

Clumped isotope thermometry in foraminifera - From calibration to Plio-Pleistocene temperature reconstructions in the Indo-Pacific Warm Pool



Niklas Meinicke

Thesis for the degree of Philosophiae Doctor (PhD)
University of Bergen, Norway
2020

UNIVERSITY OF BERGEN



Clumped isotope thermometry in foraminifera - From calibration to Plio-Pleistocene temperature reconstructions in the Indo-Pacific Warm Pool

Niklas Meinicke



Thesis for the degree of Philosophiae Doctor (PhD)
at the University of Bergen

Date of defense: 25.06.2020

© Copyright Niklas Meinicke

The material in this publication is covered by the provisions of the Copyright Act.

Year: 2020

Title: Clumped isotope thermometry in foraminifera - From calibration to Plio-Pleistocene temperature reconstructions in the Indo-Pacific Warm Pool

Name: Niklas Meinicke

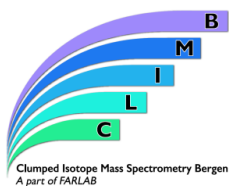
Print: Skipnes Kommunikasjon / University of Bergen

"In one drop of water are found all the secrets of all the oceans."

Khalil Gibran (1883 - 1931)

Scientific environment

The research leading to this dissertation was carried out at the Department of Earth Science and the Bjerknnes Centre for Climate Research, University of Bergen (UoB), Norway. The PhD study was part of the CLIP project funded by the Trond Mohn Foundation. Additional funding was provided by the European Research Council (ERC) under the European Union's Horizon 2020 research and innovation programme (grant agreement No 638467). This PhD project benefitted from sample material obtained during IODP Exp. 363 funded by the International Discovery Program and a close collaboration with the University of California, Santa Cruz. The supervisory committee consisted of Nele Meckler (Bjerknnes Centre for Climate Research and University of Bergen) as the main supervisor and the two co-supervisors Sze Ling Ho (National Taiwan University) and Stijn De Schepper (NORCE).



Acknowledgements

This thesis would not have been possible without the people who supported me over the last years. First, I would like to express my profound gratitude to my main supervisor, Nele Meckler, and my co-supervisors, Sze Ling Ho and Stijn De Schepper for their manifold support. Above all, thank you, Nele, for giving me the chance to spend an incredible four years in Norway and work on this exciting PhD project! I am very grateful for your scientific guidance and encouragement, for example to apply to sail on an IODP research cruise during my PhD. Your unwavering optimism inspires me and continuously entrails our group of CLIMBers, even when our mythical creatures have a bad day or two. Thank you, Ling, for your continuous support along the way and particularly for many stimulating scientific and private discussions! Stijn, thank you for being there when I needed help even though I turned my back on the North Atlantic!

Heartfelt thanks go to all members, past and present, of the clumped isotope group in Bergen! We've come a long way from the empty lab in 2015 to the exciting data being generated today. I always cherished the team spirit during long hours in the lab, countless discussions about standard measurements, mass spectrometer maintenance, daily lunch breaks and other social events, conferences and workshops, and of course our recurring group retreats. Thank you for your support and friendship, Alison Piasecki, Sze Ling Ho, Thomas Leutert, Anna Hauge Braaten, Sevasti Modestou, Alvaro Fernandez Bremer and Yves Krüger (I am aware that you are technically not a clumped isotope person)!

I am very thankful to everybody who was involved in IODP Exp. 363 for making this research cruise one of the best experiences of my life! A special thank-you to the awesome people of the nightshift who I had the pleasure to live and work alongside for nine weeks, you made this experience so much more than just a work trip!

I would like to express my gratitude to Christina Ravelo and Maria (Maya) Reimi for an exciting collaboration project and many productive zoom calls. Thank you, Maya, for all the hard work you put into the third manuscript to meet the tight deadline! Moreover, I am thankful to the Eystein Jansen, Trond Dokken, Bjørg Risebrobakken, Aradhna Tripathi, Ralf Schiebel and Dirk Nürnberg for making samples from all over the

globe available to us for my first study. Furthermore, thank you, Dirk, that you've been a constant throughout my studies, from the first lecture I attended on paleoceanography to my first publication! I would like to thank Bjarte Hannisdal for his assistance with σ and R. A sincere thanks goes to Henrik Sadatzki for proofreading my thesis.

Jordan Donn Holl, Lubna Al-Saadi, Allegra Liltved, Ulrike Proske and Raúl Tapia must be thanked for their help along the way from sample preparation to the measurements. The data presented in this thesis would not have been generated without the helping hands of Pål Tore Mørkved, Enver Alagoz, Anna Kieu-Diem Tran and Eirik Vinje Galaasen. Thank you for your tireless fight to keep the mass specs running and well-fed! Whenever I needed logistical support, for example while trying to send packages overseas, Mareile Andersson was always there to help. Thank you for your commitment!

The last years wouldn't have been the same without all my friends and colleagues from the University of Bergen and the Bjerknes Centre. In particular, I would like to thank Lukas and family, Björn, Willem, Carl, Fanny, Andreas, Tobias, Nil, Henrik, Eva and family, Sunniva, Evi, Margit, Sarah, Kerstin, Tamara, Fabian, Caroline, Hans Christian, Sonja, Morven, Jordan, Niall, Desiree, Cédric, Christos, Davide & Siri for many unforgettable memories! Thank you, Eoghan, for Kuchenzeit, the daily dip in the fjord, Kohlfahrt, Irish breakfast and all the other things that make Dorfleben awesome!

I am deeply grateful for all my friends back in Germany, especially the ones that managed to visit us in Bergen over the years: Thank you, Kaddi, Leif, Hicky, Basti, Finja, Rouven (yes, being stopped at the airport in Germany still counts), Ramona and Wolfgang! Moreover, I feel blessed to have the unconditional support of Lisa's and my family back home. Thank you for always being there for us, from the day of our move through many visits and care packages to providing accommodation during our trips to Germany!

Thank you, Lisa! There are no words to express how grateful I am for all your love and support and to have you in my life! And finally, Karlotta, thank you for not caring about my PhD and putting things in perspective! You rock my world!

Abstract

Clumped isotopes thermometry on foraminifera holds the potential to accurately reconstruct ocean temperatures on million-year timescales. In contrast to most other paleothermometers, clumped isotopes do not rely on prior knowledge regarding ocean chemistry changes thus evading a major source of uncertainty inherent to most other paleothermometers.

This thesis aims to amend our understanding of the clumped isotope signal in foraminifera and provide improvements to this paleothermometer for application to ocean sediments (Paper I). The knowledge gained is applied to Plio-Pleistocene sequences from two locations within the Indo-Pacific Warm Pool in order to address discrepancies among other temperature proxies and shed new light on long-standing debates regarding the long-term temperature evolution of this crucial region in the global ocean (Papers II and III).

The results displayed in this thesis include a clumped isotope to temperature calibration dataset for planktonic foraminifera that was combined with several existing foraminifer-based calibrations in order to elucidate potential laboratory differences as well as species effects on the paleothermometer (Paper I). Our combined calibration highlights the excellent agreement among various analytical approaches and different foraminifera species. This work thus provides a robust tool to reconstruct past ocean temperatures using various species and on million-year time scales.

The results of papers II and III constrain the Plio-Pleistocene temperature evolution of the Indo-Pacific Warm Pool independent of ocean chemistry changes. The knowledge gained can be used to disentangle the influences of these reservoir changes and the temperature signal recorded in other proxies. The paired Mg/Ca and clumped isotope records comprise evidence for the validity of Plio-Pleistocene Mg/Ca-based sea surface temperature reconstructions and argue against a systematic bias of Pliocene Mg/Ca temperature estimates by past Mg/Ca changes of seawater.

The long-term temperature evolution of the Indo-Pacific Warm Pool across the Plio-Pleistocene is illustrated by the combined mixed layer and thermocline records from IODP Sites U1488 (Paper II), U1482 and U1483 (Paper III). The evidence presented in

this thesis portrays a vertical and lateral expansion of the Indo-Pacific Warm Pool during the Pliocene relative to its modern extent, albeit without significant warming of surface waters in the central part. Our results document the strengthening of glacial periods from the Pliocene to present, while interglacial temperatures are not subject to long-term trends. Moreover, our results corroborate Mg/Ca records from the equatorial Pacific and thus support the hypothesis of a “permanent El Niño-like state” or “El Padre” during the Early Pliocene.

The potential of clumped isotope thermometry on foraminifera for the reconstruction of past ocean temperatures at different depths in the water column is demonstrated by the results included in this thesis. Applied on Cenozoic time scales this paleothermometer ideally complements other, higher resolution methods by providing the opportunity to test these proxies and deliver independent constraints on non-thermal effects such as ocean chemistry changes.

List of publications

Paper I

Meinicke, N., Ho, S.L., Hannisdal, B., Nürnberg, D., Tripathi, A., Schiebel, R. and Meckler, A.N. (2020). A robust calibration of the clumped isotopes to temperature relationship for foraminifers. *Geochimica et Cosmochimica Acta* **270**, 160-183. doi: 10.1016/j.gca.2019.11.022

Paper II

Meinicke, N., Reimi, M.A., Ravelo, A.C., and Meckler, A.N. Coupled Mg/Ca and clumped isotope measurements confirm stable Western Pacific Warm Pool sea surface temperatures over the last 6 million years.

Manuscript in preparation for Paleooceanography and Paleoclimatology

Paper III

Reimi, M.A., **Meinicke, N.**, Meckler, A.N., and Ravelo, A.C. A multi-proxy study of changes in the Indonesian Throughflow since the Pliocene.

Manuscript in preparation for Geochemistry, Geophysics and Geosystems

The published paper (I) is reprinted with permission from the journal. All rights reserved.

Contents

Scientific environment	iv
Acknowledgements	v
Abstract	vii
List of publications	ix
1 Introduction	1
1.1 Rationale.....	1
1.2 Plio-Pleistocene global climate.....	2
1.3 The Indo-Pacific Warm Pool.....	4
1.4 The Plio-Pleistocene evolution of the Indo-Pacific Warm Pool.....	7
1.5 Limitations of prevalent proxies for Plio-Pleistocene tropical temperature reconstructions.....	10
1.6 Carbonate clumped isotope thermometry.....	12
2 Objectives	16
3 Material and methods	18
4 Summary of papers	23
5 Synthesis and outlook	26
6 References	31
7 Scientific results	51
Paper I.....	51
Paper II.....	77
Paper III.....	129

1 Introduction

1.1 Rationale

The ocean is an essential part of the Earth's climate system by storing and redistributing heat and moisture. The oceans also hold information about past climate change in the sediments on the seafloor. In these sediments climate proxies can be measured providing tools to decipher information about the Earth's climate history (Emiliani, 1954). These reconstructions of past climate variability are crucial to understand mechanisms and feedbacks within Earth's climate system because they yield time series of various environmental parameters and document their relationship to each other (e.g. Rial et al., 2004).

Past time intervals such as warm periods ("interglacials") in the Pliocene (5.3 to 2.6 Ma) have been suggested as an analogue to the mean state that modern-day climate is approaching due to man-made global warming (Dowsett et al., 2009; Haywood et al., 2011). The potential of the Pliocene to help our understanding of near-future climate change has been highlighted (e.g. Dowsett, 2007b; Haywood et al., 2011; Dowsett et al., 2013; Haywood et al., 2013; Haywood et al., 2016) as it is the most recent epoch with sustained warm temperatures and atmospheric CO₂ levels similar to today (Section 1.2, Seki et al., 2010). For this reason the reconstruction of Pliocene climate has received considerable attention in previous studies (reviewed in Haywood et al., 2016; McClymont et al., 2020). However, several important issues have so far eluded a definitive answer.

The state of the Indo-Pacific Warm Pool during the Pliocene is one of these open questions (Section 1.4, Haywood et al., 2016). As the largest body of warm water on our planet the Indo-Pacific Warm Pool has been referred to as the "heat engine of the globe" (De Deckker, 2016). Due to the importance of this region for circulation patterns in the atmosphere and the ocean (Section 1.3) developing a better understanding how the warm pool evolved on million-year timescales can improve our knowledge about global climate in general. Yet, existing proxy reconstructions for this region are plagued by the limitations of the various established paleothermometers (Section 1.5).

Foraminifer-based proxies such as Mg/Ca and $\delta^{18}\text{O}$ can be used to reconstruct environmental conditions throughout the water column (reviewed in Schiebel et al., 2018). However, on million-year time scales these methods suffer from increasing uncertainty caused by ocean chemistry changes influencing the signal (Section 1.5). Being independent of ocean chemistry clumped isotope thermometry provides the potential to overcome these limitations (Section 1.6, Tripathi et al., 2010). To date, very few studies have applied this proxy to paleoceanographic research questions using foraminifera (e.g. Grauel et al., 2013; Rodríguez-Sanz et al., 2017) because it is analytically challenging and demanding with respect to the amount of sample material needed (e.g. Bernasconi et al., 2018). Although recent methodological advances have improved the applicability to small sediment samples, more work characterizing the clumped isotope signal in foraminifera is needed to facilitate the widespread use of this paleothermometer (Peral et al., 2018).

This thesis contains a study seeking to improve the calibration of the clumped isotope thermometer for foraminifera by deepening our understanding of potential laboratory- and species-specific effects on this proxy. Applying the knowledge gained from the calibration study the thesis aims at using the clumped isotope thermometer to reconstruct temperatures in the region of the Indo-Pacific Warm Pool on Plio-Pleistocene time scales.

1.2 Plio-Pleistocene global climate

The Pliocene epoch (5.3-2.6 Ma, see Figure 1) comprises a relatively stable Early Pliocene period (5.3-3.6 Ma, Pagani et al., 2010; Fedorov et al., 2013) in which global temperatures were warmer and atmospheric CO_2 concentrations likely higher than during preindustrial times (reviewed in Haywood et al., 2016). Additionally, the Late Pliocene (3.6-2.6 Ma) is marked by the onset and intensification of the Northern Hemisphere glaciation (Bartoli et al., 2005; Mudelsee & Raymo, 2005) accompanied by a transition from stable warm climates to the cooler climate and glacial-interglacial cycles of the Pleistocene (e.g. Mudelsee & Raymo, 2005; Raymo et al., 2006; Lisiecki & Raymo, 2007; Haywood et al., 2009; Ruggieri et al., 2009).

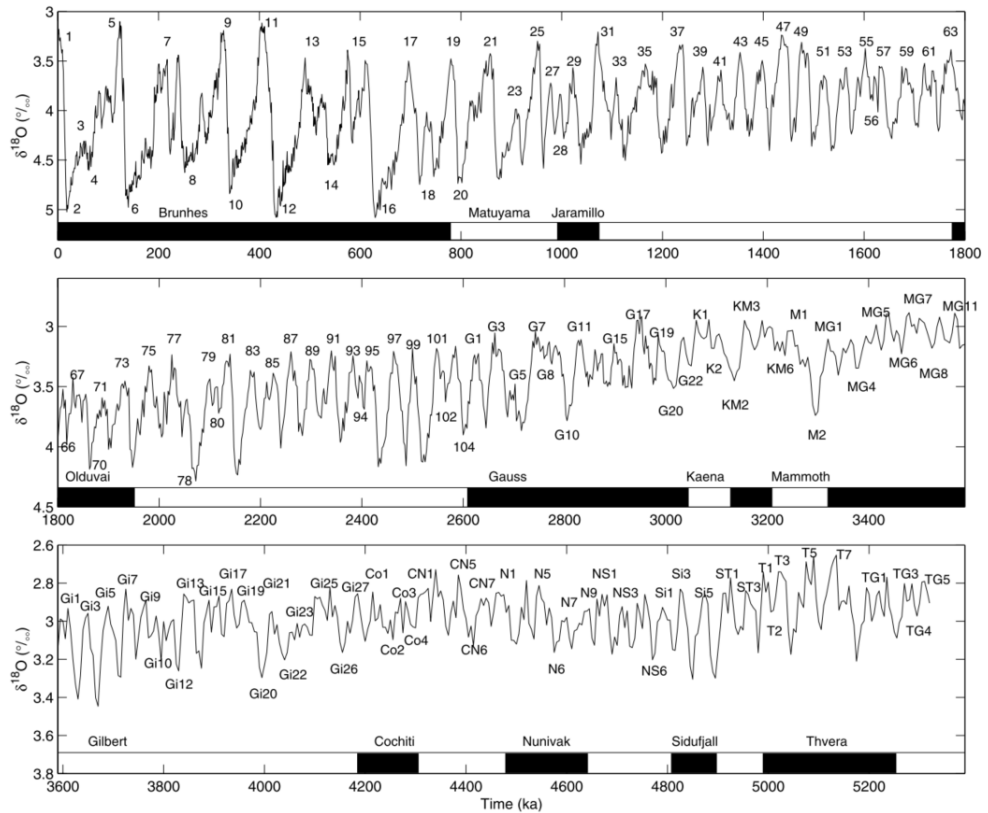


Figure 1: The benthic $\delta^{18}\text{O}$ record showing global ice volume changes over the last 5 Myrs. The vertical scale at >3.6 Ma is expanded to illustrate even small-scale climate oscillations. Numbers represent the marine isotope stages (from Lisiecki & Raymo, 2005).

The mid-Piacenzian Warm Period (mPWP, 3.3-3.0 Ma) was the most recent Pliocene interval characterized by warmer climate than today and has thus been studied in detail (e.g. Dowsett et al., 2009; Dowsett et al., 2011; Salzmann et al., 2013; Dowsett et al., 2016; Haywood et al., 2016). Climate reconstructions for this interval indicated that compared to today global temperatures were 3°C warmer (Haywood & Valdes, 2004; McClymont et al., 2020), continental ice sheets were diminished (Dolan et al., 2011), global sea-level was 10-40 m higher (Raymo et al., 2011), and the Atlantic meridional overturning circulation (AMOC) was equal (Zhang et al., 2013) or stronger (Raymo et al., 1996).

During the Late Pliocene, global climate cooled due to a gradual decrease in atmospheric CO₂ concentrations from ~400 to 280 ppm (Martínez-Botí et al., 2015). Benthic foraminiferal $\delta^{18}\text{O}$ records, which reflect bottom water temperatures and global ice volume, gradually increase from ~3.6 Ma onwards thus indicating the onset of the Northern Hemisphere glaciation. Based on temperature reconstructions using Mg/Ca and faunal assemblages the ice volume-related fraction of this signal was estimated to be ~0.4 ‰, equivalent to ~43 m of sea level lowering (Mudelsee & Raymo, 2005). At ~2.7 Ma full glacial-interglacial cycles (Figure 1), represented by a pronounced 41 kyr (obliquity) cycle (Ruggieri et al., 2009), were established (Lisiecki & Raymo, 2007; Sarnthein et al., 2009).

The long-term global cooling that started in the Pliocene continued throughout the Pleistocene epoch (2.58 Ma to 11.7 ka, e.g. Raymo et al., 2006; Lisiecki & Raymo, 2007). As shown by benthic $\delta^{18}\text{O}$ records (e.g. Pisias & Moore, 1981) the dominant periodicity of glacial-interglacial cycles changed from 41 to 100 kyr cycles during an interval called the mid-Pleistocene transition (MPT, around 900 ka). The change in frequency seen in the benthic $\delta^{18}\text{O}$ signal was accompanied by overall increased values suggesting an expansion of global ice volume to the maximum level characteristic for the Late Pleistocene ice ages (Mudelsee & Schulz, 1997; Elderfield et al., 2012).

Although alteration of climate from stable warm conditions of the Early and mid-Pliocene to glacial-interglacial cycles towards the Pleistocene (Figure 1) is the defining global feature of the Pliocene epoch, the characteristics of regional climate variability remain less well defined. In particular, regional climate change in the Indo-Pacific Warm Pool and its implications for the heat transport towards higher latitudes (e.g. via the connection to the global overturning circulation through the Indonesian Throughflow) remain a matter of debate (Haywood et al., 2016).

1.3 The Indo-Pacific Warm Pool

The Indo-Pacific Warm Pool (IPWP) covers the eastern part of the Indian Ocean and the western equatorial Pacific (Figure 2). Warmest temperatures occur in the western equatorial Pacific (Western Pacific Warm Pool, WPWP) which today is characterized by sea surface temperatures (SST) >28 °C (e.g. Wang & Mehta, 2008; Rosenthal, 2018).

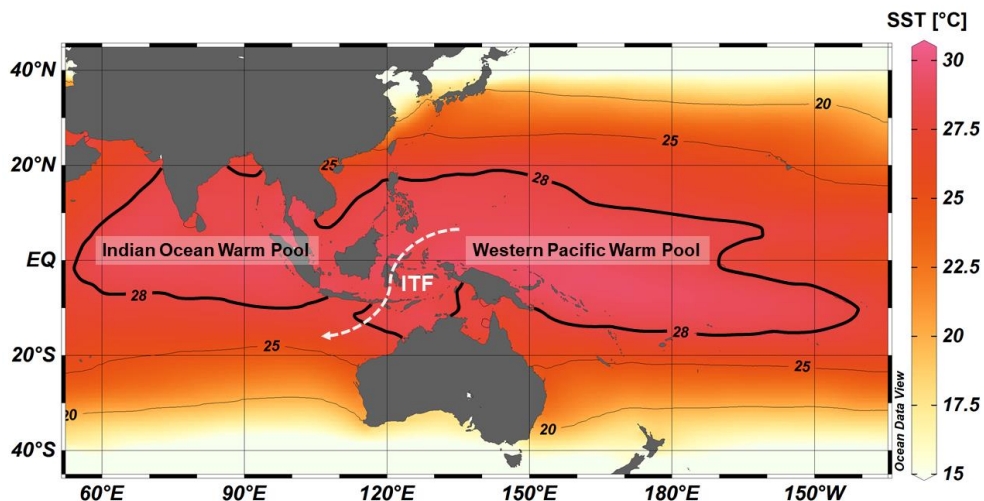


Figure 2: Annual mean sea surface temperature (Locarnini et al., 2010) in the the Indo-Pacific Warm Pool region generated using Ocean Data View (Schlitzer, 2018). The 28 °C isotherm (black line) as well as the Indonesian Throughflow (ITF, white dashed line) across the Sunda Archipelago are highlighted.

As a crucial source of heat and water vapor to the atmosphere the IPWP influences climate both on a regional and global scale through teleconnections (Molnar & Cane, 2002; Neale & Slingo, 2003): A minor change of SSTs in the IPWP may alter the position and strength of atmospheric convection over the area, thereby influencing large-scale atmospheric circulation patterns (Hadley and Walker circulation) with global implications (Sardeshmukh & Hoskins, 1988; Neale & Slingo, 2003; Wang & Mehta, 2008). The prevalent wind direction in the boreal summer (July to September) is northward towards Asia, changing to southward winds towards Australia during boreal winter (January to March). In turn, the Intertropical Convergence Zone (ITCZ) is located over the South China Sea in the boreal summer and shifts southward towards Australia in the winter (Gordon, 2005). Through its interaction with seasonal and interannual changes of precipitation patterns and the position of the ITCZ, the IPWP is connected to large-scale weather systems including the Asian monsoon and the El Niño-Southern Oscillation (ENSO, e.g. Ropelewski & Halpert, 1987; Wang & Mehta, 2008). The latter is a periodic but irregular variation of wind patterns, precipitation and sea surface temperatures of the equatorial Pacific Ocean (Philander, 1983).

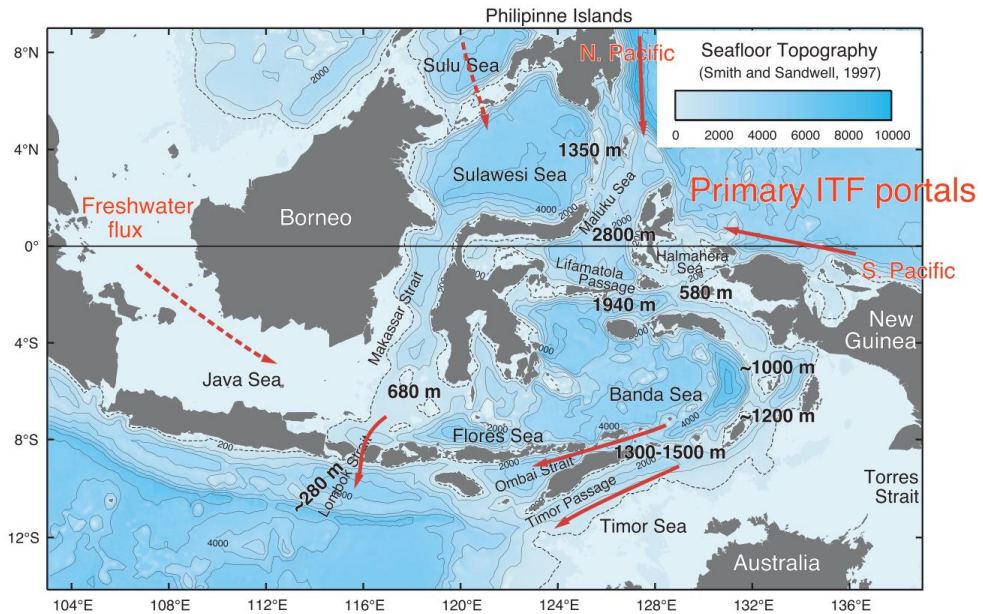


Figure 3: Seafloor topography of the Indonesian seas including the primary inflow and outflow portals of the ITF (red arrows) and sill depths in various straits. Dashed red arrows indicate secondary inflow portals delivering freshwater to the ITF (from Gordon, 2005).

Moreover, the seaways north of Australia act as a crucial pathway for ocean circulation from the Pacific to the Indian Ocean via the Indonesian Throughflow (ITF, Figure 3), thus playing an important role for the global overturning circulation (e.g. Gordon, 1986; Godfrey et al., 1993; Fine et al., 1994; Neale & Slingo, 2003). The transport of water masses through the Sunda Archipelago takes place through several straits (Figure 3). Historically, the estimated volume of water transported by the ITF varies considerably among studies from almost zero to 20 Sv ($1 \text{ Sv} = 10^6 \text{ m}^3\text{s}^{-1}$, see Godfrey, 1996). More recently, Sprintall et al. (2009) estimated the mean annual transport through Sunda Archipelago to ~ 15 Sv.

In the ITF, water masses of North Pacific and South Pacific origin mix with freshwater entering from the Sulu and Java Sea with a seasonal peak of this low-salinity contribution during boreal winter (Gordon et al., 2003). Today, North Pacific subtropical water dominates the upper thermocline of the Makassar Strait and Banda Sea while the influence of saltier South Pacific subtropical water is smaller (Gordon, 2005). The lower thermocline shows a large portion of North Pacific Intermediate

Water in the Makassar Strait and more Southern Pacific influence in the eastern pathways. The ratio of the northern and southern components varies on seasonal timescales with a larger southern component from January to March (Gordon & Fine, 1996). After entering the Indian Ocean, these Pacific water masses become the dominant source of the southward-flowing warm Leeuwin current along the west coast of Australia (Feng et al., 2003). ITF waters can also be traced as a relatively fresh surface to thermocline water mass that crosses the tropical South Indian Ocean at $\sim 12^{\circ}\text{S}$ as part of the westward-flowing South Equatorial Current (SEC, Gordon et al., 1997) which feeds into the Agulhas Current east of Africa (see Sprintall et al., 2009).

1.4 The evolution of the Indo-Pacific Warm Pool

Although the transition of global climate from the warm and stable Pliocene conditions to the glacial-interglacial cycles of the Pleistocene is well documented (Section 1.2), knowing whether the Indo-Pacific Warm Pool was stable over long time periods is crucial for our understanding of past and future climate dynamics (Dowsett, 2007a). Studies using planktonic foraminifera for Mg/Ca-based temperature reconstructions (Wara et al., 2005) as well as faunal analysis (Dowsett, 2007a) indicate relatively stable surface temperatures in the center of the WPWP since the Early Pliocene. This is valid even during climate extremes such as the mid-Pliocene warm period (~ 3 Ma, Wara et al., 2005; Dowsett, 2007a) and the coldest glacials of the late Pleistocene (e.g. Last Glacial Maximum, ~ 26.5 -19 ka, Dowsett, 2007a).

Independent of absolute temperatures in the central part of the warm pool, an expansion of warm waters both meridionally (Brierley et al., 2009) and zonally (Wara et al., 2005) has been proposed for the Early Pliocene (Fedorov et al., 2013). The reduced zonal temperature gradient across the equatorial Pacific has been referred to as a permanent El Niño-like condition (Molnar & Cane, 2002; Wara et al., 2005; Fedorov et al., 2006; Ravelo et al., 2006; Fedorov et al., 2010) or “El Padre” (Figure 4, Ravelo et al., 2014; Ford et al., 2015). This term is used to describe an Early Pliocene Pacific mean state characterized by warm surface temperatures and a deep thermocline in the eastern equatorial Pacific (Figure 4) and distinguishes it from similar patterns related to the dynamical ENSO.

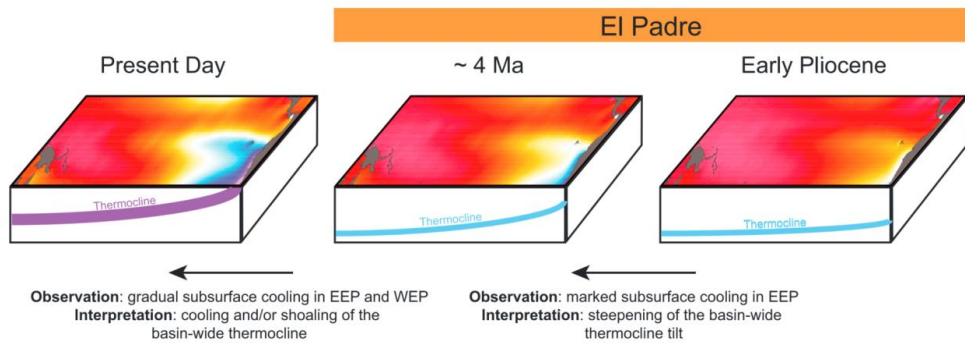


Figure 4: Schematic diagram showing the thermocline evolution from the proposed El Padre conditions in the early Pliocene to present (from Ford et al., 2015).

However, La Niña rather than El Niño-like conditions during the Early Pliocene and an “ocean thermostat” mechanism were proposed by Rickaby and Halloran (2005). Based on Mg/Ca analysis of surface and thermocline-dwelling foraminifera the authors suggested that warm surface temperatures in the western equatorial Pacific were balanced by stronger upwelling and colder temperatures in the eastern part of the ocean. Moreover, in contrast to the Mg/Ca-based evidence of stable surface temperatures in the IPWP across the last ~5 Myrs, studies based on the TEX₈₆ temperature proxy indicate a long-term cooling trend across the Plio-Pleistocene (O’Brien et al., 2014; Zhang et al., 2014). These contrasting interpretations represent a major gap in the knowledge of evolution of the IPWP (Haywood et al., 2016).

During the mid-Pliocene, tectonic changes north of Australia have been suggested as a driver for regional (and potentially global) climate change: The restriction of the Indonesian Seaway between ~4 and 3 Ma (Cane & Molnar, 2001; Karas et al., 2009; Karas et al., 2011b, 2011a; Karas et al., 2017) has been interpreted to cause a weakening (Christensen et al., 2017; De Vleeschouwer et al., 2018) and reorganization of the ITF. A shift in the dominant source of waters entering the ITF from more saline South Pacific water masses to fresher and cooler northern source water (Cane & Molnar, 2001; Karas et al., 2009) may have led to a more vigorous East Australian Current (Karas et al., 2011a) and a cooler and shallower thermocline in the tropical Indian Ocean (Karas et

al., 2009; Karas et al., 2011b). A weakening of the ITF due to tectonic changes (e.g. Cane & Molnar, 2001) and/or sea level lowstands (De Vleeschouwer et al., 2018) may also have diminished the Leeuwin Current (De Vleeschouwer et al., 2019) and triggered the onset of more arid climate in north-western Australia (Karas et al., 2011b; Christensen et al., 2017; Auer et al., 2019). A weaker Leeuwin Current in turn would have reduced the equator-to-pole heat transport (Karas et al., 2011b, 2011a; De Schepper et al., 2014), thus potentially amplifying global cooling by promoting the thermal isolation of Antarctica (De Vleeschouwer et al., 2018).

The influence of this mid-Pliocene global cooling and the reorganization of the ITF on surface water temperatures in the western Indian Ocean has been interpreted to be rather limited (Karas et al., 2011b). While Mg/Ca-based temperature records from the tropical and subtropical eastern and the tropical western Indian Ocean change reveal a similar pattern in the Early Pliocene they diverge in the Late Pliocene: A warming effect between 4 and 3.6 Ma documented in the eastern and western Indian Ocean alike (Karas et al., 2011b) is in accordance with the proposed expansion of the IPWP during the Early to mid-Pliocene (e.g. Brierley et al., 2009). However, only the record from the eastern Indian Ocean experienced a gradual long-term cooling of Mg/Ca-based surface temperatures after 3.6 Ma (Karas et al., 2011b).

1.5 Limitations of prevalent proxies for Plio-Pleistocene tropical temperature reconstructions

Although several paleotemperature proxies are available to study past climate change, reconstructing temperatures in the IPWP on million-year timescales poses a unique challenge leading to persistent discrepancies among different studies: Although warmer SSTs in the eastern equatorial Pacific during the Early Pliocene are supported by different proxies (Dekens et al., 2008; Zhang et al., 2014), the question whether Pliocene SSTs in the WPWP were warmer than those today is a matter of ongoing debate and closely connected to the limitations of various temperature proxies (Section 1.4, e.g. O'Brien et al., 2014; Ravelo et al., 2014).

The U^{K}_{37} alkenone unsaturation index (Brassell et al., 1986; Prahl & Wakeham, 1987; Prahl et al., 1988) and TEX_{86} (Schouten et al., 2002) are commonly used biomarker paleothermometers based on lipids produced by haptophyte algae and archaea, respectively. The U^{K}_{37} method is calibrated to SST but may be influenced by the seasonal productivity cycle (e.g. Schneider et al., 2010). Moreover, the U^{K}_{37} proxy is unable to reconstruct ocean temperatures above 28.5 °C (Conte et al., 2006), which hinders its use for temperature reconstructions within the IPWP (Zhang et al., 2014).

The use of the TEX_{86} proxy is mainly limited by a lack of knowledge regarding the production of the signal in the water column: There is evidence for spatial and temporal variability of the ecology and community structure of the archaea producing the TEX_{86} signal (e.g. Elling et al., 2014; Kim et al., 2015; Hertzberg et al., 2016; Polik et al., 2018). Above all, the TEX_{86} proxy is plagued by a lack of knowledge concerning the depth and season the signal originates from (reviewed in Schouten et al., 2013). This fuels an ongoing debate about the calibration of the TEX_{86} signal to water temperatures and whether this method can be used as a proxy for SST (Kim et al., 2012; Tierney & Tingley, 2015; Ho & Laepple, 2016; Zhang & Liu, 2018).

Proxy methods based on oxygen isotopes (Emiliani, 1954) as well as the Mg/Ca ratio (Nürnberg et al., 1996) in foraminifera provide the opportunity to investigate environmental conditions in different parts of the water column by selecting species with particular depth habitats (e.g. Mulitza et al., 1997). In addition to the influence of

water temperature, both $\delta^{18}\text{O}$ and Mg/Ca can be subject to biologically controlled so-called “vital effects” that can be species-specific (e.g. Bemis et al., 1998; Regenberg et al., 2009; Ezard et al., 2015). Both proxies may also be altered by post-depositional diagenetic processes (e.g. Sexton et al., 2006; Regenberg et al., 2007). These potential secondary influences on the temperature signal call for careful evaluation of regional conditions and sample preservation when using foraminifera for climate reconstructions (reviewed in Schiebel et al., 2018). A major challenge, however, accrues from the fact that in addition to water temperature, both $\delta^{18}\text{O}$ and Mg/Ca are dependent on the composition of the seawater: Beside water temperature during formation of the calcite test, the oxygen isotopes depend on the $\delta^{18}\text{O}$ of seawater which is strongly influenced by global ice volume (reviewed in Pearson, 2012). While making $\delta^{18}\text{O}$ in benthic foraminifera a useful proxy for ice volume on glacial-interglacial time scales it impedes the use of $\delta^{18}\text{O}$ for temperature reconstructions (e.g. Elderfield et al., 2012). The Mg/Ca ratio in foraminifera can be influenced to a minor extent by local salinity (e.g. Nürnberg et al., 1996; Lea et al., 1999; Mathien-Blard & Bassinot, 2009) and by carbonate chemistry (e.g. pH, Lea et al., 1999). More importantly on million-year time scales, changes of the Mg/Ca ratio of seawater can have a large effect on Mg/Ca-based temperature reconstructions if not accounted for (Evans et al., 2016). This argument has been used as a potential explanation for the observed disagreement between Mg/Ca and TEX₈₆-based temperature reconstructions across the IPWP during the Plio-Pleistocene: A Mg/Ca ratio of seawater during the Pliocene could have masked the effect of warmer surface temperatures in the Mg/Ca record of planktonic foraminifera (O’Brien et al., 2014; Zhang et al., 2014).

In order to resolve the disagreement among published temperature records from the region and develop a better understanding regarding the long-term evolution of the IPWP the persisting ambiguities related to proxy limitations need to be addressed. Clumped isotopes measured in foraminifera may provide the means to tackle this task as they can be used to reconstruct temperatures throughout the water column, while being independent of ocean chemistry changes (e.g. Tripathi et al., 2010).

1.6 Carbonate clumped isotope thermometry

The carbonate clumped isotope method rests upon the quantification of bonds between rare oxygen (^{18}O) and carbon (^{13}C) isotopes in the crystal lattice of carbonate minerals (e.g. Ghosh et al., 2006b; Schauble et al., 2006; Eiler, 2007, 2011). As a result of its lower zero-point vibrational frequencies, the ^{13}C - ^{18}O bond is more stable compared to bonds containing the more common isotopically light forms. Under equilibrium conditions, carbonate (CO_3^{2-}) ions thus possesses more bonds between two heavy isotopes than stochastically expected (Schauble et al., 2006). The extent of this excess of doubly substituted (clumped) ions increases with decreasing temperature (Bigeleisen & Mayer, 1947; Urey, 1947; Eiler & Schauble, 2004; Schauble et al., 2006). Therefore, the difference relative to a random distribution of ^{13}C - ^{18}O bonds can be utilized to determine the ambient temperature during the precipitation of the carbonate (e.g. Ghosh et al., 2006a; Schauble et al., 2006; Eiler, 2007).

With the current analytical techniques, it is not possible to determine the relative abundance of ^{13}C - ^{18}O bonds in a carbonate directly. Instead, m/z 47 isotopologues are measured on CO_2 gas extracted from the carbonate by temperature-controlled phosphoric acid digestion (Ghosh et al., 2006a; Huntington et al., 2009). Due to a proportional relationship between the relative abundance of clumped isotopes in carbonates and in acid-liberated CO_2 produced from this carbonate the carbonate's clumped isotope signal can be inferred from the CO_2 gas (Ghosh et al., 2006a). The term Δ_{47} (Equation 1) is defined as the ratio (in %) between the relative abundance of mass 47 isotopologues in a sample CO_2 gas and the abundance of this isotopologue in CO_2 gas with identical bulk isotopic composition and a stochastic distribution (Eiler & Schauble, 2004).

$$\Delta_{47} = \left[\left(\frac{R^{47}}{R^{47*}} - 1 \right) - \left(\frac{R^{46}}{R^{46*}} - 1 \right) - \left(\frac{R^{45}}{R^{45*}} - 1 \right) \right] \cdot 1000 \quad (1)$$

R^{45} , R^{46} and R^{47} represent masses 45, 46 and 47 in relation to mass 44. The theoretically expected ratios for a random distribution (R^{45*} , R^{46*} and R^{47*}) are calculated from the abundance ratios ^{13}C , ^{12}C , ^{18}O , ^{17}O and ^{16}O in the sample (Eiler, 2007).

The carbonate clumped isotope thermometer is a demanding method with respect to the measurement and correction procedure (e.g. Bernasconi et al., 2018). Due to the fact that the excess abundance of clumped isotopes at room temperature is <1 ‰, the Δ_{47} signal must be analyzed with very high precision (Huntington et al., 2009), which is achieved by long measurement time and/or replication (Fernandez et al., 2017). As a result, the sample amount requirements compared to e.g. $\delta^{18}\text{O}$ analysis are significantly increased (reviewed in Spencer & Kim, 2015; Bernasconi et al., 2018). Moreover, Δ_{47} is susceptible to several secondary effects: Even small amounts of volatile trace gases such as organics and sulfides may produce isobaric interferences during the measurement thus calling for rigorous purification of the sample gas (e.g. Eiler, 2007). Small non-linearity effects influencing the measured ratio of mass 47 to 44 as a function of isotopic composition have been described (Ghosh et al., 2006a; Huntington et al., 2009). These are caused by negative background effects on the Faraday collectors of the mass spectrometers and can be corrected for (He et al., 2012; Bernasconi et al., 2013; Fiebig et al., 2016). Moreover, scale compression takes place as a result of isotopic exchange reactions in the source of the mass spectrometer (Huntington et al., 2009; Dennis et al., 2011; He et al., 2012). Consequently, corrections for both background effects and scale compression must be applied to the data. Clumped isotope data has traditionally been corrected using CO_2 gases of various bulk isotopic composition that were either heated to 1000 °C in order to generate a stochastic distribution, or equilibrated at a defined temperature (reviewed in Huntington et al., 2009; Bernasconi et al., 2018). Following this standardization procedure and transferring the Δ_{47} data to an absolute reference frame makes results more comparable among different laboratories (Dennis et al., 2011). However, it has been argued that production and use of heated and equilibrated gases is susceptible to the introduction of additional error by user handling (Bernasconi et al., 2018).

Several recent advances in the methodological procedure of clumped isotope analysis include a push for the widespread use of carbonate standards (Bernasconi et al., 2018), daily monitoring of backgrounds for pressure baseline corrections to eliminate the need for frequent gas measurements (Meckler et al., 2014), and the adoption of the updated IUPAC-recommended parameters for ^{17}O correction (Brand et

al., 2010; Daëron et al., 2016; Schauer et al., 2016). These advances have helped to further reduce inter-laboratory differences (reviewed in Bernasconi et al., 2018; Petersen et al., 2019) while the employment of an automated micro-volume measurement approach (Schmid & Bernasconi, 2010; Schmid, 2012) and the long-integration dual-inlet (LIDI) method (Hu et al., 2014) has allowed for routine downcore analysis of small sediment samples for paleoclimate research (Müller et al., 2017).

Over the years, various theoretical, experimental, and empirical calibrations have been published to characterize the relationship between Δ_{47} and the formation temperature of carbonates (e.g. Ghosh et al., 2006a; Zaarur et al., 2013; Wacker et al., 2014; Kele et al., 2015; Kelson et al., 2017; Petersen et al., 2019). Calibrations for numerous biogenic carbonates include surface (Ghosh et al., 2006a) and deep sea corals (Ghosh et al., 2006a; Thiagarajan et al., 2011), mollusc and brachiopod shells (Came et al., 2007; Henkes et al., 2013), fish otoliths (Ghosh et al., 2007), the carbonate component of tooth enamel (Eagle et al., 2010; Wacker et al., 2016), coccoliths (Tripathi et al., 2010) and foraminifera (Tripathi et al., 2010; Grauel et al., 2013; Breitenbach et al., 2018; Peral et al., 2018; Piasecki et al., 2019). Most biogenic carbonates fall within the range of inorganic calcite suggesting that the development of a universal Δ_{47} to temperature calibration may be possible (Bonifacie et al., 2017; Kelson et al., 2017; Petersen et al., 2019). Nonetheless, potential biologically-controlled secondary effects on the Δ_{47} signal (often called “vital effects”) have been suggested for several groups of calcifying organisms (e.g. Saenger et al., 2012; Spooner et al., 2016; Bajnai et al., 2018; Daëron et al., 2019; Davies & John, 2019) emphasizing the need for more data targeting individual groups of marine calcifying organisms.

The first clumped isotope studies on foraminifera (Tripathi et al., 2010; Grauel et al., 2013) did not find evidence for species-specific effects and laid the foundation to the application of this proxy to paleoceanographic research. However, the data presented in these studies was generated following methodological procedures that are now outdated and are difficult to compare to more recent data (Peral et al., 2018). In addition, data density especially for colder temperatures (<15 °C) was sparse, and the few available data suggested potentially increased scatter at colder temperatures. More recent studies added a significant amount of measurements for planktonic (Breitenbach et al., 2018;

Peral et al., 2018) and benthic foraminifera (Peral et al., 2018; Piasecki et al., 2019) suggesting that foraminifera follow the same Δ_{47} -temperature relationship described in inorganic calibrations. These calibrations, although statistically indistinguishable from each other, yield significantly (~ 2.5 °C) different temperatures for the cold end of their calibrated range. Furthermore, the data density for individual foraminifera species has still been insufficient to test for species-specific differences with confidence. Therefore, there is a need for more work on foraminifera to further define the Δ_{47} -temperature relationship in this important group of marine calcifying organisms and rule out or quantify vital effects. Finally, the analytical approach used in the different recent calibration studies varies greatly, calling for a thorough comparison between results obtained with different approaches.

Although clumped isotope analysis is characterized by several drawbacks such as the large sample requirements, tedious measurement and correction procedures, and a low signal to noise ratio, it holds the potential to become a powerful tool for paleoceanography. Particularly, Δ_{47} in foraminifera may be used to address various long-standing questions that have eluded definitive answers using other temperature proxies due to non-thermal confounding influences on these methods. While temperatures across the water column can be studied in the same way with Δ_{47} as with the more traditional proxies $\delta^{18}\text{O}$ and Mg/Ca, Δ_{47} has the major advantage of being independent of the composition of seawater (Ghosh et al., 2006a; Eiler, 2007). This leaves diagenetic alteration of the Δ_{47} signal through processes that add inorganic calcite or replace the original biogenic calcite as the main risk for paleoceanographic applications (Leutert et al., 2019). Together with the observation that the isotopic signal is preserved even at relatively high burial temperatures $< 80\text{-}120$ °C (Passey & Henkes, 2012; Stolper & Eiler, 2015) Δ_{47} analysis in foraminifera is a promising temperature proxy particularly on million-year time scales.

2 Objectives

This PhD thesis seeks to use the clumped isotope proxy on foraminifera to close persisting gaps in our knowledge about climate change in the tropics on Plio-Pleistocene timescales. In order to tap the full potential of this method, the first goal was the improvement of the clumped isotope calibration for foraminifera making use of recent methodological advances. Applying the improved calibration to planktonic foraminifera from several sites located in the tropical Indo-Pacific, the thesis aims to shed light on the thermal evolution of the Indo-Pacific Warm Pool over the last 6 Myrs.

To attain these goals and establish the clumped isotope proxy on foraminifera for Plio-Pleistocene climate research the specific objectives were to:

- Generate a surface sediment clumped isotope calibration dataset containing various species of modern planktonic foraminifera and compare this dataset to calibrations generated with diverging measurement approaches to investigate inter-laboratory differences (Paper I).
- Utilize this multi-species dataset to investigate possible species-specific effects in foraminifera and the potential to use the proxy for reconstructing temperatures at different depths in the water column (Paper I).
- Use paired measurements of clumped isotopes and Mg/Ca on mixed layer and thermocline-dwelling foraminifera from the western equatorial Pacific to reconstruct the Plio-Pleistocene thermal evolution of the central Indo-Pacific Warm Pool (Paper II).

- Contribute to solving persistent discrepancies between Mg/Ca-based and TEX₈₆-derived temperature records (Paper II).
- Unravel the influence of the Indonesian Throughflow on Plio-Pleistocene Indian Ocean circulation and temperature patterns using paired clumped isotope and Mg/Ca measurements from two sites off northwestern Australia (Paper III).

3 Material and methods

3.1 Sediment core material

Clumped isotope measurements presented in this thesis were performed on foraminifera selected from sediment samples of various age from 16 locations (Figure 5, Tables 1 and 2).

Surface sediment samples from 13 sites were obtained from several research institutions (see Table 1) and used for a global clumped isotope to temperature calibration. The sites were chosen to represent a wide range of geographic regions and ocean conditions and contain well-preserved foraminifera of mid-Holocene to recent age. From these surface sediment samples miscellaneous species of planktonic foraminifera from different habitat depths were selected with the goal to generate a multi-species calibration dataset spanning the entire range of modern ocean temperatures (Paper I).

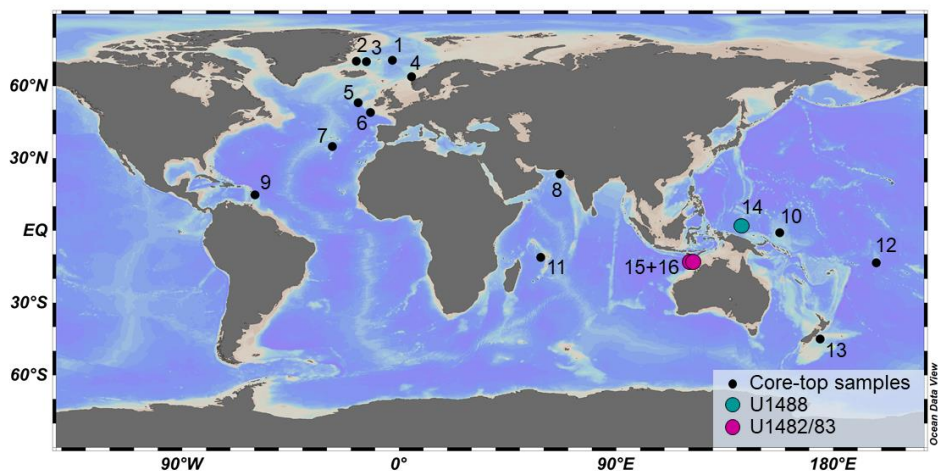


Figure 5: Sites investigated as part of this PhD project. Numbers relate to the core sites listed in Table 1 (1-13) and Table 2 (14-16). Bathymetric chart generated using Ocean Data View (ODV, Schlitzer, 2018) with bathymetric data from GlobHR (reference available in Ocean Data View).

Table 1: Locations and water depths of global surface sediment samples and the species of planktonic foraminifera used for the clumped isotope to temperature core-top calibration (Paper I).

No.	Site	Latitude °N	Longitude °E	Region	Depth [m]	Species
1 ^b	GS15-198-63MC	70.5	-2.8	Nordic Seas	2995	<i>N. pachyderma</i>
2 ^b	GS15-198-38MC	70.1	-17.7	Denmark Strait	1610	<i>N. pachyderma</i>
3 ^b	GS15-198-62MC	70.0	-13.6	Iceland Plateau	1423	<i>N. pachyderma</i>
4 ^a	GS06-144-19MC	63.8	5.2	Nordic Seas	922	<i>G. bulloides</i> , <i>G. inflata</i>
5 ^c	CD107 A ML 5A	52.9	-16.9	North Atlantic	3569	<i>G. bulloides</i> , <i>G. hirsuta</i> , <i>G. truncatulinoides</i> , <i>O. universa</i>
6 ^c	CD94 17B	48.9	-11.8	North Atlantic	1484	<i>G. bulloides</i> , <i>G. inflata</i> , <i>G. truncatulinoides</i> , <i>O. universa</i>
7 ^e	KL88	34.8	-27.7	North Atlantic	2060	<i>G. bulloides</i> , <i>G. inflata</i> , <i>G. ruber</i> white s.l., <i>G. truncatulinoides</i>
8 ^c	CD145 A150	23.3	66.7	Arabian Sea	151	<i>N. dutertrei</i>
9 ^d	SO164-25-3	14.7	-59.7	Caribbean /North Atlantic	2720	<i>G. conglobatus</i> , <i>G. ruber</i> pink, <i>G. ruber</i> white s.s., <i>G. ruber</i> white s.l., <i>P. obliquiloculata</i> , <i>T. trilobus</i>
10 ^c	OJP2016 MW0691 1.5BC11	-1.0	157.8	Ontong Java Plateau	2016	<i>T. trilobus</i>
11 ^c	WIND 33B	-11.2	58.8	Indian Ocean	2871	<i>G. menardii</i> , <i>G. ruber</i> white s.s., <i>G. tumida</i> , <i>N. dutertrei</i> , <i>O. universa</i> , <i>P. obliquiloculata</i> , <i>T. sacculifer</i> , <i>T. trilobus</i>
12 ^d	SO225-53-1	-13.5	-162.1	Manihiki Plateau	3154	<i>G. conglobatus</i> , <i>G. ruber</i> white s.s., <i>G. tumida</i> , <i>O. universa</i> , <i>P. obliquiloculata</i> , <i>T. sacculifer</i> , <i>T. trilobus</i>
13 ^d	SO213-84-2	-45.1	174.6	South Pacific	992	<i>G. bulloides</i> , <i>G. inflata</i> , <i>G. truncatulinoides</i>

Institutions samples were obtained from: a: University of Bergen, Norway, b: NORCE Norwegian Research Centre AS, Norway, c: University of California, Los Angeles, USA, d: GEOMAR, Helmholtz Centre for Ocean Research Kiel, Germany, e: Max Planck Institute for Chemistry, Mainz, Germany

The following species were used for analysis: *Globigerina bulloides*, *Globigerinoides conglobatus*, *Globigerinoides ruber* pink, *Globigerinoides ruber* white sensu lato (s.l.) and sensu stricto (s.s.), *Globorotalia hirsuta*, *Globorotalia inflata*, *Globorotalia menardii*, *Globorotalia truncatulinoides*, *Globorotalia tumida*, *Neogloboquadrina dutertrei*, *Neogloboquadrina pachyderma*, *Orbulina universa*, *Pulleniatina obliquiloculata*, *Trilobatus sacculifer*, *Trilobatus trilobus*.

Deep-sea sediments from three Sites (U1488, U1482 and U1483, Table 2) drilled during International Ocean Discovery Program (IODP) Expedition 363 were targeted for the analysis of several time intervals spanning the last 6 Myrs (Papers II and III). Our methodological approach uses intervals spanning 100 or 40 kyrs for sections younger or older than 1 Ma, respectively. By calculating mean temperatures across all samples within each interval we averaged over full glacial-interglacial cycles. Thereby, this approach avoids introducing aliasing effects to our low-resolution clumped isotope record. Moreover, in addition to reconstructing mean interval temperatures from clumped isotopes, $\delta^{18}\text{O}$ values and Mg/Ca-based temperatures are available for all individual samples within each time interval. Samples were obtained from the IODP core repository in College Station, USA. The age of the samples was determined based on shipboard calcareous nannofossil and planktonic foraminifera biostratigraphy in combination paleomagnetic data (Rosenthal, 2018; Drury in review).

Table 2: Sites, locations, water depths and species of planktonic foraminifera used for paleotemperature reconstructions in the IPWP. Downcore records were generated for sites from the western equatorial Pacific (14, Paper II) and the Indonesian Throughflow (15-16, Paper III). All three sites were drilled during IODP Exp. 363 (Rosenthal, 2018).

No.	Site	Latitude °N	Longitude °E	Region	Depth [m]	Species
14	IODP U1488	2.0	141.8	WPWP	2604	<i>G. tumida</i> , <i>T. trilobus</i>
15	IODP U1482	-15.1	120.4	ITF	1466	<i>T. trilobus</i>
16	IODP U1483	-13.1	121,8	ITF	1733	<i>T. trilobus</i>

The Plio-Pleistocene section at site U1488 from the Eauripik Rise (Figure 5) contains hemipelagic, carbonate-rich sediments (foraminifer-nannofossil ooze) with excellent to very good preservation of calcareous foraminifera tests (Rosenthal, 2018).

The preservation of samples within the intervals selected for analysis was assessed using scanning electron microscopy (SEM). Clumped isotope measurements at this site were performed on the mixed layer-dwelling species *Trilobatus trilobus* as well as the thermocline-dwelling species *Globorotalia tumida* (Paper II).

The Pliocene section of site U1482 and the Pleistocene part of site U1483 (both located on the Scott Plateau, Figure 5) were combined to generate a single clumped isotope record for the Indonesian Throughflow. The pelagic and hemipelagic sediments at both sites comprise a mixture of biogenic (mostly calcareous nannofossils and foraminifera), siliciclastic and volcanic material. Both sites are characterized in particular by a high clay content resulting in excellent preservation of the calcareous foraminifera found throughout the Plio-Pleistocene sections of the sediment (Rosenthal, 2018).

3.2 Sample preparation and analysis

All samples were wet-sieved to remove the size fraction $<63\ \mu\text{m}$ and wet or dry-sieved to isolate the size fractions designated for analysis. Individual specimens of planktonic foraminifera were selected under the light microscope and cleaned prior to clumped isotope analysis in order to remove any additional material that might potentially be attached to the outside or the inside of the foraminifer tests. Our sample preparation process involved carefully crushing the individual specimens between two glass plates to open all chambers for the cleaning procedure. The crushed foraminifera underwent several ultrasonication steps in deionized water and methanol and were rinsed numerous times with deionized water. The length of sonication steps was adjusted for individual studies: Surface sediment samples for the core top calibration study (1-13 in Figure 5, Table 1) were sonicated three times for 30 s with deionized water and 15 s with methanol. Samples from IODP sites U1488, U1482 and U1483 (14-16, Figure 5, Table 2) were sonicated for 5 s each. All cleaned samples were dried in an oven at $\leq 50\ ^\circ\text{C}$.

Clumped isotope analysis was performed on one of two Thermo Scientific MAT 253Plus dual inlet mass spectrometers coupled to KIEL IV carbonate devices (Thermo

Fisher Scientific, Bremen, Germany) at the University of Bergen. The KIEL devices were equipped with Porapak traps to remove organic contaminants (see Schmid & Bernasconi, 2010). Four carbonate standards (ETH1-4, see Bernasconi et al., 2018) were measured in equal amounts to the sample material and used for standardization as well as to monitor instrument performance. A micro-volume measurement approach (Schmid & Bernasconi, 2010; Hu et al., 2014; Meckler et al., 2014; Müller et al., 2017) that determines precise clumped isotope values of a sample from many replicate measurements of small subsamples (~100 µg) was utilized for analysis. Additionally, mean clumped isotope values including all samples from a particular time interval were calculated for the sites from the Indo-Pacific Warm Pool (14-16, Table 2). The global calibration dataset generated first was used subsequently to reconstruct water temperatures for sites U1488, U1482 and U1483. Additional information regarding the study sites, laboratory procedures and data processing can be found in the individual manuscripts (Papers I-III).

4 Summary of papers

Paper I: *A robust calibration of the clumped isotopes to temperature relationship for foraminifers*

In Paper I, we calibrate the carbonate clumped isotope thermometer for planktonic foraminifera. We build on previous studies indicating that this group of marine calcifying organisms generally follows the Δ_{47} -temperature relationship described for inorganic carbonate (e.g. Tripathi et al., 2010). Making use of recent advances in the clumped isotope method (reviewed in Bernasconi et al., 2018) we analyze small samples (<5 mg) of 14 different planktonic foraminifera species. Samples were obtained from 13 globally distributed surface sediment sites and contain species from a variety of depth habitats. We use our extensive dataset (n = 43) to investigate possible species-specific effects and assess the potential to employ Δ_{47} measured in various species of foraminifera to reconstruct temperatures in different water depths.

With the possible exception of the surface-dwelling species *Globigerinoides ruber*, our results generally confirm that species-specific effects on clumped isotopes in planktonic foraminifera are either negligible or absent. The established dataset is in excellent agreement with two recent foraminifera-based calibrations (Peral et al., 2018; Piasecki et al., 2019), one of which derived with a completely different analytical setup, and the other solely containing benthic foraminifera. Combining the available datasets, we demonstrate the conformity of data from various laboratories and measurement approaches. Together with the observation that our combined foraminifera-based calibration line concurs with an inorganic calibration resting on travertines (Kele et al., 2015), our study provides a robust tool to calculate water temperatures from foraminifera and showcases the potential of the Δ_{47} thermometer for paleoceanographic research.

Paper II: *Coupled Mg/Ca and clumped isotope measurements confirm stable sea surface temperatures in the equatorial western Pacific over the last 6 million years*

Paper II uses paired measurements of clumped isotopes and Mg/Ca in selected Plio-Pleistocene time intervals from IODP Site U1488 located in the central Indo-Pacific Warm Pool to reconstruct the long-term evolution of surface and subsurface temperatures. The Indo-Pacific Warm Pool acts as an important player in the climate system by redistributing heat and moisture on a regional as well as global scale. However, there is an ongoing discussion about Pliocene warm pool temperatures caused by limitations inherent to several paleothermometers traditionally used for climate reconstructions. Studies based on biomarkers indicate a gradual cooling by ~ 2 °C from the Pliocene to today (O'Brien et al., 2014; Zhang et al., 2014), while paleothermometers using planktonic foraminifera, such as the Mg/Ca proxy, find no evidence for long-term temperature trends on these timescales (Wara et al., 2005). It has been suggested that Mg/Ca-derived temperatures could be biased by changes of the Mg/Ca ratio of seawater (e.g. Evans et al., 2016).

Here, we use our coupled Mg/Ca and clumped isotope data to address the enigma of conflicting proxy evidence and test the influence of proposed seawater changes on Mg/Ca-based temperature reconstructions from the Pliocene. Our data confirms the absence of a long-term cooling of the Indo-Pacific Warm Pool since 6 Ma and advocates for no or relatively minor corrections for past seawater changes that could not have masked the trend visible in biomarker data. We propose that the observed disagreement between the two proxies could be explained by different water depths being recorded in biomarkers and foraminifera (also suggested by Ford et al., 2015). By verifying previously published Plio-Pleistocene Mg/Ca records from the equatorial Pacific, our data supports the hypothesis of a weaker zonal temperature gradient in the Pacific Ocean and thus a “permanent El Niño-like” conditions (Wara et al., 2005) during the Early Pliocene.

Paper III: *A multi-proxy study of changes in the Indonesian Throughflow since the Pliocene*

In Paper III, we present mixed layer temperature reconstructions based on paired Mg/Ca and clumped isotope analysis on planktonic foraminifera from a region just downstream of the Indonesian Throughflow, off North-West Australia. We apply a similar time slice approach as in Paper II to monitor long-term changes in this crucial pathway between the Pacific and Indian Oceans since the Pliocene. Warm western equatorial Pacific water flows through the Indonesian Archipelago to the Indian Ocean where it feeds several ocean currents such as the southward-flowing Leeuwin Current along the Australian margin (Feng et al., 2003). Changes in the Indonesian Throughflow, for example due to regional tectonic changes during the Pliocene, are thus believed to not only affect the hydrography in the Indian Ocean, but also influence the global climate (Cane & Molnar, 2001; Karas et al., 2009; Karas et al., 2011b, 2011a; Karas et al., 2017). Eustatic sea-level variability during the Plio-Pleistocene has been identified as an additional influencing factor potentially causing the restriction of the Indonesian Throughflow by exposing shelf areas around northern Australia and the Indonesian Archipelago during glacial sea-level lowstands (Di Nezio et al., 2016; Auer et al., 2019).

We combine two neighboring sites (IODP Sites U1482 and U1483) to obtain temperature data covering the last 6 Myrs. The paired temperature analysis confirms findings from the western equatorial Pacific (IODP Site U1488, Paper II) that argue for the use of a low-sensitivity Mg/Ca-temperature calibration and at most a minor correction for past Mg/Ca changes in seawater. Our Pliocene record indicates relatively stable surface temperatures. This result is at odds with evidence for a pronounced weakening of the southward-flowing Leeuwin Current during the Pliocene (De Vleeschouwer et al., 2019). Hence, the stable surface temperature in the Indonesian Throughflow during the Pliocene suggests that the Leeuwin Current was influenced by more localized changes such as an increased interaction with the cooler West Australian Current. The Pleistocene interval of our temperature record exhibits a cooling of surface water by ~ 3 °C between 1.4 Ma and today. This change is not observed in the central

Warm Pool (Paper II), and therefore indicates a lateral contraction of the warm pool. The trend is dominated by more pronounced cooling during glacial periods, which we attribute to restrictions of the Indonesian Throughflow caused by glacial sea-level lowstands.

5 Synthesis and outlook

The improvement of carbonate clumped isotope thermometry in foraminifera and the establishment of this method as a tool for Plio-Pleistocene paleoceanographic research are the central aspects of this thesis. The presented research significantly advances the application of clumped isotope thermometry to this important group of marine calcifying organisms and demonstrates the enormous potential of this method, especially in settings where more classical temperature proxies are hampered by uncertainty about additional, non-thermal influences. This thesis developed an improved temperature calibration for clumped isotopes in foraminifera. This calibration was used for Plio-Pleistocene temperature reconstructions, in conjunction with other proxy methods, to address long-standing scientific controversies in paleoceanography on the development of tropical climate on million-year time scales.

Paper I presents an extensive global multi-species calibration dataset that we use to further constrain the relationship between clumped isotopes and temperature in planktonic foraminifera. We show that clumped isotopes in foraminifera generally follow a very similar relationship to temperature as described for inorganic carbonates (Kele et al., 2015). Species-specific effects are either absent or small compared to the overall uncertainty of clumped isotope thermometry in foraminifera.

Furthermore, using our new data together with a methodologically homogenized dataset of recently published clumped isotope data measured on foraminifera (Breitenbach et al., 2018; Peral et al., 2018; Piasecki et al., 2019), we demonstrate the reproducibility of clumped isotope analyses that are referenced to carbonate standards, irrespective of laboratory-specific measurement approaches. This finding allows us to

combine our new data and the available foraminifera-based data to establish a comprehensive clumped isotope calibration for foraminifera. Our calibration can be utilized for temperature reconstructions throughout the water column using different species of planktonic and benthic foraminifera and thus represents an important step towards the routine use of clumped isotope thermometry in foraminifera.

Although our dataset indicates that foraminifera generally follow a single Δ_{47} to temperature relationship, some samples, particularly of the shallow-dwelling species *G. ruber*, revealed deviations from the general trend. To advance the use of clumped isotopes for foraminifera-based paleoceanographic research even further, more work on individual species of foraminifera should be conducted. In particular, shallow-dwelling species such as *G. ruber* are subject to an array of environmental factors, including temperature and salinity changes, fluctuating nutrient availability and light conditions. A potential bias on Δ_{47} due to short-lived changes in one or several of these factors cannot be resolved in a core-top dataset. Moreover, calcification temperatures of foraminifera from surface sediment samples need to be estimated, a process which is plagued by ecologically-controlled uncertainties regarding calcification depth and season (e.g. Farmer et al., 2007). Therefore, culturing studies could be used to test various influencing factors on different species of foraminifera. *G. ruber* would be an ideal first subject for a more detailed examination of individual species.

The established calibration (Paper I) was applied to Plio-Pleistocene (6 Myrs) clumped isotope records from Site U1488 in the central IPWP (Paper II) and Sites U1482 and U1483 from the ITF (Paper III) to address the conundrum of deviating SSTs reconstructed for the IPWP with different proxies. Using our multi-species calibration, we calculated water temperatures in the mixed layer (all three sites) and the thermocline (Site U1488, Paper II) from two different species of foraminifera (*T. trilobus*, *G. tumida*). These records were paired with Mg/Ca data using the same samples.

The results not only indicate that temperatures in the central IPWP (Site U1488) lack any long-term temperature trends during the Plio-Pleistocene but also suggest that Mg/Ca data from the Pliocene is not or only slightly biased by past Mg/Ca changes of seawater. Temperature reconstructions from the combined ITF record (Site U1482 and

U1483) provide an independent validation of this conclusion drawn from Paper II. Moreover, the excellent preservation of foraminifera at the two clay-rich IODP Sites U1482 and U1483 argues against diagenetic effects on the Δ_{47} signal causing a similar bias on Δ_{47} than proposed seawater Mg/Ca changes would have on Mg/Ca. This interpretation is essential as it provides important constraints on the long-term evolution of the warm pool and the credibility of Mg/Ca-based temperature reconstructions (e.g. O'Brien et al., 2014; Ravelo et al., 2014; Zhang et al., 2014). By independently confirming the lack of a cooling trend, our data point towards an alternative reason for the observed proxy discrepancies between foraminifera-based methods and TEX₈₆ data that indicate a long-term cooling. We suggest that mixed layer-dwelling foraminifera and biomarkers record different water depths.

In contrast to the observed lack of mixed layer cooling, our Mg/Ca record of thermocline-dwelling foraminifera at Site U1488 shows a distinct cooling trend. This finding is in accordance with the hypothesis that TEX₈₆-based temperature reconstructions are influenced by a subsurface production of the GDGT signal (Kim et al., 2012; Tierney & Tingley, 2015; Ho & Laepple, 2016; Richey & Tierney, 2016; Zhang & Liu, 2018).

The described disagreement between biomarker data and foraminifera-based surface temperature reconstructions in the IPWP reaches beyond the Pliocene. The long-term cooling trend in TEX₈₆ data has been described back to 12 Ma (Zhang et al., 2014). Hence, extending paired Mg/Ca and Δ_{47} measurements on foraminifera further back in time would allow assessing the magnitude of Mg/Ca changes in the ocean on even longer timescales. A distinct advantage of these longer records would be the potentially larger temperature changes that can be resolved more easily with clumped isotope thermometry. In a collaboration with the University of California, Santa Cruz we are indeed already working on extending our paired Mg/Ca and Δ_{47} measurements from Site U1488 back to 9.5 Ma. Beyond 9.5 Ma the influence of diagenetic alteration on the sample material increases significantly, complicating foraminifera-based temperature reconstructions (Rosenthal, 2018).

While Mg/Ca-based studies found surface temperatures in the central WPWP to be relatively stable on Plio-Pleistocene time scales (Wara et al., 2005), the ITF has been described to behave more dynamically (Karas et al., 2011b). Besides supplying additional evidence regarding the validity of Plio-Pleistocene Mg/Ca records, our ITF records (Paper III) provide new insights into local surface water changes in this crucial region.

Regional tectonic changes during the Pliocene (Cane & Molnar, 2001; Karas et al., 2009; Karas et al., 2011b, 2011a; Karas et al., 2017) and eustatic sea-level variations particularly during the Pleistocene glaciations (Di Nezio et al., 2016) have been suggested to influence water mass transport through the ITF region by exposing shelf areas around northern Australia and Indonesia. These changes in the transport of warm Pacific water to the Indian Ocean, in turn, have been proposed as drivers for global climate change e.g. by promoting the Pleistocene global cooling (Cane & Molnar, 2001; De Vleeschouwer et al., 2018). Sites U1482 and U1483 are situated closer to the main path of the ITF than previously analyzed records from the Pliocene (e.g. De Vleeschouwer et al., 2018) making them an ideal target for reconstructions of surface temperature changes at the outflow of the ITF.

The data presented in paper III documents different patterns during the Pliocene and Pleistocene. Records from the eastern Indian Ocean and the Leeuwin Current, which is fed by water masses from the ITF (Feng et al., 2003), reveal a Pliocene cooling trend that was previously attributed to ITF restrictions (Karas et al., 2011b). Our data does not support a cooling of ITF surface water masses during the Pliocene. It thus indicates a more localized mechanism such as stronger vertical mixing of cooler southern source waters to be responsible for the observed temperature changes in the eastern Indian Ocean. In contrast, a clear cooling trend by ~ 3 °C from the mid-Pleistocene onwards (Paper III) documents substantial changes in the ITF during this time while the ITF source area in the central WPWP does not reveal the same cooling (Paper II). Based on the observation that this cooling in the ITF is particularly pronounced during glacial periods, glacial sea-level lowstands restricting the inflow of warm waters from the equatorial Pacific are the most likely explanation.

Our paired Δ_{47} and Mg/Ca temperature record generated for several high-resolution time intervals has distinct advantages over a single low-resolution record. By calculating mean interval temperatures from clumped isotopes and Mg/Ca we average over full glacial-interglacial cycles and thus avoid introducing aliasing effects to the data. Our approach also reduces the amount of sample material needed by distributing clumped isotope measurements over a longer time interval. At the same time, Mg/Ca and $\delta^{18}\text{O}$ data can be interpreted for individual samples providing information about short-term changes within each time interval. However, due to the dynamic nature of the ITF region (e.g. Auer et al., 2019) and its importance for heat exchange between the Pacific and Indian Ocean with global implications (Karas et al., 2017), our time slice approach bears the risk of missing crucial changes in between individual time intervals. Hence, Sites U1482 and U1483 are promising targets to generate an additional continuous record of surface temperature changes in this region. Moreover, the investigation of subsurface-dwelling species of planktonic foraminifera (as performed in Paper II) can deliver insights about the vertical temperature structure of the ITF and thermocline temperature changes. This way the full potential of the combined foraminifera-based approach to contribute to a more holistic understanding of Plio-Pleistocene climate dynamics in this region could be realized.

The Δ_{47} measurements presented in Papers II and III provide the first temperature constraints from foraminifera independent of changes in seawater composition and are therefore a significant advance of our knowledge regarding the evolution of the IPWP on million-year time scales. Combining clumped isotopes and Mg/Ca on the same samples increases the confidence in foraminifera-based temperature reconstructions. Our approach unites the strengths of the high-resolution Mg/Ca method with the independence from ocean chemistry that is characteristic of the clumped isotope thermometer. Demonstrating the potential of this multi-proxy approach on million-year timescales, our results advocate for putting clumped isotopes into the standard toolbox for paleoceanographers.

6 References

- Auer, G., De Vleeschouwer, D., Smith, R. A., Bogus, K., Groeneveld, J., Grunert, P., . . . Henderiks, J. (2019). Timing and Pacing of Indonesian Throughflow Restriction and Its Connection to Late Pliocene Climate Shifts. *Paleoceanography and Paleoclimatology*. doi:10.1029/2018pa003512
- Bajnai, D., Fiebig, J., Tomasovych, A., Milner Garcia, S., Rollion-Bard, C., Raddatz, J., . . . Brand, U. (2018). Assessing kinetic fractionation in brachiopod calcite using clumped isotopes. *Sci Rep*, 8(1), 533. doi:10.1038/s41598-017-17353-7
- Bartoli, G., Sarnthein, M., Weinelt, M., Erlenkeuser, H., Garbe-Schönberg, D., & Lea, D. W. (2005). Final closure of Panama and the onset of northern hemisphere glaciation. *Earth and Planetary Science Letters*, 237(1-2), 33-44. doi:10.1016/j.epsl.2005.06.020
- Bemis, B. E., Spero, H. J., Bijma, J., & Lea, D. W. (1998). Reevaluation of the oxygen isotopic composition of planktonic foraminifera: Experimental results and revised paleotemperature equations. *Paleoceanography*, 13(2), 150-160. doi:10.1029/98PA00070
- Bernasconi, S. M., Hu, B., Wacker, U., Fiebig, J., Breitenbach, S. F., & Rutz, T. (2013). Background effects on Faraday collectors in gas-source mass spectrometry and implications for clumped isotope measurements. *Rapid Commun Mass Spectrom*, 27(5), 603-612. doi:10.1002/rcm.6490
- Bernasconi, S. M., Müller, I. A., Bergmann, K. D., Breitenbach, S. F. M., Fernandez, A., Hodell, D. A., . . . Ziegler, M. (2018). Reducing Uncertainties in Carbonate Clumped Isotope Analysis Through Consistent Carbonate-Based Standardization. *Geochemistry, Geophysics, Geosystems*. doi:10.1029/2017gc007385
- Bigeleisen, J., & Mayer, M. G. (1947). Calculation of Equilibrium Constants for Isotopic Exchange Reactions. *The Journal of Chemical Physics*, 15(5), 261. doi:10.1063/1.1746492

- Bonifacie, M., Calmels, D., Eiler, J. M., Horita, J., Chaduteau, C., Vasconcelos, C., . . . Bourrand, J.-J. (2017). Calibration of the dolomite clumped isotope thermometer from 25 to 350°C, and implications for a universal calibration for all (Ca, Mg, Fe)CO₃ carbonates. *Geochimica et Cosmochimica Acta*, *200*, 255-279. doi:10.1016/j.gca.2016.11.028
- Brand, W. A., Assonov, S. S., & Coplen, T. B. (2010). Correction for the 17O interference in δ (13C) measurements when analyzing CO₂ with stable isotope mass spectrometry (IUPAC Technical Report). *Pure and Applied Chemistry*, *82*(8), 1719-1733. doi:10.1351/PAC-REP-09-01-0510.1351/PAC-REP-09-01-05
- Brassell, S., Eglinton, G., Marlowe, I., Pflaumann, U., & Sarnthein, M. (1986). Molecular stratigraphy: a new tool for climatic assessment. *Nature*, *320*, 129-133. doi:10.1038/320129a0
- Breitenbach, S. F. M., Mloneck-Vautravers, M. J., Grauel, A.-L., Lo, L., Bernasconi, S. M., Müller, I. A., . . . Hodell, D. A. (2018). Coupled Mg/Ca and clumped isotope analyses of foraminifera provide consistent water temperatures. *Geochimica et Cosmochimica Acta*. doi:https://doi.org/10.1016/j.gca.2018.03.010
- Brierley, C. M., Fedorov, A. V., Liu, Z., Herbert, T. D., Lawrence, K. T., & LaRiviere, J. P. (2009). Greatly Expanded Tropical Warm Pool and Weakened Hadley Circulation in the Early Pliocene. *Science*, *323*(5922), 1714-1718. doi:10.1126/science.1167625
- Came, R. E., Eiler, J. M., Veizer, J., Azmy, K., Brand, U., & Weidman, C. R. (2007). Coupling of surface temperatures and atmospheric CO₂ concentrations during the Palaeozoic era. *Nature*, *449*(7159), 198-201. doi:10.1038/nature06085
- Cane, M. A., & Molnar, P. (2001). Closing of the Indonesian seaway as a precursor to east African aridification around 3-4 million years ago. *Nature*, *411*(6834), 157-162. doi:10.1038/35075500
- Christensen, B. A., Renema, W., Henderiks, J., De Vleeschouwer, D., Groeneveld, J., Castañeda, I. S., . . . Fulthorpe, C. S. (2017). Indonesian Throughflow drove Australian climate from humid Pliocene to arid Pleistocene. *Geophysical Research Letters*, *44*(13), 6914-6925. doi:10.1002/2017gl072977

- Conte, M. H., Sicre, M.-A., Rühlemann, C., Weber, J. C., Schulte, S., Schulz-Bull, D., & Blanz, T. (2006). Global temperature calibration of the alkenone unsaturation index (UK'37) in surface waters and comparison with surface sediments. *Geochemistry, Geophysics, Geosystems*, 7(2), n/a-n/a. doi:10.1029/2005gc001054
- Daëron, M., Blamart, D., Peral, M., & Affek, H. (2016). Absolute isotopic abundance ratios and the accuracy of $\Delta 47$ measurements. *Chemical Geology*, 442, 83-96. doi:10.1016/j.chemgeo.2016.08.014
- Daëron, M., Drysdale, R. N., Peral, M., Huyghe, D., Blamart, D., Coplen, T. B., . . . Zanchetta, G. (2019). Most Earth-surface calcites precipitate out of isotopic equilibrium. *Nat Commun*, 10(1), 429. doi:10.1038/s41467-019-08336-5
- Davies, A. J., & John, C. M. (2019). The clumped ($^{13}\text{C}^{18}\text{O}$) isotope composition of echinoid calcite: Further evidence for “vital effects” in the clumped isotope proxy. *Geochimica et Cosmochimica Acta*, 245, 172-189. doi:10.1016/j.gca.2018.07.038
- De Deckker, P. (2016). The Indo-Pacific Warm Pool: critical to world oceanography and world climate. *Geoscience Letters*, 3(1), 20. doi:10.1186/s40562-016-0054-3
- De Schepper, S., Gibbard, P. L., Salzmann, U., & Ehlers, J. (2014). A global synthesis of the marine and terrestrial evidence for glaciation during the Pliocene Epoch. *Earth-Science Reviews*, 135, 83-102. doi:https://doi.org/10.1016/j.earscirev.2014.04.003
- De Vleeschouwer, D., Auer, G., Smith, R., Bogus, K., Christensen, B., Groeneveld, J., . . . Pälike, H. (2018). The amplifying effect of Indonesian Throughflow heat transport on Late Pliocene Southern Hemisphere climate cooling. *Earth and Planetary Science Letters*, 500, 15-27. doi:10.1016/j.epsl.2018.07.035
- De Vleeschouwer, D., Petrick, B. F., & Martínez-García, A. (2019). Stepwise Weakening of the Pliocene Leeuwin Current. *Geophysical Research Letters*, 46(14), 8310-8319. doi:10.1029/2019GL083670

- Dekens, P. S., Ravelo, A. C., McCarthy, M. D., & Edwards, C. A. (2008). A 5 million year comparison of Mg/Ca and alkenone paleothermometers. *Geochemistry, Geophysics, Geosystems*, 9(10). doi:10.1029/2007gc001931
- Dennis, K. J., Affek, H. P., Passey, B. H., Schrag, D. P., & Eiler, J. M. (2011). Defining an absolute reference frame for 'clumped' isotope studies of CO₂. *Geochimica et Cosmochimica Acta*, 75(22), 7117-7131. doi:10.1016/j.gca.2011.09.025
- Di Nezio, P. N., Timmermann, A., Tierney, J. E., Jin, F.-F., Otto-Bliesner, B., Rosenbloom, N., . . . Montenegro, A. (2016). The climate response of the Indo-Pacific warm pool to glacial sea level. *Paleoceanography*, 31(6), 866-894. doi:10.1002/2015pa002890
- Dolan, A. M., Haywood, A. M., Hill, D. J., Dowsett, H. J., Hunter, S. J., Lunt, D. J., & Pickering, S. J. (2011). Sensitivity of Pliocene ice sheets to orbital forcing. *Palaeogeography, Palaeoclimatology, Palaeoecology*, 309(1-2), 98-110. doi:10.1016/j.palaeo.2011.03.030
- Dowsett, H., Dolan, A., Rowley, D., Pound, M., Salzmann, U., Robinson, M., . . . Haywood, A. (2016). The PRISM4 (mid-Piacenzian) palaeoenvironmental reconstruction. *Climate of the Past Discussions*, 12, 1519-1538. doi:10.5194/cp-2016-33
- Dowsett, H. J. (2007a). Faunal re-evaluation of Mid-Pliocene conditions in the western equatorial Pacific. *Micropaleontology*, 53(6), 447-456. doi:10.2113/gsmicropal.53.6.447
- Dowsett, H. J. (2007b). The PRISM palaeoclimate reconstruction and Pliocene sea-surface temperature. In N. Williams, Haywood, A.M., Gregory, F.J., Schmidt, D.N. (Ed.), *Deep-time perspectives on climate change: marrying the signal from computer models and biological proxies* (pp. 459-480). London: The Geological Society for The Micropalaeontological Society.
- Dowsett, H. J., Chandler, M. A., & Robinson, M. M. (2009). Surface temperatures of the Mid-Pliocene North Atlantic Ocean: implications for future climate. *Philos Trans A Math Phys Eng Sci*, 367(1886), 69-84. doi:10.1098/rsta.2008.0213

- Dowsett, H. J., Foley, K. M., Stoll, D. K., Chandler, M. A., Sohl, L. E., Bentsen, M., . . . Zhang, Z. (2013). Sea surface temperature of the mid-Piacenzian ocean: a data-model comparison. *Sci Rep*, 3, 2013. doi:10.1038/srep02013
- Dowsett, H. J., Haywood, A. M., Valdes, P. J., Robinson, M. M., Lunt, D. J., Hill, D. J., . . . Foley, K. M. (2011). Sea surface temperatures of the mid-Piacenzian Warm Period: A comparison of PRISM3 and HadCM3. *Palaeogeography, Palaeoclimatology, Palaeoecology*, 309(1-2), 83-91. doi:10.1016/j.palaeo.2011.03.016
- Drury, A. J., Weserhold, T., Ravelo, A.C., Kulhanek, D.K., Mountain, G., Holbourn, A., Rosenthal, Y., Wilkens, R., Röhl, U. (in review). Composite depth scale and splice revision for IODP Site U1488 (Expedition 363 Western Pacific Warm Pool) using XRF core scanning data and composite core images. *Proceedings of the Integrated Ocean Drilling Program*, 363.
- Eagle, R. A., Schauble, E. A., Tripathi, A. K., Tutken, T., Hulbert, R. C., & Eiler, J. M. (2010). Body temperatures of modern and extinct vertebrates from (13)C-(18)O bond abundances in bioapatite. *Proc Natl Acad Sci U S A*, 107(23), 10377-10382. doi:10.1073/pnas.0911115107
- Eiler, J. M. (2007). “Clumped-isotope” geochemistry—The study of naturally-occurring, multiply-substituted isotopologues. *Earth and Planetary Science Letters*, 262(3-4), 309-327. doi:10.1016/j.epsl.2007.08.020
- Eiler, J. M. (2011). Paleoclimate reconstruction using carbonate clumped isotope thermometry. *Quaternary Science Reviews*, 30(25-26), 3575-3588. doi:10.1016/j.quascirev.2011.09.001
- Eiler, J. M., & Schauble, E. (2004). 18O13C16O in Earth’s atmosphere. *Geochimica et Cosmochimica Acta*, 68(23), 4767-4777. doi:10.1016/j.gca.2004.05.035
- Elderfield, H., Ferretti, P., Greaves, M., Crowhurst, S., McCave, I. N., Hodell, D., & Piotrowski, A. M. (2012). Evolution of Ocean Temperature and Ice Volume Through the Mid-Pleistocene Climate Transition. *Science*, 337(6095), 704-709. doi:10.1126/science.1221294

- Elling, F. J., Könneke, M., Lipp, J. S., Becker, K. W., Gagen, E. J., & Hinrichs, K.-U. (2014). Effects of growth phase on the membrane lipid composition of the thaumarchaeon *Nitrosopumilus maritimus* and their implications for archaeal lipid distributions in the marine environment. *Geochimica et Cosmochimica Acta*, *141*, 579-597. doi:<https://doi.org/10.1016/j.gca.2014.07.005>
- Emiliani, C. (1954). Temperatures of Pacific bottom waters and polar superficial waters during the Tertiary. *Science*, *119*(3103), 853-855. Retrieved from www.jstor.org/stable/1681508. Accessed 26 Mar. 2020.
- Evans, D., Brierley, C., Raymo, M. E., Erez, J., & Müller, W. (2016). Planktic foraminifera shell chemistry response to seawater chemistry: Pliocene–Pleistocene seawater Mg/Ca, temperature and sea level change. *Earth and Planetary Science Letters*, *438*, 139-148. doi:10.1016/j.epsl.2016.01.013
- Ezard, T. H. G., Edgar, K. M., & Hull, P. M. (2015). Environmental and biological controls on size-specific $\delta^{13}\text{C}$ and $\delta^{18}\text{O}$ in recent planktonic foraminifera. *Paleoceanography*, *30*(3), 151-173. doi:10.1002/2014pa002735
- Farmer, E. C., Kaplan, A., de Menocal, P. B., & Lynch-Stieglitz, J. (2007). Corroborating ecological depth preferences of planktonic foraminifera in the tropical Atlantic with the stable oxygen isotope ratios of core top specimens. *Paleoceanography*, *22*(3), n/a-n/a. doi:10.1029/2006PA001361
- Fedorov, A. V., Brierley, C. M., & Emanuel, K. (2010). Tropical cyclones and permanent El Niño in the early Pliocene epoch. *Nature*, *463*(7284), 1066-1070. doi:10.1038/nature08831
- Fedorov, A. V., Brierley, C. M., Lawrence, K. T., Liu, Z., Dekens, P. S., & Ravelo, A. C. (2013). Patterns and mechanisms of early Pliocene warmth. *Nature*, *496*(7443), 43-49. doi:10.1038/nature12003
- Fedorov, A. V., Dekens, P. S., McCarthy, M., Ravelo, A. C., deMenocal, P. B., Barreiro, M., . . . Philander, S. G. (2006). The Pliocene Paradox (Mechanisms for a Permanent El Niño). *Science*, *312*(5779), 1485-1489. doi:10.1126/science.1122666

- Feng, M., Meyers, G., Pearce, A., & Wijffels, S. (2003). Annual and interannual variations of the Leeuwin Current at 32 S. *Journal of Geophysical Research: Oceans*, 108(C11). doi:10.1029/2002JC001763
- Fernandez, A., Müller, I. A., Rodríguez-Sanz, L., van Dijk, J., Looser, N., & Bernasconi, S. M. (2017). A Reassessment of the Precision of Carbonate Clumped Isotope Measurements: Implications for Calibrations and Paleoclimate Reconstructions. *Geochemistry, Geophysics, Geosystems*, 18(12), 4375-4386. doi:10.1002/2017gc007106
- Fiebig, J., Hofmann, S., Löffler, N., Lüdecke, T., Methner, K., & Wacker, U. (2016). Slight pressure imbalances can affect accuracy and precision of dual inlet-based clumped isotope analysis. *Isotopes in environmental and health studies*, 52(1-2), 12-28. doi:10.1080/10256016.2015.1010531
- Fine, R. A., Lukas, R., Bingham, F. M., Warner, M. J., & Gammon, R. H. (1994). The western equatorial Pacific: A water mass crossroads. *Journal of Geophysical Research: Oceans*, 99(C12), 25063-25080. doi:10.1029/94jc02277
- Ford, H. L., Ravelo, A. C., Dekens, P. S., LaRiviere, J. P., & Wara, M. W. (2015). The evolution of the equatorial thermocline and the early Pliocene El Padre mean state. *Geophysical Research Letters*, 42(12), 4878-4887. doi:10.1002/2015gl064215
- Ghosh, P., Adkins, J., Affek, H., Balta, B., Guo, W., Schauble, E. A., . . . Eiler, J. M. (2006a). ^{13}C – ^{18}O bonds in carbonate minerals: A new kind of paleothermometer. *Geochimica et Cosmochimica Acta*, 70(6), 1439-1456. doi:10.1016/j.gca.2005.11.014
- Ghosh, P., Eiler, J., Campana, S. E., & Feeney, R. F. (2007). Calibration of the carbonate ‘clumped isotope’ paleothermometer for otoliths. *Geochimica et Cosmochimica Acta*, 71(11), 2736-2744. doi:10.1016/j.gca.2007.03.015
- Ghosh, P., Garzzone, C. N., & Eiler, J. M. (2006b). Rapid uplift of the Altiplano revealed through ^{13}C - ^{18}O bonds in paleosol carbonates. *Science*, 311(5760), 511-515.

- Godfrey, J. (1996). The effect of the Indonesian throughflow on ocean circulation and heat exchange with the atmosphere: A review. *Journal of Geophysical Research: Oceans*, 101(C5), 12217-12237. doi:10.1029/95JC03860
- Godfrey, J., Wilkin, J., & Hirst, A. (1993). Why does the Indonesian throughflow appear to originate from the North Pacific? *Journal of Physical Oceanography*, 23(6), 1087-1098. doi:10.1175/1520-0485(1993)023<1087:WDTITA>2.0.CO;2
- Gordon, A. L. (1986). Interocean exchange of thermocline water. *Journal of Geophysical Research: Oceans*, 91(C4), 5037-5046. doi:10.1029/JC091iC04p05037
- Gordon, A. L. (2005). Oceanography of the Indonesian seas and their throughflow. *Oceanography*, 18(4), 14-27.
- Gordon, A. L., & Fine, R. A. (1996). Pathways of water between the Pacific and Indian oceans in the Indonesian seas. *Nature*, 379(6561), 146-149. doi:10.1038/379146a0
- Gordon, A. L., Ma, S., Olson, D. B., Hacker, P., Ffield, A., Talley, L. D., . . . Baringer, M. (1997). Advection and diffusion of Indonesian throughflow water within the Indian Ocean South Equatorial Current. *Geophysical Research Letters*, 24(21), 2573-2576. doi:10.1029/97GL01061
- Gordon, A. L., Susanto, R. D., & Vranes, K. (2003). Cool Indonesian throughflow as a consequence of restricted surface layer flow. *Nature*, 425(6960), 824-828. doi:10.1038/nature02038
- Grauel, A.-L., Schmid, T. W., Hu, B., Bergami, C., Capotondi, L., Zhou, L., & Bernasconi, S. M. (2013). Calibration and application of the ‘clumped isotope’ thermometer to foraminifera for high-resolution climate reconstructions. *Geochimica et Cosmochimica Acta*, 108, 125-140. doi:10.1016/j.gca.2012.12.049
- Haywood, A. M., Dolan, A. M., Pickering, S. J., Dowsett, H. J., McClymont, E. L., Prescott, C. L., . . . Valdes, P. J. (2013). On the identification of a Pliocene time slice for data-model comparison. *Philos Trans A Math Phys Eng Sci*, 371(2001), 20120515. doi:10.1098/rsta.2012.0515

- Haywood, A. M., Dowsett, H. J., & Dolan, A. M. (2016). Integrating geological archives and climate models for the mid-Pliocene warm period. *Nat Commun*, 7, 10646. doi:10.1038/ncomms10646
- Haywood, A. M., Dowsett, H. J., Valdes, P. J., Lunt, D. J., Francis, J. E., & Sellwood, B. W. (2009). Introduction. Pliocene climate, processes and problems. *Philos Trans A Math Phys Eng Sci*, 367(1886), 3-17. doi:10.1098/rsta.2008.0205
- Haywood, A. M., Ridgwell, A., Lunt, D. J., Hill, D. J., Pound, M. J., Dowsett, H. J., . . . Williams, M. (2011). Are there pre-Quaternary geological analogues for a future greenhouse warming? *Philosophical Transactions of the Royal Society A: Mathematical, Physical and Engineering Sciences*, 369(1938), 933-956. doi:10.1098/rsta.2010.0317
- Haywood, A. M., & Valdes, P. J. (2004). Modelling Pliocene warmth: contribution of atmosphere, oceans and cryosphere. *Earth and Planetary Science Letters*, 218(3-4), 363-377. doi:10.1016/s0012-821x(03)00685-x
- He, B., Olack, G. A., & Colman, A. S. (2012). Pressure baseline correction and high-precision CO₂ clumped-isotope (δ^{47}) measurements in bellows and micro-volume modes. *Rapid Commun Mass Spectrom*, 26(24), 2837-2853. doi:10.1002/rcm.6436
- Henkes, G. A., Passey, B. H., Wanamaker, A. D., Grossman, E. L., Ambrose, W. G., & Carroll, M. L. (2013). Carbonate clumped isotope compositions of modern marine mollusk and brachiopod shells. *Geochimica et Cosmochimica Acta*, 106, 307-325. doi:10.1016/j.gca.2012.12.020
- Hertzberg, J. E., Schmidt, M. W., Bianchi, T. S., Smith, R. W., Shields, M. R., & Marcantonio, F. (2016). Comparison of eastern tropical Pacific TEX₈₆ and Globigerinoides ruber Mg/Ca derived sea surface temperatures: Insights from the Holocene and Last Glacial Maximum. *Earth and Planetary Science Letters*, 434, 320-332. doi:https://doi.org/10.1016/j.epsl.2015.11.050
- Ho, S. L., & Laepple, T. (2016). Flat meridional temperature gradient in the early Eocene in the subsurface rather than surface ocean. *Nature Geoscience*, 9, 606. doi:10.1038/ngeo2763

- Hu, B., Radke, J., Schluter, H. J., Heine, F. T., Zhou, L., & Bernasconi, S. M. (2014). A modified procedure for gas-source isotope ratio mass spectrometry: the long-integration dual-inlet (LIDI) methodology and implications for clumped isotope measurements. *Rapid Commun Mass Spectrom*, 28(13), 1413-1425. doi:10.1002/rcm.6909
- Huntington, K. W., Eiler, J. M., Affek, H. P., Guo, W., Bonifacie, M., Yeung, L. Y., . . . Came, R. (2009). Methods and limitations of 'clumped' CO₂ isotope (Delta47) analysis by gas-source isotope ratio mass spectrometry. *J Mass Spectrom*, 44(9), 1318-1329. doi:10.1002/jms.1614
- Karas, C., Nürnberg, D., Bahr, A., Groeneveld, J., Herrle, J. O., Tiedemann, R., & deMenocal, P. B. (2017). Pliocene oceanic seaways and global climate. *Scientific Reports*, 7, 39842. doi:10.1038/srep39842
- Karas, C., Nürnberg, D., Gupta, A. K., Tiedemann, R., Mohan, K., & Bickert, T. (2009). Mid-Pliocene climate change amplified by a switch in Indonesian subsurface throughflow. *Nature Geoscience*, 2(6), 434-438. doi:10.1038/ngeo520
- Karas, C., Nürnberg, D., Tiedemann, R., & Garbe-Schönberg, D. (2011a). Pliocene climate change of the Southwest Pacific and the impact of ocean gateways. *Earth and Planetary Science Letters*, 301(1), 117-124. doi:https://doi.org/10.1016/j.epsl.2010.10.028
- Karas, C., Nürnberg, D., Tiedemann, R., & Garbe-Schönberg, D. (2011b). Pliocene Indonesian Throughflow and Leeuwin Current dynamics: Implications for Indian Ocean polar heat flux. *Paleoceanography*, 26(2), n/a-n/a. doi:10.1029/2010pa001949
- Kele, S., Breitenbach, S. F. M., Capezzuoli, E., Meckler, A. N., Ziegler, M., Millan, I. M., . . . Bernasconi, S. M. (2015). Temperature dependence of oxygen- and clumped isotope fractionation in carbonates: A study of travertines and tufas in the 6–95°C temperature range. *Geochimica et Cosmochimica Acta*, 168, 172-192. doi:10.1016/j.gca.2015.06.032

- Kelson, J. R., Huntington, K. W., Schauer, A. J., Saenger, C., & Lechler, A. R. (2017). Toward a universal carbonate clumped isotope calibration: Diverse synthesis and preparatory methods suggest a single temperature relationship. *Geochimica et Cosmochimica Acta*, 197, 104-131. doi:10.1016/j.gca.2016.10.010
- Kim, J.-H., Romero, O. E., Lohmann, G., Donner, B., Laepple, T., Haam, E., & Sinninghe Damsté, J. S. (2012). Pronounced subsurface cooling of North Atlantic waters off Northwest Africa during Dansgaard–Oeschger interstadials. *Earth and Planetary Science Letters*, 339-340, 95-102. doi:https://doi.org/10.1016/j.epsl.2012.05.018
- Kim, J.-H., Schouten, S., Rodrigo-Gámiz, M., Rampen, S., Marino, G., Huguet, C., . . . Sinninghe Damsté, J. S. (2015). Influence of deep-water derived isoprenoid tetraether lipids on the TEX86H paleothermometer in the Mediterranean Sea. *Geochimica et Cosmochimica Acta*, 150, 125-141. doi:https://doi.org/10.1016/j.gca.2014.11.017
- Lea, D. W., Mashiotta, T. A., & Spero, H. J. (1999). Controls on magnesium and strontium uptake in planktonic foraminifera determined by live culturing. *Geochimica et Cosmochimica Acta*, 63(16), 2369-2379. doi:http://dx.doi.org/10.1016/S0016-7037(99)00197-0
- Leutert, T. J., Sexton, P. F., Tripathi, A., Piasecki, A., Ho, S. L., & Meckler, A. N. (2019). Sensitivity of clumped isotope temperatures in fossil benthic and planktic foraminifera to diagenetic alteration. *Geochimica et Cosmochimica Acta*, 257, 354-372. doi:https://doi.org/10.1016/j.gca.2019.05.005
- Lisiecki, L. E., & Raymo, M. E. (2005). A Pliocene-Pleistocene stack of 57 globally distributed benthic $\delta^{18}\text{O}$ records. *Paleoceanography*, 20(1), n/a-n/a. doi:10.1029/2004pa001071
- Lisiecki, L. E., & Raymo, M. E. (2007). Plio–Pleistocene climate evolution: trends and transitions in glacial cycle dynamics. *Quaternary Science Reviews*, 26(1), 56-69. doi:https://doi.org/10.1016/j.quascirev.2006.09.005

- Locarnini, R., Mishonov, A., Antonov, J., Boyer, T., Garcia, H., Baranova, O., . . . Johnson, D. (2010). World Ocean Atlas 2009, Volume 1: Temperature. S. Levitus, Ed. NOAA Atlas NESDIS 68, US Government Printing Office, Washington, DC, 184 pp. In.
- Martínez-Botí, M. A., Foster, G. L., Chalk, T. B., Rohling, E. J., Sexton, P. F., Lunt, D. J., . . . Schmidt, D. N. (2015). Plio-Pleistocene climate sensitivity evaluated using high-resolution CO₂ records. *Nature*, *518*(7537), 49-54. doi:10.1038/nature14145
- Mathien-Blard, E., & Bassinot, F. (2009). Salinity bias on the foraminifera Mg/Ca thermometry: Correction procedure and implications for past ocean hydrographic reconstructions. *Geochemistry, Geophysics, Geosystems*, *10*(12). doi:doi:10.1029/2008GC002353
- McClymont, E. L., Ford, H. L., Ho, S. L., Tindall, J. C., Haywood, A. M., Alonso-Garcia, M., . . . White, S. (2020). Lessons from a high CO₂ world: an ocean view from ~3 million years ago. *Clim. Past Discuss.*, *2020*, 1-27. doi:10.5194/cp-2019-161
- Meckler, A. N., Ziegler, M., Millan, M. I., Breitenbach, S. F., & Bernasconi, S. M. (2014). Long-term performance of the Kiel carbonate device with a new correction scheme for clumped isotope measurements. *Rapid Commun Mass Spectrom*, *28*(15), 1705-1715. doi:10.1002/rcm.6949
- Molnar, P., & Cane, M. A. (2002). El Niño's tropical climate and teleconnections as a blueprint for pre-Ice Age climates. *Paleoceanography*, *17*(2), 11-11-11-11. doi:10.1029/2001pa000663
- Mudelsee, M., & Raymo, M. E. (2005). Slow dynamics of the Northern Hemisphere glaciation. *Paleoceanography*, *20*(4), n/a-n/a. doi:10.1029/2005pa001153
- Mudelsee, M., & Schulz, M. (1997). The Mid-Pleistocene climate transition: onset of 100 ka cycle lags ice volume build-up by 280 ka. *Earth and Planetary Science Letters*, *151*(1), 117. doi:10.1016/S0012-821X(97)00114-3
- Mulitza, S., Dürkoop, A., Hale, W., Wefer, G., & Stefan Niebler, H. (1997). Planktonic foraminifera as recorders of past surface-water stratification. *Geology*, *25*(4), 335. doi:10.1130/0091-7613(1997)025<0335:PFAROP>2.3.CO;2

- Müller, I. A., Fernandez, A., Radke, J., van Dijk, J., Bowen, D., Schwieters, J., & Bernasconi, S. M. (2017). Carbonate clumped isotope analyses with the long-integration dual-inlet (LIDI) workflow: scratching at the lower sample weight boundaries. *Rapid Communications in Mass Spectrometry*, *31*(12), 1057-1066. doi:10.1002/rcm.7878
- Neale, R., & Slingo, J. (2003). The Maritime Continent and Its Role in the Global Climate: A GCM Study. *Journal of Climate*, *16*(5), 834-848. doi:10.1175/1520-0442(2003)016<0834:Tmcair>2.0.Co;2
- Nürnberg, D., Bijma, J., & Hemleben, C. (1996). Assessing the reliability of magnesium in foraminiferal calcite as a proxy for water mass temperatures. *Geochimica et Cosmochimica Acta*, *60*(5), 803-814. doi:http://dx.doi.org/10.1016/0016-7037(95)00446-7
- O'Brien, C. L., Foster, G. L., Martínez-Botí, M. A., Abell, R., Rae, J. W. B., & Pancost, R. D. (2014). High sea surface temperatures in tropical warm pools during the Pliocene. *Nature Geoscience*, *7*(8), 606-611. doi:10.1038/ngeo2194
- Pagani, M., Liu, Z., LaRiviere, J., & Ravelo, A. C. (2010). High Earth-system climate sensitivity determined from Pliocene carbon dioxide concentrations. *Nature Geoscience*, *3*(1), 27-30. doi:10.1038/ngeo724
- Passey, B. H., & Henkes, G. A. (2012). Carbonate clumped isotope bond reordering and geospeedometry. *Earth and Planetary Science Letters*, *351-352*, 223-236. doi:https://doi.org/10.1016/j.epsl.2012.07.021
- Pearson, P. N. (2012). Oxygen isotopes in foraminifera: Overview and historical review. *Paleontological Society Papers*, *18*, 1-38. doi:10.1017/S1089332600002539
- Peral, M., Daëron, M., Blamart, D., Bassinot, F., Dewilde, F., Smialkowski, N., . . . Waelbroeck, C. (2018). Updated calibration of the clumped isotope thermometer in planktonic and benthic foraminifera. *Geochimica et Cosmochimica Acta*. doi:10.1016/j.gca.2018.07.016

- Petersen, S. V., Defliese, W. F., Saenger, C., Daëron, M., Huntington, K. W., John, C. M., . . . Winkelstern, I. Z. (2019). Effects of Improved $\delta^{17}O$ Correction on Inter-Laboratory Agreement in Clumped Isotope Calibrations, Estimates of Mineral-Specific Offsets, and Temperature Dependence of Acid Digestion Fractionation. *Geochemistry, Geophysics, Geosystems*. doi:10.1029/2018gc008127
- Philander, S. G. H. (1983). El Niño Southern Oscillation phenomena. *Nature*, 302(5906), 295-301. doi:10.1038/302295a0
- Piasecki, A., Bernasconi, S. M., Grauel, A.-L., Hannisdal, B., Ho, S. L., Leutert, T. J., . . . Meckler, N. (2019). Application of Clumped Isotope Thermometry to Benthic Foraminifera. *Geochemistry, Geophysics, Geosystems*, 0(ja). doi:10.1029/2018GC007961
- Pisias, N. G., & Moore, T. C. (1981). The evolution of Pleistocene climate: A time series approach. *Earth and Planetary Science Letters*, 52(2), 450-458. doi:https://doi.org/10.1016/0012-821X(81)90197-7
- Polik, C. A., Elling, F. J., & Pearson, A. (2018). Impacts of Paleoecology on the TEX86 Sea Surface Temperature Proxy in the Pliocene-Pleistocene Mediterranean Sea. *Paleoceanography and Paleoclimatology*, 33(12), 1472-1489. doi:doi:10.1029/2018PA003494
- Prahl, F. G., Muehlhausen, L. A., & Zahnle, D. L. (1988). Further evaluation of long-chain alkenones as indicators of paleoceanographic conditions. *Geochimica et Cosmochimica Acta*, 52(9), 2303-2310. doi:https://doi.org/10.1016/0016-7037(88)90132-9
- Prahl, F. G., & Wakeham, S. G. (1987). Calibration of unsaturation patterns in long-chain ketone compositions for palaeotemperature assessment. *Nature*, 330(6146), 367-369. Retrieved from http://dx.doi.org/10.1038/330367a0
- Ravelo, A. C., Dekens, P. S., & McCarthy, M. (2006). Evidence for El Niño-like conditions during the Pliocene. *GSA Today*, 16(3), 4. doi:10.1130/1052-5173(2006)016<4:efenlc>2.0.co;2
- Ravelo, A. C., Lawrence, K. T., Fedorov, A., & Ford, H. L. (2014). Comment on “A 12-million-year temperature history of the tropical Pacific Ocean”. *Science*, 346(6216), 1467-1467. doi:10.1126/science.1257618

- Raymo, M. E., Grant, B., Horowitz, M., & Rau, G. H. (1996). Mid-Pliocene warmth: stronger greenhouse and stronger conveyor. *Marine Micropaleontology*, 27(1–4), 313-326. doi:[http://dx.doi.org/10.1016/0377-8398\(95\)00048-8](http://dx.doi.org/10.1016/0377-8398(95)00048-8)
- Raymo, M. E., Lisiecki, L. E., & Nisancioglu, K. H. (2006). Plio-Pleistocene ice volume, Antarctic climate, and the global $\delta^{18}\text{O}$ record. *Science*, 313(5786), 492-495. doi:10.1126/science.1123296
- Raymo, M. E., Mitrovica, J. X., O’Leary, M. J., DeConto, R. M., & Hearty, P. J. (2011). Departures from eustasy in Pliocene sea-level records. *Nature Geoscience*, 4(5), 328-332. doi:10.1038/ngeo1118
- Regenberg, M., Nürnberg, D., Schönfeld, J., & Reichert, G.-J. (2007). Early diagenetic overprint in Caribbean sediment cores and its effect on the geochemical composition of planktonic foraminifera. *Biogeosciences*, 4(6), 957-973. doi:10.5194/bg-4-957-2007.
- Regenberg, M., Steph, S., Nürnberg, D., Tiedemann, R., & Garbe-Schönberg, D. (2009). Calibrating Mg/Ca ratios of multiple planktonic foraminiferal species with $\delta^{18}\text{O}$ -calcification temperatures: Paleothermometry for the upper water column. *Earth and Planetary Science Letters*, 278(3-4), 324-336. doi:10.1016/j.epsl.2008.12.019
- Rial, J. A., Pielke, R. A., Beniston, M., Claussen, M., Canadell, J., Cox, P., . . . Reynolds, J. F. (2004). Nonlinearities, feedbacks and critical thresholds within the Earth's climate system. *Climatic change*, 65(1-2), 11-38. doi:10.1023/B:CLIM.0000037493.89489.3f
- Richey, J. N., & Tierney, J. E. (2016). GDGT and alkenone flux in the northern Gulf of Mexico: Implications for the TEX86 and UK'37 paleothermometers. *Paleoceanography*, 31(12), 1547-1561. doi:10.1002/2016pa003032
- Rickaby, R. E. M., & Halloran, P. (2005). Cool La Niña During the Warmth of the Pliocene? *Science*, 307(5717), 1948-1952. doi:10.1126/science.1104666
- Rodríguez-Sanz, L., Bernasconi, S. M., Marino, G., Heslop, D., Müller, I. A., Fernandez, A., . . . Rohling, E. J. (2017). Penultimate deglacial warming across the Mediterranean Sea revealed by clumped isotopes in foraminifera. *Scientific Reports*, 7(1), 16572. doi:10.1038/s41598-017-16528-6

- Ropelewski, C. F., & Halpert, M. S. (1987). Global and Regional Scale Precipitation Patterns Associated with the El Niño/Southern Oscillation. *Monthly Weather Review*, 115(8), 1606-1626. doi:10.1175/1520-0493(1987)115<1606:Garspp>2.0.Co;2
- Rosenthal, Y., Holbourn, A.E., Kulhanek, D.K., and the Expedition 363 Scientists. (2018). Western Pacific Warm Pool. In *Proceedings of the International Ocean Discovery Program, 363*. College Station, TX (International Ocean Discovery Program).
- Ruggieri, E., Herbert, T., Lawrence, K. T., & Lawrence, C. E. (2009). Change point method for detecting regime shifts in paleoclimatic time series: Application to $\delta^{18}O$ time series of the Plio-Pleistocene. *Paleoceanography*, 24(1), n/a-n/a. doi:10.1029/2007pa001568
- Saenger, C., Affek, H. P., Felis, T., Thiagarajan, N., Lough, J. M., & Holcomb, M. (2012). Carbonate clumped isotope variability in shallow water corals: Temperature dependence and growth-related vital effects. *Geochimica et Cosmochimica Acta*, 99, 224-242. doi:10.1016/j.gca.2012.09.035
- Salzmann, U., Dolan, A. M., Haywood, A. M., Chan, W.-L., Voss, J., Hill, D. J., . . . Chandler, M. A. (2013). Challenges in quantifying Pliocene terrestrial warming revealed by data–model discord. *Nature Climate Change*, 3(11), 969-974. doi:10.1038/nclimate2008
- Sardeshmukh, P. D., & Hoskins, B. J. (1988). The Generation of Global Rotational Flow by Steady Idealized Tropical Divergence. *Journal of the Atmospheric Sciences*, 45(7), Sardeshmukh and Hoskins1228-1251. doi:10.1175/1520-0469(1988)045<1228:Tgogrf>2.0.Co;2
- Sarnthein, M., Bartoli, G., Prange, M., Schmittner, A., Schneider, B., Weinelt, M., . . . Garbe-Schönberg, D. (2009). Mid-Pliocene shifts in ocean overturning circulation and the onset of Quaternary-style climates. doi:10.5194/cp-5-269-2009

- Schauble, E. A., Ghosh, P., & Eiler, J. M. (2006). Preferential formation of ^{13}C – ^{18}O bonds in carbonate minerals, estimated using first-principles lattice dynamics. *Geochimica et Cosmochimica Acta*, 70(10), 2510-2529. doi:10.1016/j.gca.2006.02.011
- Schauer, A. J., Kelson, J., Saenger, C., & Huntington, K. W. (2016). Choice of (17) O correction affects clumped isotope ($\Delta 47$) values of CO_2 measured with mass spectrometry. *Rapid Commun Mass Spectrom*, 30(24), 2607-2616. doi:10.1002/rcm.7743
- Schiebel, R., Smart, S. M., Jentzen, A., Jonkers, L., Morard, R., Meilland, J., . . . Haug, G. H. (2018). Advances in planktonic foraminifer research: New perspectives for paleoceanography. *Revue de Micropaléontologie*, 61(3), 113-138. doi:https://doi.org/10.1016/j.revmic.2018.10.001
- Schlitzer, R. (2018). Ocean data view. <http://odv.awi.de>.
- Schmid, T. W., & Bernasconi, S. M. (2010). An automated method for 'clumped-isotope' measurements on small carbonate samples. *Rapid Commun Mass Spectrom*, 24(14), 1955-1963. doi:10.1002/rcm.4598
- Schmid, T. W. R., Jens; Bernasconi, Stefano M. . (2012). Clumped-Isotope Measurements on Small Carbonate Samples with a Kiel IV Carbonate Device and a MAT 253 Mass Spectrometer. *30233*.
- Schneider, B., Leduc, G., & Park, W. (2010). Disentangling seasonal signals in Holocene climate trends by satellite-model-proxy integration. *Paleoceanography*, 25(4). doi:10.1029/2009pa001893
- Schouten, S., Hopmans, E. C., & Damsté, J. S. S. (2013). The organic geochemistry of glycerol dialkyl glycerol tetraether lipids: a review. *Organic geochemistry*, 54, 19-61. doi:10.1016/j.orggeochem.2012.09.006
- Schouten, S., Hopmans, E. C., Schefuß, E., & Sinninghe Damsté, J. S. (2002). Distributional variations in marine crenarchaeotal membrane lipids: a new tool for reconstructing ancient sea water temperatures? *Earth and Planetary Science Letters*, 204(1), 265-274. doi:https://doi.org/10.1016/S0012-821X(02)00979-2

- Seki, O., Foster, G. L., Schmidt, D. N., Mackensen, A., Kawamura, K., & Pancost, R. D. (2010). Alkenone and boron-based Pliocene pCO₂ records. *Earth and Planetary Science Letters*, 292(1-2), 201-211. doi:10.1016/j.epsl.2010.01.037
- Sexton, P. F., Wilson, P. A., & Pearson, P. N. (2006). Microstructural and geochemical perspectives on planktic foraminiferal preservation: “Glassy” versus “Frosty”. *Geochemistry, Geophysics, Geosystems*, 7(12). doi:doi:10.1029/2006GC001291
- Spencer, C., & Kim, S.-T. (2015). Carbonate clumped isotope paleothermometry: a review of recent advances in CO₂ gas evolution, purification, measurement and standardization techniques. *Geosciences Journal*, 19(2), 357-374. doi:10.1007/s12303-015-0018-1
- Spooner, P. T., Guo, W., Robinson, L. F., Thiagarajan, N., Hendry, K. R., Rosenheim, B. E., & Leng, M. J. (2016). Clumped isotope composition of cold-water corals: A role for vital effects? *Geochimica et Cosmochimica Acta*, 179, 123-141. doi:10.1016/j.gca.2016.01.023
- Sprintall, J., Wijffels, S. E., Molcard, R., & Jaya, I. (2009). Direct estimates of the Indonesian Throughflow entering the Indian Ocean: 2004–2006. *Journal of Geophysical Research: Oceans*, 114(C7). doi:10.1029/2008JC005257
- Stolper, D. A., & Eiler, J. M. (2015). The kinetics of solid-state isotope-exchange reactions for clumped isotopes: A study of inorganic calcites and apatites from natural and experimental samples. *American Journal of Science*, 315(5), 363-411. doi:10.2475/05.2015.01
- Thiagarajan, N., Adkins, J., & Eiler, J. (2011). Carbonate clumped isotope thermometry of deep-sea corals and implications for vital effects. *Geochimica et Cosmochimica Acta*, 75(16), 4416-4425. doi:10.1016/j.gca.2011.05.004
- Tierney, J. E., & Tingley, M. P. (2015). A TEX86 surface sediment database and extended Bayesian calibration. *Scientific Data*, 2(1). doi:10.1038/sdata.2015.29
- Tripati, A. K., Eagle, R. A., Thiagarajan, N., Gagnon, A. C., Bauch, H., Halloran, P. R., & Eiler, J. M. (2010). 13C–18O isotope signatures and ‘clumped isotope’ thermometry in foraminifera and coccoliths. *Geochimica et Cosmochimica Acta*, 74(20), 5697-5717. doi:10.1016/j.gca.2010.07.006

- Urey, H. C. (1947). The thermodynamic properties of isotopic substances. *Journal of the Chemical Society (Resumed)*, 562-581. doi:10.1039/jr9470000562
- Wacker, U., Fiebig, J., Tödter, J., Schöne, B. R., Bahr, A., Friedrich, O., . . . Joachimski, M. M. (2014). Empirical calibration of the clumped isotope paleothermometer using calcites of various origins. *Geochimica et Cosmochimica Acta*, 141, 127-144. doi:10.1016/j.gca.2014.06.004
- Wacker, U., Rutz, T., Löffler, N., Conrad, A. C., Tütken, T., Böttcher, M. E., & Fiebig, J. (2016). Clumped isotope thermometry of carbonate-bearing apatite: Revised sample pre-treatment, acid digestion, and temperature calibration. *Chemical Geology*, 443, 97-110. doi:https://doi.org/10.1016/j.chemgeo.2016.09.009
- Wang, H., & Mehta, V. M. (2008). Decadal Variability of the Indo-Pacific Warm Pool and Its Association with Atmospheric and Oceanic Variability in the NCEP–NCAR and SODA Reanalyses. *Journal of Climate*, 21(21), 5545-5565. doi:10.1175/2008jcli2049.1
- Wara, M. W., Ravelo, A. C., & Delaney, M. L. (2005). Permanent El Nino-like conditions during the Pliocene warm period. *Science*, 309(5735), 758-761. doi:10.1126/science.1112596
- Zaarur, S., Affek, H. P., & Brandon, M. T. (2013). A revised calibration of the clumped isotope thermometer. *Earth and Planetary Science Letters*, 382, 47-57. doi:10.1016/j.epsl.2013.07.026
- Zhang, Y. G., & Liu, X. (2018). Export Depth of the TEX86 Signal. *Paleoceanography and Paleoclimatology*. doi:10.1029/2018pa003337
- Zhang, Y. G., Pagani, M., & Liu, Z. (2014). A 12-million-year temperature history of the tropical Pacific Ocean. *Science*, 344(6179), 84-87. doi:10.1126/science.1246172
- Zhang, Z. S., Nisancioglu, K. H., Chandler, M. A., Haywood, A. M., Otto-Bliesner, B. L., Ramstein, G., . . . Ueda, H. (2013). Mid-pliocene Atlantic Meridional Overturning Circulation not unlike modern. *Climate of the Past*, 9(4), 1495-1504. doi:10.5194/cp-9-1495-2013

**A robust calibration of the clumped isotopes to
temperature relationship for foraminifers**

Niklas Meinicke, S. Ling Ho, Bjarte Hannisdal, Dirk Nürnberg, Aradhna
Tripathi, Ralf Schiebel and A. Nele Meckler

*Published in Geochimica et Cosmochimica Acta (2020),
doi: 10.1016/j.gca.2019.11.022*



A robust calibration of the clumped isotopes to temperature relationship for foraminifers

N. Meinicke^{a,*}, S.L. Ho^{a,b}, B. Hannisdal^a, D. Nürnberg^c, A. Tripathi^{d,e},
R. Schiebel^f, A.N. Meckler^a

^aBjerknes Centre for Climate Research and Department of Earth Science, University of Bergen, Norway

^bInstitute of Oceanography, National Taiwan University, Taipei City, Taiwan

^cGEOMAR Helmholtz Centre for Ocean Research Kiel, Germany

^dDepartment of Earth, Planetary, and Space Sciences, Department of Atmospheric and Oceanic Sciences, Institute for the Environment and Sustainability, American Indian Studies Center, Center for Diverse Leadership in Science, UCLA, USA

^eInstitut Universitaire Européen de la Mer (IUEM), France

^fMax Planck Institute for Chemistry, Mainz, Germany

Received 13 May 2019; accepted in revised form 18 November 2019; available online 26 November 2019

Abstract

The clumped isotope (Δ_{47}) proxy is a promising geochemical tool to reconstruct past ocean temperatures far back in time and in unknown settings, due to its unique thermodynamic basis that renders it independent from other environmental factors like seawater composition. Although previously hampered by large sample-size requirements, recent methodological advances have made the paleoceanographic application of Δ_{47} on small (<5 mg) foraminifer samples possible.

Previous studies show a reasonable match between Δ_{47} calibrations based on synthetic carbonate and various species of planktonic foraminifers. However, studies performed before recent methodological advances were based on relatively few species and data treatment that is now outdated. To overcome these limitations and elucidate species-specific effects, we analyzed 14 species of planktonic foraminifers in sediment surface samples from 13 sites, covering a growth temperature range of ~0–28 °C. We selected mixed layer-dwelling and deep-dwelling species from a wide range of ocean settings to evaluate the feasibility of temperature reconstructions for different water depths. Various techniques to estimate foraminifer calcification temperatures were tested in order to assess their effects on the calibration and to find the most suitable approach.

Results from this study generally confirm previous findings that there are no species-specific effects on the Δ_{47} -temperature relationship in planktonic foraminifers, with one possible exception. Various morphotypes of *Globigerinoides ruber* were found to often deviate from the general trend determined for planktonic foraminifers.

Our data are in excellent agreement with a recent foraminifer calibration study that was performed with a different analytical setup, as well as with a calibration based exclusively on benthic foraminifers. A combined, methodologically homogenized dataset also reveals very good agreement with an inorganic calibration based on travertines. Our findings highlight the potential of the Δ_{47} paleothermometer to be applied to recent and extinct species alike to study surface ocean temperatures as well as thermocline variability for a multitude of settings and time scales.

© 2019 The Authors. Published by Elsevier Ltd. This is an open access article under the CC BY license (<http://creativecommons.org/licenses/by/4.0/>).

Keywords: Carbonate clumped isotopes; Foraminifera; Paleothermometry

1. INTRODUCTION

* Corresponding author.

E-mail address: niklas.meinicke@uib.no (N. Meinicke).

The investigation of past climate change relies to a large degree on reconstructions of ocean conditions. Not only is

the ocean a major player in the global climate system responsible for storage and redistribution of heat; ocean sediments also constitute vital archives that can be used for climate reconstructions on various time scales (e.g. Zachos et al., 2001). Several geochemical proxies have been used to reconstruct ocean conditions, such as sea surface temperature, prior to the instrumental era. These include paleothermometers, for instance stable oxygen isotopes ($\delta^{18}\text{O}$) measured in calcareous tests of foraminifers (Urey, 1947; Epstein et al., 1951; Emiliani, 1966; Pearson, 2012), Mg/Ca ratios of foraminifers (Nürnberg et al., 1996; Lea et al., 1999), the unsaturation of organic ketone molecules (U_{37}^K) produced by marine nannoplankton (Brassell et al., 1986; Prahl et al., 1988) and the TEX₈₆ proxy based on membrane lipids of archaea (Schouten et al., 2002).

Although each of these proxies is characterized by its individual strengths and weaknesses, two sources of uncertainty are particularly problematic for the application on longer time scales: First, temperature proxies such as $\delta^{18}\text{O}$ and Mg/Ca in foraminifers that depend on the fluid composition the signal is formed from require precise knowledge of the seawater composition ($\delta^{18}\text{O}_{\text{seawater}}$ and Mg/Ca, respectively) at the time of formation. Second, the recorded signal in most proxies is to some extent influenced by biological processes that need to be accounted for. These so-called vital effects can be species-specific (e.g. Bemis et al., 1998; Turich et al., 2007; Regenberg et al., 2009; Ho et al., 2014; Ezard et al., 2015; Jentzen et al., 2018; Polik et al., 2018), thus increasing the uncertainty of environmental reconstructions, particularly for data that is derived from extinct species. Clumped isotopes have the potential to circumvent both of these problems.

The carbonate clumped isotope method is based upon the fact that the abundance of doubly substituted carbonate ions containing both rare isotopes ^{18}O and ^{13}C increases with colder temperature. While carbonate formed under equilibrium conditions generally contains more bonds between two heavy isotopes than expected for a random (stochastic) distribution, the amount of this excess is temperature dependent (e.g. Bigeleisen and Mayer, 1947; Urey, 1947; Eiler and Schauble, 2004; Schauble et al., 2006). Temperature-dependent equilibrium constants determine the relative abundance of the $^{13}\text{C}^{18}\text{O}^{16}\text{O}^{16}\text{O}^{2-}$ isotopologue in isotope exchange reactions (e.g. Wang et al., 2004; Schauble et al., 2006).

The relative abundance of these multiply substituted (clumped) isotopologues in a carbonate can therefore be used as a measure for its formation temperature (e.g. Eiler and Schauble, 2004; Ghosh et al., 2006; Schauble et al., 2006; Eiler, 2007). An important aspect distinguishing this paleothermometer from other approaches is its independence from the isotopic composition of the aqueous solution it precipitated from (Ghosh et al., 2006; Eiler, 2007). The Δ_{47} value measured in acid-liberated CO_2 reflects the excess abundance (in ‰) of doubly substituted molecules relative to a random distribution that is calculated for each sample (Ghosh et al., 2006). The relationship between the normalized Δ_{47} value and carbonate formation temperature has been defined by theoretical, experimental, and empirical calibrations (e.g. Ghosh

et al., 2006; Ghosh et al., 2007; Tripati et al., 2010; Grauel et al., 2013; Henkes et al., 2013; Zaarur et al., 2013; Wacker et al., 2014; Kele et al., 2015; Bonifacie et al., 2017; Kelson et al., 2017; Breitenbach et al., 2018; Peral et al., 2018; Petersen et al., 2019).

The first two studies of foraminifers (Grauel et al., 2013; Tripati et al., 2010) indicated that within their sample sets there is evidence that foraminifers follow a single Δ_{47} -temperature relationship. Hence these studies paved the way for the application of clumped isotope thermometry on foraminifers from sedimentary archives (e.g. Tripati et al., 2014). However, due to a relative lack of data for the cold temperature end of these foraminifer calibrations, coupled with recent developments in data processing and correction methods, additional studies have been underway: The more recent works (Breitenbach et al., 2018; Peral et al., 2018; Piasecki et al., 2019) have utilized progress made in community-wide efforts to facilitate inter-laboratory data comparison using the recalibration of absolute isotope ratios (Daëron et al., 2016; Schauer et al., 2016), and further redefinition of carbonate standards (Bernasconi et al., 2018), building on the definition of an “absolute” reference frame by Dennis et al. (2011), as well as newly developed analytical approaches (Hu et al., 2014).

Peral et al. (2018) and Piasecki et al. (2019) focused mostly on planktonic and benthic foraminifers, respectively, and both concluded that foraminifer-based Δ_{47} -T calibrations agree with inorganic calibrations. Although the two equations are statistically indistinguishable from each other temperatures calculated with these calibrations diverge towards the cold end of ocean temperatures ($\sim 0^\circ\text{C}$) by more than 2.5°C . A challenge for surface sediment-based calibrations using foraminifers is the difficulty in determining the actual calcification temperature, particularly for planktonic foraminifers.

Additionally, the small temperature range recorded in foraminifers poses a persisting problem for foraminifer Δ_{47} -T calibrations, because large datasets are required to extract an accurate linear relationship from the relatively large uncertainty of individual measurements (Fernandez et al., 2017). The relatively low signal to noise ratio compared to other geochemical proxies such as $\delta^{18}\text{O}$ might mask smaller, potentially species-specific, secondary effects. These potential secondary effects include pH or kinetic effects suggested for other types of marine biogenic carbonates/marine invertebrate organisms (e.g. Bajnai et al., 2018; Daëron et al., 2019; Davies and John, 2019). Divergences among older foraminifer-based calibrations can partly be explained by methodological or inter-laboratory differences such as the ^{17}O correction (Schauer et al., 2016; Bernasconi et al., 2018; Petersen et al., 2019), the choice of standards (Bernasconi et al., 2018), the acid digestion temperature (Defiense et al., 2015) and the common acid bath vs. the micro-volume approach (reviewed in Spencer and Kim, 2015).

These uncertainties underline the importance of further studies investigating method- and laboratory-specific differences as well as potential species effects. Ultimately the aim is to determine a common foraminifer calibration to enable a widespread application of clumped isotope analysis in for-

aminifers. At the same time, using clumped isotopes on foraminifers yields enormous potential for paleoceanographic reconstructions when coupled with other proxies: As highlighted by Breitenbach et al. (2018) and Evans et al. (2018), clumped isotope measurements can be combined with other foraminifer-based proxies to disentangle ocean temperature from other influences, such as changing seawater composition (e.g. past Mg/Ca changes, Evans et al. (2018)).

Similarly to other foraminifer-based proxies such as $\delta^{18}\text{O}$ (e.g. Mulitza et al., 1997), the Δ_{47} signal in foraminifers could be used to reconstruct temperature gradients in the water column by comparing species from different depth habitats. In the case of Δ_{47} using a single calibration is advantageous as it allows for a direct comparison of data from various species without any additional uncertainty introduced by individual, species-specific calibrations.

Here, we present new foraminifer-based Δ_{47} data analyzed on 14 species of planktonic foraminifers from surface sediments from 13 sites, covering a calcification temperature range of ~ 0 – 28 °C. We study potential species-specific effects on the clumped isotope measurements and compare our results to recent Δ_{47} -T calibrations. Data from our study are combined with data from Peral et al. (2018) and Piasecki et al. (2019) to determine a common foraminifer-based calibration and compare it to inorganic Δ_{47} -T calibrations. Finally, we evaluate whether temperature reconstructions for different depth levels of the water column are feasible with the reduced sample requirements of our analytical approach.

2. MATERIAL AND METHODS

2.1. Sites and samples

Surface sediment samples (mostly 0–1 cm, see Table 1) from 13 sites in the Nordic Seas, the North Atlantic, Indian Ocean, and Pacific Ocean were used in this calibration study (Fig. 1 and Table 1). The sites were selected to cover a wide range of oceanographic conditions and species of foraminifers.

Monospecific samples of surface- as well as deep-dwelling foraminifers covering a growth temperature range of ~ 0 – 28 °C (see Section 2.4) were measured. A total number of 43 samples from 14 species of planktonic foraminifers was selected (Tables 1 and 2), including *Globigerina bulloides*, *Globigerinoides conglobatus*, *Globigerinoides ruber* pink, *Globigerinoides ruber* white sensu lato (s.l.) and sensu stricto (s.s.), *Globorotalia hirsuta*, *Globorotalia inflata*, *Globorotalia menardii*, *Globorotalia truncatulinoides*, *Globorotalia tumida*, *Neoglobobulimina dutertrei*, *Neoglobobulimina pachyderma*, *Orbulina universa*, *Pulleniatina obliquiloculata*, *Trilobatus sacculifer*, *Trilobatus trilobus*.

Species characteristics and assumptions regarding their ecology are crucial to the interpretation of the Δ_{47} data, in particular when various species are compared to each other. Table 2 provides a summary of the species-specific characteristics considered, such as the presence of photobiotic symbionts, spatial and seasonal distribution, preferred habitat depth, the tendency to form gametogenetic calcite prior to reproduction and the accumulation of thick calcite crusts.

2.2. Sample preparation

All samples were wet-sieved over a 63 μm sieve and dried at ≤ 50 °C. The coarse fraction was then dry-sieved into size fractions of < 150 μm , 150–250 μm , 250–315 μm , 315–355 μm and 355–400 μm , 400–500 μm and > 500 μm . For each sample, at least 2 mg of foraminifer tests of each species were collected under the microscope. The preservation of all individual specimens was assessed under the microscope and translucent specimens were preferred for analysis where available. Only fully intact pristine-looking tests were selected for analysis. Broken specimens as well as specimens containing substantial infillings, secondary calcite overgrowth or oxide coatings were excluded from analysis. Additionally, SEM images were used for selected samples to confirm that the foraminifers were well preserved. The size fractions used for the analysis were individually selected for each sample (Table 3). We attempted to obtain enough adult specimen of each species to allow an accurate isotope analysis while keeping the size range as narrow as possible in order to limit ontogenetic effects. Therefore, the size fraction in which most of the adult specimens at a given site were found was selected for analysis. Size fractions with a small number of very large individuals were excluded as well as smaller size fractions potentially containing juvenile specimens.

A modified version of the cleaning protocol for foraminifer Mg/Ca analysis published by Barker et al. (2003) was used to remove contaminants. Batches of 200 to 1300 μg of foraminifer tests were cleaned at a time with each sample being represented by at least three individually cleaned sub-samples. The foraminifers were placed between two glass plates and carefully crushed in order to crack open all chambers and allow for subsequent cleaning. The crushed tests were sonicated three times for 30 s with DI water and rinsed with DI water after each sonication step. Samples were then sonicated once for 15 s with methanol and subsequently rinsed three times with DI water. After removing excess DI water, the cleaned samples were dried in an oven at ≤ 50 °C. The comparison of several cleaning steps and intensities (Piasecki et al., 2019; see also Grauel et al., 2013, Peral et al., 2018) led to the decision to leave out the H_2O_2 treatment suggested by Barker et al. (2003) to remove organic material for Mg/Ca analysis.

2.3. Measurement procedure

All measurements took place between November 2016 and March 2018 with replicate measurements of individual samples spread over several weeks to months. Measurements were performed using a Thermo Scientific MAT 253Plus mass spectrometer coupled to a KIEL IV carbonate device (Thermo Fisher Scientific, Bremen, Germany) equipped with a Porapak trap to capture organic contaminants (Schmid and Bernasconi, 2010). The Porapak trap was operated at -20 °C during the measurement. Between runs, the trap was heated to 120 °C for at least one hour for cleaning. In the Kiel device, each aliquot is reacted individually with phosphoric acid at 70 °C.

We measured 15 to 30 (average $n = 19$) aliquots (100–130 μg each) for every sample. Average values for stable

Table 1
 Sites from which planktonic foraminiferal specimens used in this study were selected.

Station	Latitude °N	Longitude °E	Region	Depth [m]	Depth in the core [cm]	Age [ka BP]	Species
GS15-198-63MC	70.5	-2.8	Nordic Seas	2995	0-1	<625 ± 20 conventional ¹⁴ C age	<i>N. pachyderma</i>
GS15-198-38MC	70.1	-17.7	Denmark Strait	1610	0-1	<410 ± 15 conventional ¹⁴ C age	<i>N. pachyderma</i>
GS15-198-62MC	70.0	-13.6	Iceland Plateau	1423	0-1	<2995 ± 15 conventional ¹⁴ C age	<i>N. pachyderma</i>
GS06-144-19MC	63.8	5.2	Nordic Seas	922	0-7	recent (Yu et al., 2013)	<i>G. bulloides</i> , <i>G. inflata</i>
CD107 A ML 5A	52.9	-16.9	North Atlantic	3569	surface sediment		<i>G. bulloides</i> , <i>G. hirsuta</i> , <i>G. truncatulinoides</i> , <i>O. universa</i>
CD94 17B (OMEX)	48.9	-11.8	North Atlantic	1484	surface sediment		<i>G. bulloides</i> , <i>G. inflata</i> , <i>G. truncatulinoides</i> , <i>O. universa</i>
KL88	34.8	-27.7	North Atlantic	2060	surface sediment		<i>G. bulloides</i> , <i>G. inflata</i> , <i>G. ruber</i> white s.l., <i>G. truncatulinoides</i>
CD145 A150	23.3	66.7	Arabian Sea	151	0-1		<i>N. dutertrei</i>
SO164-25-3	14.7	-59.7	Caribbean/North Atlantic	2720	0-1	1915 ± 30 (Regenberg et al., 2006)	<i>G. conglobatus</i> , <i>G. ruber</i> pink, <i>G. ruber</i> white s.s., <i>G. ruber</i> white s.l., <i>P. obliquiloculata</i> , <i>T. trilobus</i>
OIP2016 MW0691	-1.0	157.8	Ontong Java Plateau	2016	0-5		<i>T. trilobus</i>
WIND 33B	-11.2	58.8	Indian Ocean	2871	0-2		<i>G. menardii</i> , <i>G. ruber</i> white s.s., <i>G. tumida</i> , <i>N. dutertrei</i> , <i>O. universa</i> , <i>P. obliquiloculata</i> , <i>T. sacculifer</i> , <i>T. trilobus</i>
SO225-53-1	-13.5	-162.1	Mamihiki Plateau	3154	0-1	6230 ± 50 (Raddatz et al., 2017)	<i>G. conglobatus</i> , <i>G. ruber</i> white s.s., <i>G. tumida</i> , <i>O. universa</i> , <i>P. obliquiloculata</i> , <i>T. sacculifer</i> , <i>T. trilobus</i>
SO213-84-2	-45.1	174.6	South Pacific	992	0-1	4952 ± 238 (Molina-Kescher et al., 2014)	<i>G. bulloides</i> , <i>G. inflata</i> , <i>G. truncatulinoides</i>

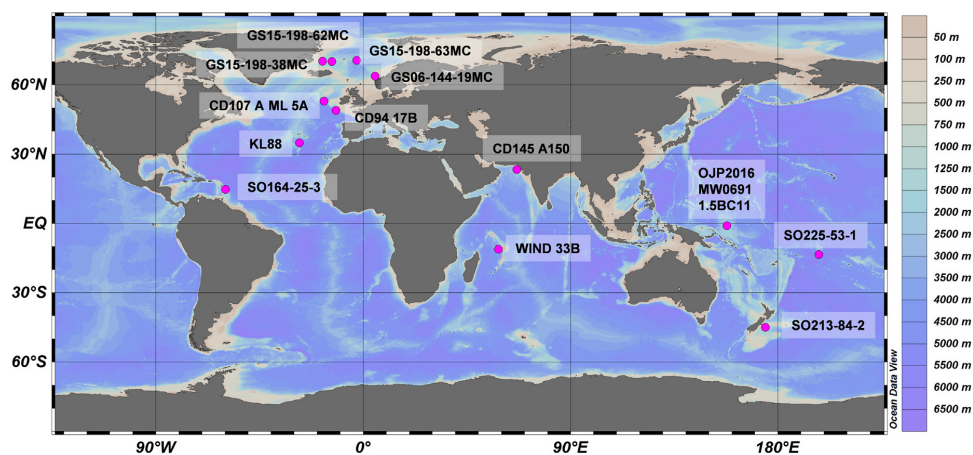


Fig. 1. Bathymetric chart generated using Ocean Data View (ODV, Schlitzer, 2018) showing surface sediment locations (pink filled circles), from which foraminifer specimens were selected. Bathymetric data from GlobHR (reference available in Ocean Data View).

carbon ($\delta^{13}\text{C}$) and oxygen isotopes ($\delta^{18}\text{O}$) as well as Δ_{47} were then calculated and used for the calibration. Samples were measured using the long-integration dual-inlet (LIDI) method described by Hu et al. (2014). This method measures the sample and reference gas separately with decreasing pressure from a micro-volume. Samples were measured first for 400 seconds with signals typically decreasing from $\sim 16\text{ V}$ to $\sim 10\text{ V}$ ($m/z = 44$). Afterwards the reference gas was adjusted to the same initial pressure and measured accordingly. The shot noise limit for these intensities and integration times is 0.03‰ when applying a typical scale decomposition factor for this system.

Peak scans (varying high voltage between 9.4 and 9.6 kV) at m/z 44 intensities of 5, 10, 15, 20 and 25 V were performed once a day for the pressure baseline correction following Bernasconi et al. (2013) and Meckler et al. (2014). This and subsequent corrections were applied using the Easotope software package (John and Bowen, 2016). The “Brand parameters” suggested by Daëron et al. (2016) and Schauer et al. (2016) were used for the ^{17}O correction. In every run (maximum 46 aliquots), the sample measurements were bracketed by five blocks consisting of the four ETH carbonate standards ETH1 to ETH4 using the values reported in Bernasconi et al. (2018). Three of these standards were used to transfer the results into the absolute reference frame (Dennis et al., 2011), which corrects the measurements for offsets and scale compression, while the fourth standard was treated like a sample to monitor the corrections applied to the data. In addition, the long-term averages of ETH 1 and 2 were used to monitor the pressure baseline correction which should result in the same Δ_{47} values (Bernasconi et al., 2018). Baseline-corrected Δ_{48} values were used as a contamination monitor. No contamination was detected in any of the samples.

The average long-term reproducibility (1SD) of Δ_{47} measured in the carbonate standards after correction varies from 0.031‰ to 0.038‰ (see Appendix Table A1). Each

replicate measurement was corrected using a total number of 60–80 standard measurements from the same and adjacent days. The exact number was chosen according to the instrument stability (see Piasecki et al., 2019 for more information). In addition to correcting for instrumental drift using carbonate standards, we distributed replicate measurements of all samples over long time intervals of up to several months to ensure that aliquots from as many samples as possible were measured in parallel.

The ETH standard values adopted in this study were reported by Bernasconi et al. (2018), who used a $+0.062\text{‰}$ correction (Defliese et al., 2015) for differences in acid fractionation between digestion at 70 °C and the classical 25 °C digestion temperature. Applying the recently updated acid fractionation correction of 0.066‰ for this temperature difference (Petersen et al., 2019) would increase all of our Δ_{47} values by 0.004‰ . Should the ETH standard values be updated in the future it is possible to recalculate the values from this study using the replicate level raw data that is provided in the EarthChem database (<https://doi.org/doi:10.1594/IEDA/111435>).

2.4. Foraminifer calcification temperature estimates

In order to establish a calibration relating the Δ_{47} signal in planktonic foraminifers to water temperature, the calcification temperature for each species at each site needs to be estimated. Since our sample set comprises a large number of different species from a wide range of geographical regions, the estimation of calcification temperatures is subject to a number of uncertainties. Calcification temperatures were hence calculated using different approaches (Method 1 to 3) in order to find the optimal solution.

Method 1: If calcification depths and possible seasonality effects are known for the species and geographical regions, the water temperature can be taken from reanalysis data presented in the World Ocean Atlas (WOA; Locarnini

Table 2
Summary of species-specific characteristics for the planktonic foraminifers analyzed in this study (Schiebel and Hemleben, 2017, and references therein).

Species	Spinose	Symbiont-bearing	Typical habitat	Spatial distribution	Seasonality	Gametogenic calcite reported	Other secondary calcite reported	Remarks
<i>Globigerina bulloides</i>	yes	yes	mixed layer	temperate to sub-polar waters and upwelling regions	found year round with lower abundances in summer, typical of the spring bloom	yes	no	
<i>Globigerinoides conglobatus</i>	yes	yes	mixed layer	tropical and subtropical waters	more abundant in fall	yes	no	
<i>Globigerinoides ruber</i> pink	yes	yes	mixed layer	tropical to subtropical waters in the Atlantic Ocean	most abundant at highest T	no	no	
<i>Globigerinoides ruber</i> white s.l.	yes	yes	mixed layer	tropical to subtropical waters	low in stratified tropical waters	no	no	
<i>Globigerinoides ruber</i> white s.s.	no	no	upper mixed layer	tropical to subtropical waters	low in stratified tropical waters	no	no	
<i>Globorotalia hirsuta</i>	no	no	subsurface	temperate to subtropical waters	unclear	no	yes	
<i>Globorotalia inflata</i>	no	no	mixed layer to subsurface	subtropical to subpolar waters, hydrologic fronts	depending on front dynamics	no	yes	only specimens without calcite veneer selected for analysis
<i>Globorotalia menardii</i>	no	yes	thermocline	tropical to subtropical waters	low in stratified tropical waters	no	yes	
<i>Globorotalia truncatulinoides</i>	no	no	subsurface	tropical to temperate waters	more abundant in winter	no	yes	
<i>Globorotalia tumida</i>	no	no	thermocline	tropical to subtropical waters	low in stratified tropical waters	no	yes	
<i>Neogoboloboaquadrina duerrei</i>	no	yes	mixed layer to thermocline	tropical to temperate waters	low in stratified tropical waters	no	yes	
<i>Neogoboloboaquadrina pachyderma</i>	no	no	mixed layer	polar waters	polar summer	no	yes	only left-coiling specimens selected for analysis
<i>Orbulina universa</i>	yes	yes	mixed layer to thermocline	tropical to temperate waters	summer in temperate waters	yes	no	
<i>Pulleniatina obliquiloculata</i>	no	no	lower mixed layer to thermocline	tropical to subtropical waters	more abundant in winter	yes	no	only smooth tests without gametogenic calcite selected for analysis
<i>Trilobatus sacculifer</i>	yes	yes	mixed layer	tropical to subtropical waters	low in stratified tropical waters	yes	no	
<i>Trilobatus trilobus</i>	yes	yes	mixed layer	tropical to subtropical waters	low in stratified tropical waters	yes	no	

Table 3

The specifications (site, species, size fraction, number of replicates) and average isotopic compositions (Δ_{47} , $\delta^{13}\text{C}_{\text{calcite}}$ and $\delta^{18}\text{O}_{\text{calcite}}$) of individual samples with corresponding $\delta^{18}\text{O}_{\text{seawater}}$ data (LeGrande and Schmidt, 2006), assumed calcification depth (Rippert et al., 2016; Schiebel and Hemleben, 2017, and references therein) and four different estimates of calcification temperature based on the World Ocean Atlas 2009 (Method 1), Shackleton (1974) (Methods 2 and 3) and Kim and O'Neil (1997) (Method 2). The calculated apparent calcification depth (ACD) is given for the Method 3.

Site and species	Size fraction [μm]	N*	Δ_{47} [‰]	SE	$\delta^{13}\text{C}_c$ [‰]	SE	$\delta^{18}\text{O}_c$ [‰]	SE	$\delta^{18}\text{O}_{\text{sw}}$ [‰]	Assumed CD [m]	SE	T M1 [°C]*	SD T M2 [°C]*	T S74 M2 [°C]*	SE T S74 M3 [°C]*	T S74 M3 [°C]*	SE T S74 M3 [°C]*	ACD M3 [m]*	T K97 M2 [°C]*	SE	
CD94 17B (OMEX)																					
<i>G. bulloides</i>	250–315	16	0.706	0.006	-0.440	0.030	0.72	0.02	0.57	0–100	0.02	12.9	1.9	15.5	1.0	13.5	0.2	15	14.1	1.2	
<i>G. truncat.</i>	355–500	15	0.713	0.008	1.050	0.040	1.48	0.03	0.55	200–500	0.02	11.0	0.3	12.3	1.2	11.6	0.8	204	10.6	1.4	
<i>G. inflata</i>	355–400	15	0.710	0.008	0.960	0.010	1.35	0.03	0.56	0–500	0.02	12.0	1.6	13.0	1.2	12.3	1.0	115	11.3	1.4	
<i>O. universa</i>	355–400	15	0.707	0.008	2.080	0.040	1.18	0.03	0.57	20–150	0.02	12.2	1.5	13.6	1.3	13.1	0.8	46	12.1	1.5	
CD107 A ML 5A																					
<i>G. bulloides</i>	250–355	30	0.714	0.006	-0.410	0.020	1.38	0.04	0.52	0–100	0.02	11.9	1.5	12.6	1.6	11.6	0.8	99	10.9	1.8	
<i>G. truncat.</i> *	355–500	15	0.713	0.008	1.180	0.020	1.58	0.02	0.48	200–500	0.02	10.3	0.3	11.7	1.1	11.1	0.9	186	9.9	1.2	
<i>O. universa</i>	355–500	15	0.704	0.005	2.030	0.020	1.05	0.02	0.52	20–150	0.02	11.5	1.2	14.0	1.2	12.1	0.5	32	12.4	1.3	
<i>G. hirsuta</i>	>355	19	0.723	0.007	1.170	0.020	2.08	0.02	0.44	500–700	0.02	9.4	0.4	9.5	1.2	9.6	1.1	497	7.5	1.2	
CD145 AI50																					
<i>N. datervei</i>	355–500	20	0.679	0.008	1.420	0.040	-1.12	0.02	0.72	25–125	0.02	23.4	2.1	23.5	1.2	23.3	0.7	62	23.6	1.4	
GS06-144-19MC																					
<i>G. bulloides</i>	250–315	18	0.713	0.006	-0.410	0.030	1.61	0.02	0.29	0–100	0.02	8.6	1.6	10.8	1.2	9.0	0.2	12	8.9	1.3	
<i>G. inflata</i>	250–315	18	0.719	0.007	0.920	0.010	1.95	0.01	0.37	0–500	0.01	7.6	1.8	9.7	1.1	8.7	0.4	39	7.7	1.2	
GS15-198-38MC																					
<i>N. pachyderma</i>	150–250	20	0.755	0.008	0.540	0.010	3.60	0.01	-0.17	0–50	0.01	0.2	1.5	1.0	1.2	0.4	0.3	111	-1.2	1.2	
GS15-198-62MC																					
<i>N. pachyderma</i>	150–250	28	0.756	0.006	0.770	0.010	3.66	0.01	0.01	0–50	0.01	0.8	1.5	1.5	1.1	0.8	0.5	65	-0.7	1.0	
GS15-198-63MC																					
<i>N. pachyderma</i>	250–315	21	0.750	0.006	0.390	0.010	2.78	0.01	0.28	0–50	0.01	4.2	1.7	6.1	1.1	4.3	0.3	18	3.9	1.1	
KL88																					
<i>G. ruber</i> w. s.l.	315–355	18	0.715	0.008	1.050	0.030	0.61	0.02	1.03	30–50	0.02	19.4	1.9	17.7	1.2	17.0	1.1	120	16.7	1.3	
<i>G. bulloides</i>	250–315	15	0.708	0.006	-1.180	0.040	1.41	0.03	1.01	0–100	0.03	19.3	2.3	14.4	1.4	13.0	1.1	414	13.0	1.5	
<i>G. truncat.</i> *	355–400	16	0.723	0.008	0.930	0.030	1.64	0.04	0.71	200–500	0.04	13.9	1.2	12.3	1.5	11.8	1.1	537	10.6	1.6	
<i>G. inflata</i>	355–400	16	0.721	0.007	0.800	0.030	1.74	0.03	0.88	0–500	0.03	16.9	3.0	12.6	1.6	11.3	1.0	595	10.9	1.7	
OJP2016 MW0691 1.5BC11																					
<i>T. trilobus</i>	355–400	16	0.669	0.005	2.220	0.030	-2.05	0.02	0.36	75–150	0.02	26.4	1.9	25.7	1.2	26.0	0.8	123	26.4	1.5	

SO164-25-3																				
<i>G. ruber</i> w. s.s.	315–355	20	0.653	0.006	1.190	0.050	-2.29	0.02	0–30	0.72	0.20	27.4	0.8	28.1	1.2	27.3	0.2	20	29.5	1.6
<i>G. ruber</i> w. s.l.	250–315	18	0.682	0.006	0.670	0.050	-2.21	0.03	30–50	0.81	0.20	27.1	0.7	28.1	1.3	27.3	0.2	22	29.5	1.7
<i>G. ruber</i> pink	315–355	18	0.678	0.008	1.450	0.020	-2.18	0.02	0–50	0.74	0.21	27.3	0.8	27.8	1.2	27.3	0.2	24	29.0	1.5
<i>T. trilobus</i>	315–355	17	0.665	0.009	1.380	0.050	-1.85	0.04	50–100	0.98	0.23	26.0	0.9	27.4	1.6	27.0	0.4	42	28.6	2.0
<i>P.</i>	355–500	16	0.664	0.005	1.230	0.040	-0.91	0.02	100–125	1.13	0.20	24.2	0.8	24.2	1.2	24.2	0.8	113	24.5	1.4
<i>obliquiloculata</i>	>400	16	0.670	0.008	2.300	0.060	-1.30	0.03	75–125	1.09	0.21	24.8	1.1	25.6	1.4	25.5	0.7	87	26.3	1.7
<i>G. conglobatus</i>																				
SO213-84-2																				
<i>G. bulloides</i>	315–355	30	0.729	0.005	0.400	0.030	2.02	0.03	100–150	0.01	0.20	8.3	0.4	8.0	1.4	7.7	0.9	271	6.0	1.5
<i>G. truncat.</i> *	315–355	16	0.731	0.007	1.010	0.030	2.17	0.03	200–500	-0.01	0.20	7.4	0.6	7.3	1.3	7.3	0.9	361	5.2	1.3
<i>G. inflata</i>	315–355	20	0.729	0.008	1.240	0.010	1.90	0.02	0–500	0.04	0.20	8.8	0.9	8.6	1.2	8.1	1.0	214	6.6	1.3
SO225-53-1																				
<i>G. ruber</i> w. s.s.	250–355	17	0.684	0.007	1.750	0.050	-1.59	0.02	50–150	0.68	0.21	26.6	1.4	25.1	1.2	25.4	0.9	132	25.7	1.5
<i>T. trilobus</i>	250–355	22	0.683	0.006	1.850	0.040	-1.40	0.03	75–150	0.71	0.21	26.2	1.2	24.6	1.5	24.6	0.9	147	25.0	1.8
<i>T. sacculifer</i>	>355	15	0.676	0.005	2.480	0.060	-1.37	0.04	75–150	0.71	0.21	26.2	1.2	24.4	1.4	24.5	0.9	150	24.8	1.8
<i>P.</i>	355–500	21	0.678	0.006	1.500	0.030	-0.24	0.06	150–200	0.72	0.20	23.3	1.2	19.9	1.9	19.1	1.1	253	19.3	2.2
<i>obliquiloculata</i>	>355	16	0.672	0.007	3.170	0.050	-1.26	0.06	50–200	0.68	0.21	25.8	2.1	23.8	1.8	24.0	0.9	160	24.1	2.2
<i>O. universa</i>	355–500	20	0.690	0.007	2.360	0.020	-1.23	0.04	100–200	0.72	0.20	24.8	1.8	23.9	1.6	23.9	0.9	163	24.1	2.0
<i>G. conglobatus</i>	>355	16	0.688	0.006	2.280	0.040	0.10	0.06	125–300	0.61	0.25	21.6	3.5	18.1	2.1	17.3	1.1	282	17.2	2.4
WIND 33B																				
<i>G. ruber</i> w. s.s.	250–355	19	0.686	0.008	1.590	0.030	-1.74	0.02	0–30	0.40	0.20	26.9	1.2	24.6	1.1	24.6	1.0	58	25.0	1.4
<i>T. trilobus</i>	250–355	23	0.671	0.005	1.670	0.030	-1.51	0.02	50–100	0.32	0.21	23.0	2.1	23.4	1.2	23.5	1.0	71	23.6	1.4
<i>T. sacculifer</i>	>355	25	0.675	0.006	2.350	0.030	-1.55	0.02	50–100	0.32	0.21	23.0	2.1	23.5	1.2	23.7	1.0	69	23.7	1.5
<i>N. dutertrei</i>	355–400	20	0.678	0.005	1.720	0.020	-0.64	0.03	20–125	0.34	0.21	23.5	3.2	20.0	1.4	19.7	0.8	112	19.4	1.7
<i>P.</i>	355–500	21	0.680	0.005	0.990	0.010	-0.80	0.03	100–125	0.31	0.21	19.6	2.5	20.5	1.4	20.4	0.8	104	20.0	1.7
<i>obliquiloculata</i>	>400	19	0.679	0.006	2.370	0.030	-1.37	0.03	20–150	0.34	0.21	22.6	3.8	22.9	1.4	22.8	1.0	78	22.9	1.7
<i>O. universa</i>	>400	20	0.702	0.006	1.520	0.020	0.40	0.06	20–100	0.35	0.21	24.5	2.5	15.9	1.8	15.6	0.9	182	14.6	2.1
<i>G. menardii</i>	>355	20	0.700	0.005	1.660	0.020	0.71	0.05	125–300	0.29	0.20	15.1	2.5	14.4	1.6	14.2	0.9	215	12.9	1.8

* N = number of replicate measurements, CD = calcification depth, S74 = Shackleton 1974, K97 = Kim and O'Neil, 1997, M1-3 = Methods 1–3, G. truncat. = *Globorotalia truncatulinoides*.

et al., 2010). Due to the fact that typical foraminifer water depth habitats vary over time, both dependent on the availability of prey and ontogeny (Schiebel and Hemleben, 2017), the environmental signal recorded by the bulk foraminifer tests is rather an average across the entire life cycle of individuals and assemblages (e.g. Deuser and Ross, 1989). We therefore used published apparent calcification depths from studies utilizing other temperature proxies such as oxygen isotopes and Mg/Ca on planktonic foraminifers (e.g. Schiebel and Hemleben, 2017 and references therein) as basis for atlas-based calcification temperatures (Table 3). This approach suffers from insufficient information regarding foraminiferal calcification depths for individual regions and species. Also, the temperature information derived from the World Ocean Atlas may not provide the same accuracy everywhere because the data is interpolated to all ocean regions and standard depth levels. Here we used the annual mean water temperature of the assumed calcification depth as basis for further calculations. Seasonal temperature variability was factored into the uncertainty calculations. For Method 1, the overall temperature uncertainty is given by the standard deviation of all monthly temperatures at the assumed calcification depth of each species at a given site.

Method 2: Calcification temperatures can be derived from oxygen isotope ($\delta^{18}\text{O}$) measurements of each foraminifer sample by applying empirical calibration equations, which relate the $\delta^{18}\text{O}$ of the calcite tests ($\delta^{18}\text{O}_{\text{calcite}}$) to water temperature (e.g. Shackleton et al., 1973). For this approach, the $\delta^{18}\text{O}$ of the seawater ($\delta^{18}\text{O}_{\text{seawater}}$) is needed, which we obtained for the assumed calcification depths from the database of LeGrande and Schmidt (2006). Due to species-specific disequilibrium effects (suggested by Urey, 1947; Shackleton et al., 1973), specific $\delta^{18}\text{O}$ -T calibrations have been derived for certain species and ocean regions (reviewed in Pearson, 2012). However, as such calibrations are only available for some of the species studied here, we decided to apply the multi-species $\delta^{18}\text{O}$ -temperature equations of Kim and O'Neil (1997) and Shackleton (1974) for the entire dataset, acknowledging that some of the reconstructed temperatures may be biased by species-specific effects. The extent of such effects, however, is still a matter of debate (Niebler et al., 1999; Schiebel and Hemleben, 2017). We tested the sensitivity of our results to corrections for species-specific differences using the available information (Appendix Table A2). Applying species-specific $\delta^{18}\text{O}$ corrections led to a calibration line within the error of the uncorrected $\delta^{18}\text{O}$ data (Table A3). Furthermore, using species-specific corrections hardly changes the influence of individual species on the slope of the calibration line (Fig. A1). Because of the uncertainty introduced by the large spread of published values for species-specific corrections and the lack of improvement to our fit when applying a correction, we decided against applying any correction to the $\delta^{18}\text{O}_{\text{calcite}}$ data used for the calibration. Temperature estimates from two commonly used calibrations (Shackleton, 1974, equation D; Kim and O'Neil, 1997 modified by Bemis et al., 1998 Table 1) were compared. Following the recommendation of Bemis et al. (1998) and Pearson (2012), factors of 0.20‰ (Epstein et al., 1953) and 0.27‰ (Hut, 1987) were used to convert from VSMOW to VPDB for the $\delta^{18}\text{O}$ -T calibrations of

Shackleton (1974) and Kim and O'Neil (1997), respectively. The uncertainty of each calcification temperature estimate was calculated as a combination of several individual uncertainties: We used the standard deviation of the measured $\delta^{18}\text{O}_{\text{calcite}}$ values to account for the variability of the sample material and the uncertainty of the isotope measurement. Mean $\delta^{18}\text{O}_{\text{seawater}}$ values were calculated for the depth intervals that were assumed to best represent the calcification depths (Table 3, same as in Method 1) of the samples. The standard deviation of $\delta^{18}\text{O}_{\text{seawater}}$ over this depth interval was taken as uncertainty. An additional 0.2‰ were added to account for the uncertainty introduced by the gridded dataset (following Peral et al. (2018)).

Method 3: In order to avoid relying on assumed depth habitats, calcification temperatures were also estimated from hypothetical $\delta^{18}\text{O}$ depth profiles of calcite formed in the water column ($\delta^{18}\text{O}_{\text{calculated}}$). For this approach, the WOA temperature data are used in combination with a published $\delta^{18}\text{O}$ -T calibration (Shackleton, 1974) to produce vertical profiles of hypothetical $\delta^{18}\text{O}$ to which the measured foraminiferal $\delta^{18}\text{O}_{\text{calcite}}$ is compared, in order to determine the apparent calcification depth (ACD) and subsequently the corresponding WOA temperature. This approach has previously been applied in Mg/Ca-temperature calibration studies on foraminifers (e.g. Groeneveld and Chiessi, 2011). The $\delta^{18}\text{O}_{\text{calculated}}$ of calcite is calculated for the entire water column at each sample site, combining WOA water temperature data (Locarnini et al., 2010) and $\delta^{18}\text{O}_{\text{seawater}}$ values (LeGrande and Schmidt, 2006). Method 3 has the advantage that no assumptions regarding habitat depth are needed, neither for the atlas-derived water temperature nor for the $\delta^{18}\text{O}$ of the water. This way, seasonal or ontogenetic variations in the calcification depth are accounted for as well.

If the measured $\delta^{18}\text{O}_{\text{calcite}}$ of a sample was not found in the $\delta^{18}\text{O}_{\text{calculated}}$ values (calculated temperatures warmer/colder than the observed maximum/minimum annual mean water temperature), the annual mean water temperature at 0 m depth was used. Therefore, extreme temperature cases not represented in WOA are excluded with this method, eliminating temperatures warmer or colder than observed at these sites. Nonetheless, Method 3 is associated with several uncertainties stemming from both the analytical and the natural variability of foraminiferal $\delta^{18}\text{O}$, as well as from the atlas $\delta^{18}\text{O}_{\text{seawater}}$. Uncertainties were propagated using a Monte Carlo approach. First, assuming a conservative error of 0.2‰ for the atlas $\delta^{18}\text{O}_{\text{seawater}}$ (following Peral et al. (2018)), we generated 10,000 iterations of $\delta^{18}\text{O}_{\text{calculated}}$ (Step 1 in Fig. 2A), using the equation of choice. For all these iterations, we then performed Step 2 (Fig. 2B) considering the uncertainty in $\delta^{18}\text{O}_{\text{calcite}}$ measurements (estimated from the standard deviation of replicate measurements) to obtain the ACD and calcification temperatures. We then calculated average ACDs and calcification temperatures for each sample from the individual iterations. Temperature estimates using all three approaches are compared in Table 3.

2.5. Linear regression

In order to account for the uncertainty in both Δ_{47} and calcification temperature, we calculate regression slopes and

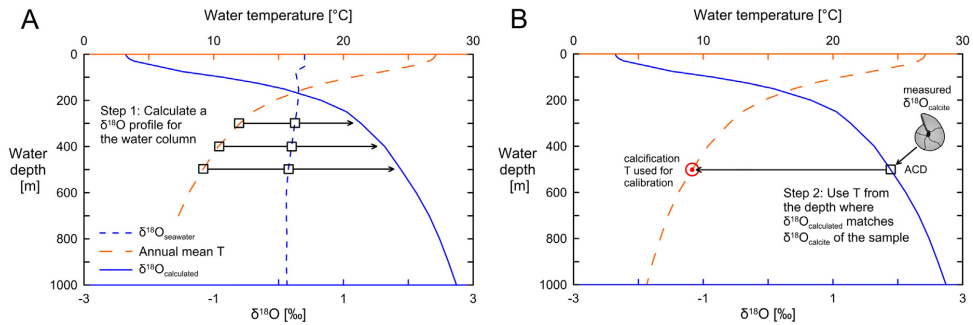


Fig. 2. Schematic drawing illustrating the two-step process (Method 3) used to assess apparent calcification temperatures from a combination of WOA-based temperature data and a $\delta^{18}\text{O}$ -T calibration. A: Annual mean temperature data (Locarnini et al., 2010) and $\delta^{18}\text{O}_{\text{seawater}}$ data (LeGrande and Schmidt, 2006) are used to generate a vertical $\delta^{18}\text{O}_{\text{calculated}}$ profile for calcite formed at any given location. B: The comparison between the measured $\delta^{18}\text{O}_{\text{calcite}}$ value of a foraminifer sample and the theoretical $\delta^{18}\text{O}_{\text{calculated}}$ profile is used to find the apparent calcification depth (ACD) of a foraminifer species. The annual mean water temperature at the ACD serves as best estimate for the calcification temperature of the foraminifer.

intercepts using the method of York et al. (2004). This method is commonly used in regression analysis of clumped isotope calibration data (e.g. Huntington et al., 2009; Grauel et al., 2013; Peral et al., 2018), thus helps facilitate the intercomparison of calibrations across studies. We estimated the uncertainty on the slope and intercept and 95% confidence envelopes on the regression lines using quantiles of 100,000 bootstrap samples. These were obtained by randomly resampling with replacement from the original data with its associated uncertainties, therefore maintaining the original sample size.

3. RESULTS

3.1. Δ_{47} , $\delta^{18}\text{O}$ and $\delta^{13}\text{C}$ data

Average data for each sample as well as environmental parameters such as the estimated $\delta^{18}\text{O}_{\text{seawater}}$ values and calcification temperatures reconstructed using various approaches (see Section 2.4) are summarized in Table 3. The average Δ_{47} data cover a range of 0.103‰ with a standard error of the mean for individual samples of 0.005–0.009. The lowest (0.653‰) and highest (0.756‰) Δ_{47} value correspond to the lowest (−2.29‰) and highest (3.66‰) $\delta^{18}\text{O}_{\text{calcite}}$ values, respectively (Fig. 3 A). Overall, there is a strong positive correlation (0.95 using Pearson's product-moment correlation) between both variables for the calculated averages. The standard deviation of replicate $\delta^{18}\text{O}$ measurements is 0.05–0.26‰ (standard error: 0.01–0.06‰). Mean $\delta^{13}\text{C}$ values for the samples measured in this study range between −1.2‰ and 3.2‰ with standard deviations between 0.04 and 0.24‰ (Fig. 3 B) and standard errors between 0.01 and 0.06‰. The $\delta^{13}\text{C}$ values and the Δ_{47} signal do not show a clear relationship. The standard errors of the mean and the standard deviations are not correlated with the mean Δ_{47} , $\delta^{18}\text{O}$ and $\delta^{13}\text{C}$, respectively. Moreover, there is no systematic difference in the isotopic composition between species with and without photosymbionts.

3.2. Calcification temperatures

Because the calcification temperatures of planktonic foraminifers are challenging to estimate, we approximated them using three approaches (see Section 2.4). All three methods reveal strong correlations (correlation coefficient between −0.91 and −0.95 using Pearson's product moment correlation) between estimated calcification temperature ($10^6/T^2$, T in K) and Δ_{47} . Detailed information on the regression lines derived from the different temperature estimates can be found in the Appendix (Table A3). Despite the strong correlations that were found for all the different methods, calcification temperature datasets differ from each other (Fig. 4A–D, Table 3).

The differences in estimated calcification temperature are largest between Method 1 using the World Ocean Atlas 2009 and the methods using $\delta^{18}\text{O}$ -T relationships (Fig. 4D). While the slopes of linear regression models for Methods 1 and 2 are similar (Fig. 4A), the dataset using WOA-based temperatures is characterized by larger variability (up to 13 °C temperature difference for similar Δ_{47} values, Fig. 4A). This is reflected in a lower correlation coefficient (−0.91 compared to −0.95 using Pearson's product-moment correlation). Hence, the uncertainty related to insufficient ecological information for certain species and/or regions seems to lead to a larger uncertainty for temperature estimates using Method 1 compared to $\delta^{18}\text{O}$ -based approaches (Methods 2 and 3).

When comparing calcification temperatures which were derived from two different $\delta^{18}\text{O}$ -T calibration equations (Shackleton, 1974; Kim and O'Neil, 1997) using Method 2 (Fig. 4D), temperature estimates for the tropical species largely agree (average temperature difference 0.7 °C), while towards the cold end of the calibration temperature estimates increasingly deviate from each other (maximum 2.2 °C). As a result, the regression calculated using the Kim and O'Neil (1997) $\delta^{18}\text{O}$ -T calibration reveals a flatter slope (Fig. 4B). The coldest temperature estimates

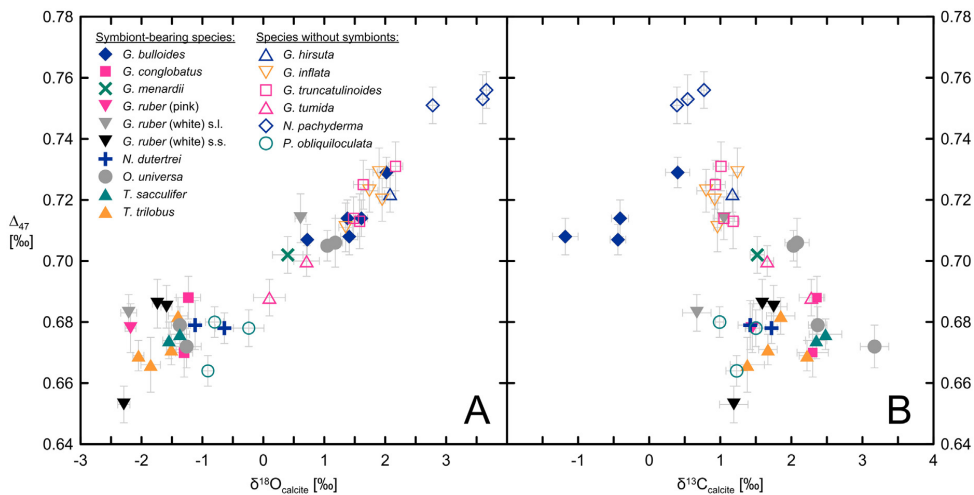


Fig. 3. Stable oxygen (A) and carbon isotopes (B) plotted against Δ_{47} . Symbols and colors represent different planktonic foraminifer species. Error bars illustrate one standard error for Δ_{47} and one standard deviation for $\delta^{18}\text{O}$ and $\delta^{13}\text{C}$. Note the positive correlation between $\delta^{18}\text{O}_{\text{calcite}}$ and Δ_{47} .

calculated using Kim and O'Neil (1997) are well below 0°C . These temperature estimates do not agree with the available temperature data from the WOA, neither with the annual mean temperature nor seasonal extremes. In contrast, temperatures calculated using the $\delta^{18}\text{O}$ -T calibration of Shackleton (1974) are in agreement with the temperature ranges reported in the WOA.

Temperatures estimated using Method 3 show a good agreement within the error estimates with those derived from Method 2 (Fig. 4C and D), and both datasets reveal similar correlation coefficients with Δ_{47} . The slopes of both linear regressions agree within error (Fig. 4C). Most samples reveal less than 1°C temperature differences between both methods (Methods 2 and 3). In most cases with larger offsets the measured $\delta^{18}\text{O}$ value of the sample is lighter (on average 0.22‰) than the $\delta^{18}\text{O}_{\text{calculated}}$ value at the sea surface. As Method 3 uses the temperature at sea surface whenever the $\delta^{18}\text{O}_{\text{calcite}}$ value is lighter than the $\delta^{18}\text{O}_{\text{calculated}}$ value at 0 m , the resulting temperature estimate is lower than the one that is only based on the $\delta^{18}\text{O}$ -T calibration.

4. DISCUSSION

4.1. Relationship between Δ_{47} and foraminifer calcification temperature

The method used to estimate calcification temperatures of planktonic foraminifers has an influence on the resulting Δ_{47} vs. temperature calibration. Fig. 4D demonstrates that the differences between Method 1 and Method 2 are pronounced for some of the samples, whereas others are less sensitive to the choice of method. We attribute this result to the varying accuracy of the ecological assumptions made for individual sites and species when using Method 1.

Therefore, the WOA-based temperature estimates generated using Method 1 appear less applicable for a temperature calibration than temperature estimates based on the better established $\delta^{18}\text{O}$ -T-relationship (Methods 2 and 3). Selecting an appropriate $\delta^{18}\text{O}$ -T calibration for the reconstruction of calcification temperatures from the $\delta^{18}\text{O}$ values is however crucial, as there are systematic differences between temperature estimates generated with different calibrations (Fig. 4D).

It is unlikely that the coldest temperature estimates generated with the calibration of Kim and O'Neil (1997) are accurate, as they do not agree with the WOA temperature data at these sites. A possible cause for this discrepancy between the two calibrations is inherent in the way they were generated: Both calibrations use data from a temperature range of $0\text{--}500^\circ\text{C}$ by combining foraminifer data and inorganic calcite data from a study of O'Neil et al. (1969). The calibration of Shackleton (1974) combined this extensive inorganic dataset with foraminifer samples covering a temperature range of $0\text{--}7^\circ\text{C}$ and was specifically proposed to represent cold temperature carbonate samples (Shackleton, 1974; reviewed in Pearson, 2012). In contrast, the calibration of Kim and O'Neil (1997) used samples from a temperature range of $10\text{--}40^\circ\text{C}$. Therefore, the latter equation may be less suitable to be applied to foraminifers calcifying at low water temperatures that are beyond the calibrated range. While acknowledging a remaining uncertainty related to the choice of $\delta^{18}\text{O}$ -T calibration, we surmise that the calibration of Shackleton (1974) is the most reliable basis for temperature reconstructions from diverse settings and for a large number of different species based on the arguments outlined above.

Whether this equation is used directly (Method 2) or combined with available temperature data (Method 3) has only minor influence on the resulting calibration line

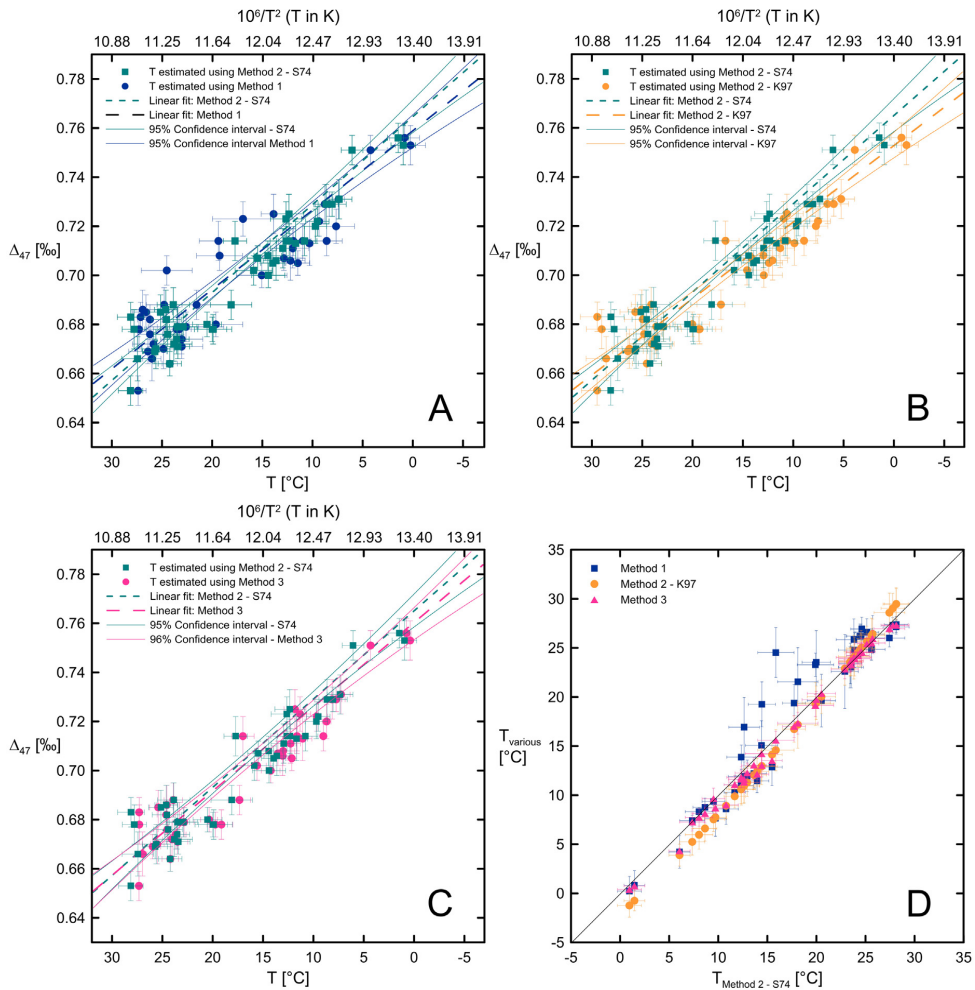


Fig. 4. Calcification temperatures estimated from three different methods versus Δ_{47} (A–C) and against each other (D). A: Method 1 using WOA-based temperature data (Locarnini et al., 2010) and a linear regression model (blue dots and blue dashed line) compared to Method 2 using the Shackleton (1974) equation (green filled squares and green dashed line). The 95% confidence intervals for Method 1 (blue) and Method 2 (green) are shown as solid lines. B: Method 2 using the Kim and O'Neil (1997) equation (orange dots and orange dashed line) and the Shackleton (1974) equation (green filled squares and green dashed line). Solid lines represent the 95% confidence intervals. C: Comparing Method 2 (green filled squares and green dashed line) to Method 3 (pink dots and pink dashed line), both approaches using the same $\delta^{18}\text{O}_{\text{calcite}}$ vs. temperature calibration (Shackleton, 1974). Solid lines represent the 95% confidence intervals. D: Comparison of temperatures estimated using Method 2 (Shackleton, 1974) with other temperature datasets used in A–C (blue dots: Method 1; orange dots: Method 2 using Kim and O'Neil (1997); pink dots: Method 3). Error bars represent the temperature uncertainty (A–D) in x direction and one standard error of the mean Δ_{47} (A–C) or the uncertainty of the temperature estimates (D) in y direction, as given in Table 3. (For interpretation of the references to colour in this figure legend, the reader is referred to the web version of this article.)

(Fig. 4C and D). One potential weakness of Method 3 compared to Method 2 is indicated by the observation that some sea surface sample values are not represented by the $\delta^{18}\text{O}_{\text{calculated}}$ profile. This could be explained by some unaccounted-for species-specific disequilibrium effects. Another reason for these $\delta^{18}\text{O}_{\text{calcite}}$ values that point to

warmer temperatures than the annual mean SST could be seasonality effects in the life cycle of certain foraminifer species. These effects may bias the signal towards summer temperatures. This could for example affect samples of *G. ruber* pink as well as *N. pachyderma* since both species may calcify relatively close to the sea surface and are reported to

reach maximum abundances during summer season (Table 2).

On the other hand, assumptions regarding foraminifer ecology might not represent all of the data equally well and can potentially introduce errors, as evident from Fig. 4A. Consequently, the advantage of Method 3 over Method 2 is its independence from any assumptions concerning the calcification depth of the analyzed specimens. Moreover, since the calcification temperatures are derived from WOA data, extreme temperature values outside the observed annual mean temperature are excluded. We therefore use calcification temperatures derived with Method 3 for all subsequent calculations.

The relationship between Δ_{47} and calcification temperatures, which were derived from Method 3 and the application of the York regression, leads to the following regression equation:

$$\Delta_{47} = (0.0397 \pm 0.0021) * 10^6 / T^2 + (0.2259 \pm 0.0255) \quad (T \text{ in K}) \quad (1)$$

The Δ_{47} data for all measured species follow a clear linear relationship (Fig. 5) albeit with noticeable scatter, which is most pronounced at the warm end of the calibration (>22 °C). Interestingly, earlier studies (Tripathi et al., 2010, Grauel et al., 2013) have observed the opposite (i.e., larger variability at the cold temperature end, see Section 4.2). The observed variability is not related to a specific site being systematically offset from the general trend (Fig. 5A), but may stem from a variety of reasons as discussed in the following.

The small amounts (<5 mg) of sample material measured in this study may have led to a slightly larger scatter than observed in the recent foraminifer-based Δ_{47} -T calibration by Peral et al. (2018) where 16–20 mg were used. The samples in this study integrate over fewer individual specimens (minimum ~100) than studies measuring larger samples and could be affected by individual tests that deviate from the mean Δ_{47} values. Hence, the scatter of the Δ_{47} signal could likely be reduced further by measuring more replicates at the expense of slightly larger sample requirements.

Besides the measurement procedure, there are several potential reasons for individual samples to deviate from the described Δ_{47} -T relationship, related to either the calcification temperatures that were calculated from $\delta^{18}\text{O}_{\text{calcite}}$ or the Δ_{47} values. Because calcification temperatures can only be estimated, any divergence from the true calcification temperature can potentially cause affected samples to deviate from the general trend. Surface water conditions in particular can be highly variable (e.g. on a seasonal scale), potentially influencing the isotopic signal recorded by the foraminifers (e.g. Curry et al., 1983). However, potential seasonal temperature effects are largely accounted for by the combined approach of calculating $\delta^{18}\text{O}$ values and using WOA-based water temperatures (Method 3).

Despite the fact that planktonic foraminifers appear to calcify slightly offset from isotopic equilibrium with respect to stable oxygen isotopes of ambient seawater (Daeron et al., 2019), we do not see clear evidence that species-specific disequilibrium effects on $\delta^{18}\text{O}$ enhanced variability in our dataset. Species-specific correction for disequilibrium

effects using published values would result in colder temperature estimates for several tropical surface species (Appendix Table A2). However, since there is a wide range of published disequilibrium correction factors (e.g. 0.0–1.0‰ for *G. ruber* (white), Niebler et al. (1999)), it remains difficult to assess its influence on the temperature estimates. Depending on the choice of correction factor for each species, the scatter of tropical surface-dwelling species in the Δ_{47} signal may in fact increase. In any case, a disequilibrium correction of the $\delta^{18}\text{O}_{\text{calcite}}$ signal moves the data of several warm-water surface species in the same direction and thus will not reduce the scatter of the data (Appendix Table A2 and Fig. A1).

Early diagenetic alterations such as secondary calcite precipitates grown at colder water temperatures may bias calcification temperature reconstructions from $\delta^{18}\text{O}$ measurements towards colder values (e.g. Pearson, 2012). However, such alteration should affect both the $\delta^{18}\text{O}$ and the Δ_{47} signal and bias all samples from the same site towards colder temperatures. Especially if two species from the same site are characterized by similar calcification depths, early diagenetic effects should be similar for both. Yet, the calculated calcification temperatures from $\delta^{18}\text{O}_{\text{calcite}}$ of different surface-dwelling species from the same sites generally agree well: For example, at site SO164-25-3 located in the Caribbean differences of up to 0.029‰ in the Δ_{47} signal were observed for surface species assumed to calcify at similar depth. For the same species the $\delta^{18}\text{O}$ -based temperature estimates are characterized by a relatively small difference ≤ 1.8 °C (see Fig. 5A) and SEM images taken for several species at this site did not reveal any signs of secondary calcification. Moreover, we take the aforementioned good agreement between the temperatures calculated from $\delta^{18}\text{O}$ (Method 2) and temperature estimates based on WOA data in combination with published calcification depths (Method 1) as indication that the $\delta^{18}\text{O}$ signal is not altered (average temperature difference for tropical species: 0.7 °C). Due to the fact that clumped isotopes are only dependent on the mineral formation temperature, a stronger influence of early diagenesis on the Δ_{47} signal than on $\delta^{18}\text{O}$ is unlikely and has not been observed, even in samples as old as 44 Ma (Leutert et al., 2019).

Possible short-term variability of the surface water $\delta^{18}\text{O}$ due to salinity changes could introduce larger variability of the $\delta^{18}\text{O}_{\text{calcite}}$ signal of surface-dwelling species (reviewed in Pearson, 2012). For instance, site SO164-25-3 is located in an area that is influenced by the Amazon and Orinoco River plumes and may thus be experiencing considerable salinity changes (Schmuker and Schiebel, 2002). A surface-water salinity effect that influences the oxygen isotope signal of the upper water column could potentially bias the estimated calcification temperature of surface species at site SO164-25-3. For this site, however, we measured several surface-dwelling species including three morphotypes of the same species, *G. ruber* (*G. ruber* white s.s., s.l. and *G. ruber* pink). Although the $\delta^{18}\text{O}_{\text{calcite}}$ measurements from all three morphotypes agree well, not only among this species but also with other species from the same site, the Δ_{47} signal of these three samples reveals notable differences (~0.03‰). Moreover, none of the species measured for this site is characterized by a particularly variable $\delta^{18}\text{O}_{\text{calcite}}$

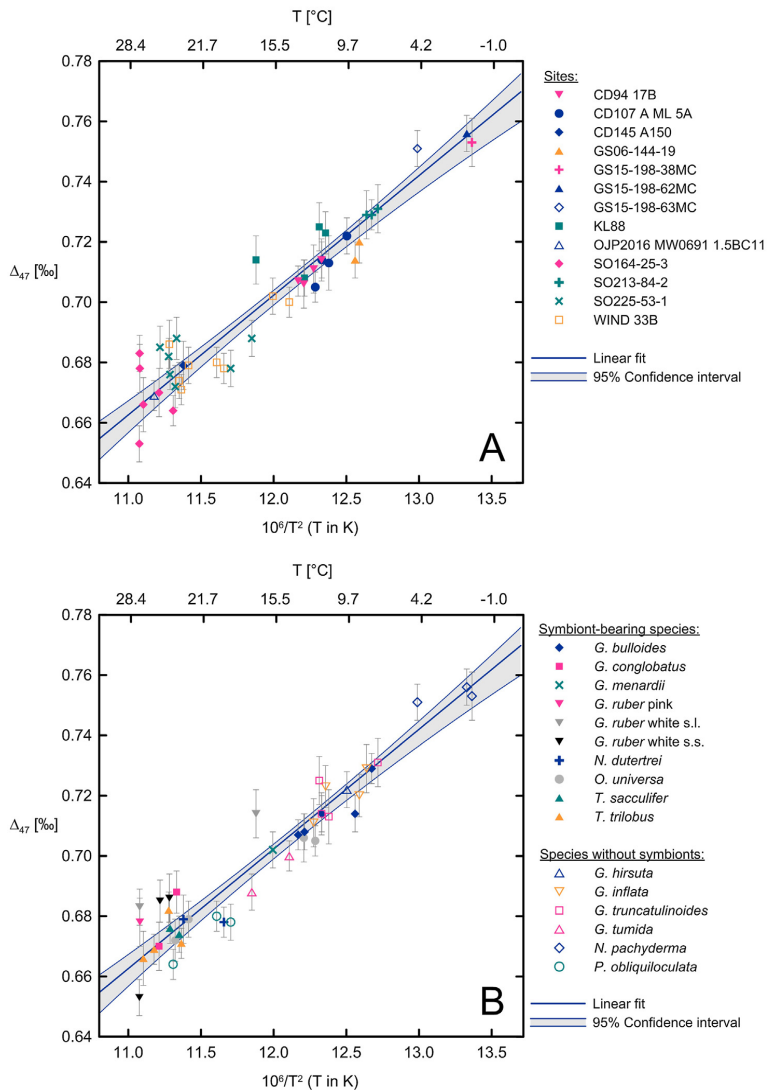


Fig. 5. The Δ_{47} -temperature relationship for planktonic foraminifers measured in this study by site (A) and species (B). Error bars represent the standard error of the mean Δ_{47} values (in per mil) (Table 3). Calcification temperatures are given in $10^6/T^2$ (T in K) and °C. The blue line and gray shaded area show the linear regression (Eq. (1)) and 95% confidence interval.

signal (SD of 0.09–0.16) and the calculated calcification temperatures are similar to the WOA-based estimates.

As suggested by various studies (e.g. Spero et al., 1997), pH affects the $\delta^{18}\text{O}$ signal of foraminiferal calcite towards more negative values with increasing pH. This effect was estimated by Zeebe (1999) to amount to -1.42‰ per unit of pH. The presence of photosymbionts is expected to increase the internal pH of foraminifers by up to 0.5 pH units (Rink et al., 1998) and thereby could bias tempera-

tures calculated from $\delta^{18}\text{O}_{\text{calcite}}$ towards warmer values (reviewed in Pearson, 2012). For benthic foraminifers, on the other hand, Marchitto et al. (2014) found no clear pH effect. If pH had a strong influence on the calcification temperatures estimated from $\delta^{18}\text{O}_{\text{calcite}}$ in this study we would expect all symbiont-bearing species to reveal systematically warmer temperatures and disagree with atlas-based (Method 1) temperatures. Although this is not the case we cannot exclude that pH effects contributed some

additional scatter to the $\delta^{18}\text{O}_{\text{calcite}}$ signal of surface-dwelling species. Potential pH effects on the Δ_{47} signal will be discussed in Section 4.2. We suggest that the number of replicate measurements is the most important factor causing scatter in our foraminiferal Δ_{47} -T dataset. Nonetheless, we will investigate the data for species-specific effects possibly contributing to the scatter of the Δ_{47} signal in the following section.

4.2. Species-specific effects

The question whether the Δ_{47} in planktonic foraminifers is influenced by any species-specific effects is of vital importance to the application of this proxy for paleoceanography, since the absence of species effects would imply that Δ_{47} can be applied far back in time, despite evolutionary changes in species composition. Previous Δ_{47} -T calibration studies on foraminifers found large scatter and a potential discrepancy between foraminifers and inorganic calibrations at the cold end of the calibration (Tripathi et al., 2010; Grauel et al., 2013), which were attributed to kinetic effects during the calcification process on foraminifers in cold-water conditions resulting in lower and more variable Δ_{47} values. In this study, in contrast, we observe neither increased scatter nor deviations towards low Δ_{47} in the cold-end foraminifer samples (Fig. 5). Cold-water species such as *N. pachyderma* from multiple sites do not reveal systematically negative, larger residuals. While most species are distributed relatively close to the calibration line ($\leq 0.01\text{‰}$) and do not reveal any systematic offset, there are a few exceptions (Fig. 6A): One of two samples measured on *G. conglobatus* (site SO225-53-1 from the Manihiki Plateau) plots $\sim 0.015\text{‰}$ above the linear fit. Furthermore, all but one of the *G. ruber* samples from multiple sites are

characterized by higher Δ_{47} values (residuals 0.01–0.02‰). This includes all three morphotypes of *G. ruber* measured in this study. Furthermore, all three samples of *P. obliquiloculata* show lower Δ_{47} values with two of them $< -0.010\text{‰}$.

Taking the uncertainty of the calcification temperature estimates and the clumped isotope measurements into account, the measured, species-specific Δ_{47} data from this study do not reveal any statistically significant deviation from the linear relationship determined for the entire dataset. Some species are only represented by a single sample, whereas up to six samples from different sites were included for species that are frequently used for paleoceanography (such as *G. bulloides*, *G. ruber* and *N. pachyderma*). The limited temperature ranges of individual species do not allow for the calculation of individual, species-specific regression lines.

To further test the influence of individual species or genera on the Δ_{47} -T calibration, we removed consecutively certain taxa from the dataset and compared the resulting slopes of the calibrations to the slope of the entire dataset (Fig. 6B). All of the slopes calculated for such data subsets fall within the 95% confidence interval of the slope calculated for the entire dataset. The two species that have the largest influence on the slope are *N. pachyderma* and *G. ruber*. This observation could be related to the position of the data from these two species at the cold (*N. pachyderma*) and warm end (*G. ruber*) of the dataset as the regression line is particularly sensitive to data at both ends of the temperature range. The dataset without *N. pachyderma* is characterized by a flatter slope (0.0380 compared to 0.0397 for the entire dataset). This deviation could be explained by the fact that the exclusion of this cool ($< 10\text{ °C}$), high-latitude species from the dataset reduces the entire temperature-range by 7 °C and hence raises the uncertainty of the

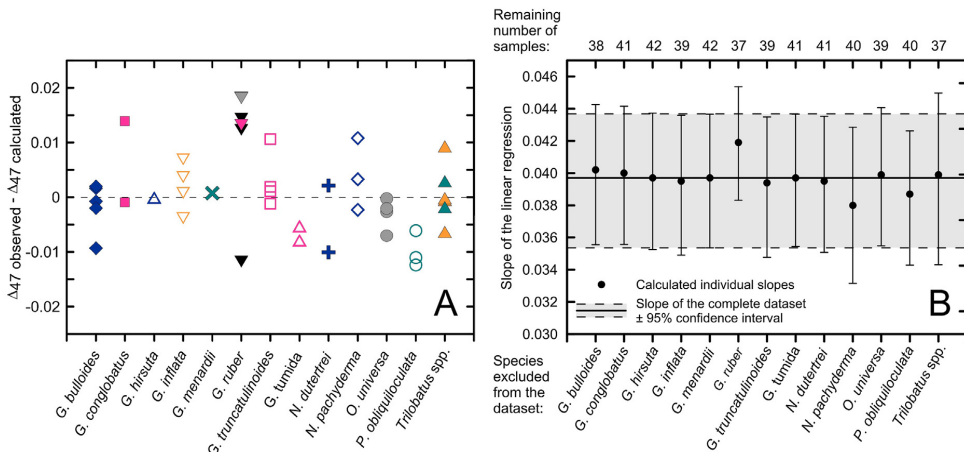


Fig. 6. Evaluation of possible species-specific effects on the calibration; A: Δ_{47} residuals of single foraminifer species, calculated as deviation from the linear regression presented in Fig. 5 (individual species/species groups are displayed by different symbols and colors similar to Fig. 5B). The residuals show no significant trend. B: Calculated slopes of the linear regression for subsets of the data (black dots) excluding one species at a time to test the influence of individual species on the calibration. The black line represents the slope of the complete dataset (grey area: 95% confidence interval of the mean slope). Error bars represent the 95% confidence intervals of the slopes.

Δ_{47} -T calibration (standard error raised from 0.0021‰ to 0.0025‰).

For *G. ruber*, all but one sample are offset by on average 0.015‰ to a higher Δ_{47} value (lower temperature) from the calculated Δ_{47} -T regression line of the entire dataset (Figs. 5B, 6A). The linear fit calculated for the dataset without *G. ruber* exhibits the steepest slope (0.0419) of any of the subsets presented in Fig. 6B, suggesting that these data exert the strongest influence on the regression, albeit not significant at the 95% confidence level. This relatively large effect on the slope despite the temperature range of the dataset being largely unaltered may imply that the *G. ruber* Δ_{47} -T dependency is different from other planktonic foraminifer species. However, the observation that not all *G. ruber* data show the offset to higher Δ_{47} values is inconsistent with this hypothesis. For Caribbean site SO164-25-3, for example, we analyzed three different morphotypes of *G. ruber* (*G. ruber* white s.s. s.l. and *G. ruber* pink). Two of these samples (*G. ruber* white s.l. and *G. ruber* pink) show the offset to higher Δ_{47} , whereas the third morphotype (*G. ruber* white s.s.) reveals a lower (by ~ 0.03 ‰) Δ_{47} value than the other two and plots below the regression line (Fig. 5B). Moreover, Δ_{47} in *G. ruber* was also analyzed in the recent study by Peral et al. (2018), which did not reveal systematic species-specific behavior of *G. ruber*, although one of three samples was characterized by slightly higher Δ_{47} . Overall, evidence regarding species-specific effects in *G. ruber* is inconclusive and we do not consider *G. ruber* to calcify systematically offset from other species of foraminifers with respect to Δ_{47} . Individual samples of other species (such as *G. conglobatus*) also deviate from the linear regression to a similar degree. A combination of the intrinsic uncertainty of the clumped isotope measurement together with natural variability of the sample material could explain the observed scatter of the Δ_{47} -T data, including the apparent deviation of *G. ruber* from the trend.

However, we cannot rule out the existence of relatively small and possibly variable secondary influences on the Δ_{47} signal during the calcification process in the surface water. The fact that the shallowest surface-dwelling species *G. ruber* shows the strongest deviation of individual samples from the general Δ_{47} -T relationship raises the question, whether there could be additional effects besides temperature on Δ_{47} in species living close to the sea surface. This has been described for other groups of marine calcifying organisms as well. Tropical shallow-water corals, for example, show increasing Δ_{47} with increasing calcification rates (Saenger et al., 2012). Kinetic effects on the Δ_{47} signal related to growth rates in brachiopods were shown by Bajnai et al. (2018). Moreover, Davies and John (2019) reported evidence for a constant offset of echinoid Δ_{47} values from inorganic calcite that might be related to internal pH of the calcifying fluid in echinoids being offset from seawater pH. If this was true for foraminifers as well, the effect would be expected to be larger for symbiont-bearing species such as *G. ruber* because the internal pH in these species was reported to be higher (Rink et al., 1998). In contrast to this hypothesis, however, Tang et al. (2014) observed in inorganic calcite precipitation experiments that the Δ_{47} -T relationship is largely insensitive to pH and growth

rate at the external and internal conditions expected during foraminifer calcification. Tripathi et al. (2015) also found that even major changes in ocean chemistry (pH and salinity) expected during the Cenozoic have only small to negligible effects on the Δ_{47} signal of marine carbonates.

One potential explanation for increased scatter of the Δ_{47} values in surface-dwelling planktonic foraminifers could be the additional influence of photosynthesis on the calcification process: Photosymbionts may potentially cause disequilibrium effects on the recorded Δ_{47} signal because they are not only altering the microenvironment from which calcite is excreted but also by affecting calcification rates (de Nooijer et al., 2014). An effect of strong photosynthesis in plants on Δ_{47} measured in residual CO_2 gas was demonstrated by Laskar and Liang (2016), who also reported plant photosynthesis to decouple the $\delta^{18}\text{O}$ and Δ_{47} values. However, studies investigating photosynthesis in foraminifers found that both the kind of symbionts and the concentration of chlorophyll as a measure for photosynthetic activity in *G. ruber* are similar to other species, such as *T. sacculifer* (Fujiki et al., 2014; Takagi et al., 2019). This would suggest

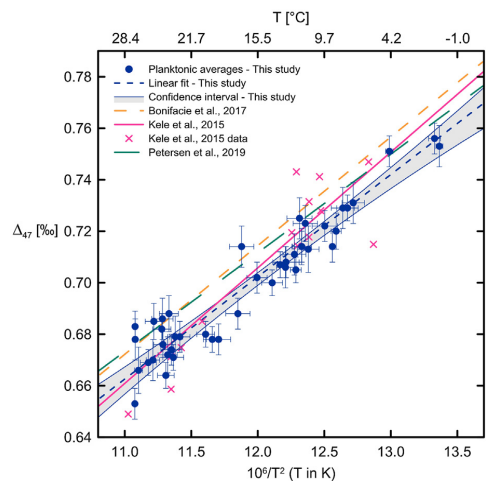


Fig. 7. Comparison of various Δ_{47} -T calibrations. Clumped isotope data from this study (blue symbols) and the calculated linear regression (dashed blue line) including confidence intervals (gray shaded area) is compared with published data and calibration lines including the compilation of Bonifacie et al. (2017; yellow dashed line), the travertine calibration of Kele et al. (2015; pink line and symbols) recalculated by Bernasconi et al. (2018), and the composite synthetic carbonate calibration of Petersen et al. (2019; green dashed line). The calibration of Bonifacie et al. (2017) and Petersen et al. (2019) contain data from several individual studies that were measured, standardized, and corrected in various ways. Therefore, the individual data of the Bonifacie et al. (2017) and Petersen et al. (2019) compilations are characterized by a larger variability and thus, are not presented here. Error bars in x and y-direction represent the temperature uncertainty and one standard error of the mean Δ_{47} , respectively, as presented in Table 3. (For interpretation of the references to colour in this figure legend, the reader is referred to the web version of this article.)

that any effect photosynthesis may have on Δ_{47} in *G. ruber* should also occur in other symbiont-bearing species, whereas we do not observe any systematic difference between symbiont-bearing and non-symbiotic foraminifer species (Fig. 5B). Because *G. ruber* has a shallower habitat depth than most other planktonic foraminifers (e.g. Wang, 2000), the influence of photosynthesis might be larger on this species than on deeper-dwelling symbiotic species. A higher symbiont density under high-light conditions likely affects the calcification process of *G. ruber* as already suggested for boron isotopes (see Hönisch and Hemming, 2004). However, this effect cannot explain the differences of the Δ_{47} signal in three morphotypes of *G. ruber* from the same site (see Fig. 5). In particular the *G. ruber* (white) s.s. morphotype reported to live closest to the sea surface yields Δ_{47} values closest to the calibration line. More work is needed to test possible secondary influences on the incorporation of the Δ_{47} signal and evaluate whether there might be any significant species-specific effects in *G. ruber* and similar shallow-dwelling species.

4.3. Comparison with other clumped isotope calibrations

Our data is in overall good agreement with recent clumped isotope calibrations of Bonifacie et al. (2017), Kele et al. (2015) as recalculated by Bernasconi et al. (2018), and Petersen et al. (2019) (Fig. 7). Our linear regression has a slope between the flatter Petersen et al. (2019) calibration and steeper slopes published by Bonifacie et al. (2017) and Kele et al. (2015) (Table 4). Since the slope and intercept are negatively correlated for the regression analysis the intercept of our regression is higher than the ones published by Bonifacie et al. (2017) and Kele et al. (2015). The Petersen et al. (2019) calibration, which is based on a compilation of synthetic carbonate data shows a slight but apparently systematic offset towards higher Δ_{47} values compared to our data. Most of the datasets included in this compilation, as well as in the compilation by Bonifacie et al.

(2017), however, used different analytical and data correction procedures compared to our study.

Bonifacie et al. (2017) combines data from various existing calibrations that were generated on a variety of analytical setups and using different standards. Also, several of the datasets included in the Bonifacie et al. (2017) calibration were calculated with the parameter set for ^{17}O correction by Gonfiantini et al. (1995), which were later shown to have caused discrepancies among samples with very different bulk compositions (Daëron et al., 2016; Schauer et al., 2016). For example, the intercept of the travertine calibration of Kele et al. (2015) decreased by 0.038‰ with the updated ^{17}O abundance correction of Brand et al. (2010) (Bernasconi et al., 2018). However, the original data are included in the compilation of Bonifacie et al. (2017). Recalculating the calibration of Bonifacie et al. (2017) using the updated Kele dataset might therefore lead to a lower intercept and move this calibration closer to our calibration (Eq. (1)).

The underlying data of the (fully recalculated, see Bernasconi et al., 2018) travertine calibration by Kele et al. (2015) agree well with our foraminifer data (Fig. 7). This is most likely due to similarity in analytical set-up, raw data treatment and correction using the same carbonate standard values. Differences in data correction and/or analytical procedures may thus explain some degree of systematic offset between calibrations. In addition, Fernandez et al. (2017) pointed out that a small temperature range of some Δ_{47} -T calibrations is among the important factors that can explain discrepancies between various calibration lines. Given the small temperature range biogenic samples like foraminifers cover, the slight discrepancies between calibrations are not surprising.

4.4. Comparison of foraminifer-based calibrations

Comparing our data to recent Δ_{47} -T calibrations of Peral et al. (2018), Piasecki et al. (2019) and Breitenbach et al. (2018) (Fig. 8) contributes to the ongoing debate regarding

Table 4

Our foraminifer-based Δ_{47} -T calibration compared to recent clumped isotope calibrations in the 25 °C reference frame. All calibrations except for Bonifacie et al. (2017) and Petersen et al. (2019) were calculated using ETH carbonate standards and the correction for temperature dependent acid fractionation that was published by Defliese et al. (2015). The equation published by Bonifacie et al. (2017) was converted to the 25 °C reference frame using a correction for temperature-dependent acid fractionation of 0.082‰ (Defliese et al., 2015) on the intercept. The intercept of the Petersen et al. (2019) calibration was lowered by -0.004‰ (see Section 2.3) for comparability with equations based on the acid fractionation factors published by Defliese et al. (2015).

Regression	Slope * $10^6/\text{T}^2 \pm 1$ SE	Intercept ± 1 SE	Type of material
Bonifacie et al. (2017)	0.0422 \pm 0.0019	0.208 \pm 0.0207	Various – compilation of existing calibration data
Breitenbach et al. (2018) (foraminifer dataset)	0.0315 \pm 0.008	0.313 \pm 0.1	Foraminifers
Breitenbach et al. (2018) (Cambridge calibration)	0.0448 \pm 0.007	0.154 \pm 0.08	Natural cave carbonates (cave pearls)
Kele et al. (2015) (fully recalculated)	0.0449 \pm 0.001	0.167 \pm 0.01	Inorganic carbonates (travertines, tufas)
Peral et al. (2018)	0.04163 \pm 0.00084	0.2056 \pm 0.0011	Foraminifers
Petersen et al. (2019)	0.0383 \pm 1.7E ⁻⁶	0.258 \pm 1.7E ⁻⁵	Compilation of synthetic carbonate data
Piasecki et al. (2019)	0.0460 \pm 0.005	0.159 \pm 0.064	Benthic foraminifers
This study	0.0397 \pm 0.0021	0.2259 \pm 0.0255	Planktonic foraminifers
Combined calibration (Breitenbach et al., 2018, Peral et al., 2018, Piasecki et al., 2019, this study)	0.0418 \pm 0.0016	0.2017 \pm 0.0195	Foraminifers
Combined calibration (Peral et al., 2018, Piasecki et al., 2019, this study)	0.0431 \pm 0.0016	0.1876 \pm 0.0189	Foraminifers

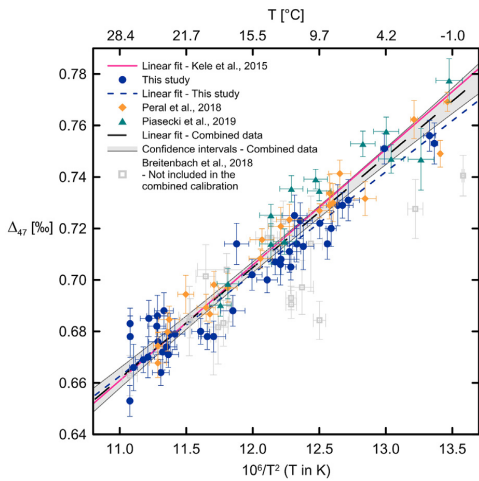


Fig. 8. Compilation of available foraminiferal Δ_{47} -T calibrations. The planktonic foraminiferal data from this study (blue symbols and dashed line) are compared to foraminiferal data from Peral et al. (2018) with temperatures recalculated using Method 3 (orange diamonds), benthic foraminiferal data (site averages) from Piasecki et al. (2019) (green triangles) and planktonic foraminiferal data from Breitenbach et al. (2018) with recalculated temperatures using Method 3 (gray squares). Moreover, a combined foraminiferal calibration (black dashed line) including 95% confidence intervals (gray shaded area) for the data from this study, Peral et al. (2018), and Piasecki et al. (2019) is presented with the recalculated calibration line of Kele et al. (2015; pink line) for comparison. Error bars in y-direction represent one standard error of the mean Δ_{47} . Error bars in x-direction show the calculated temperature uncertainty for Breitenbach et al. (2018), Peral et al. (2018) and this study and an assigned constant uncertainty of ± 1 °C for Piasecki et al., 2019. Note that the foraminiferal data from Breitenbach et al. (2018) were not included in the combined calibration due to the larger variability of the dataset (also discussed in Breitenbach et al., 2018). (For interpretation of the references to colour in this figure legend, the reader is referred to the web version of this article.)

inter-laboratory differences and improves foraminiferal-based Δ_{47} -T calibration efforts. In order to treat the datasets consistently, we recalculated calcification temperatures for the datasets of Peral et al. (2018) and Breitenbach et al. (2018) using Method 3. The previously published bottom water temperatures for the benthic dataset of Piasecki et al. (2019) were kept. Bottom water conditions are assumed to be relatively constant over time, such that instrumental measurements can be regarded as reliable to calibrate Δ_{47} -data of benthic foraminifera. Such an approach independently verifies that the calculated planktonic calcification temperatures are realistic, provided that neither planktonic nor benthic foraminifera record Δ_{47} values significantly offset from the inorganic Δ_{47} -T relationship.

In general, the datasets are in good agreement across the entire temperature range from -1 to 28 °C. The benthic foraminiferal Δ_{47} data of Piasecki et al. (2019) was generated in the same laboratory as the data from this study and seem to

indicate a slight deviation from our planktonic Δ_{47} -T calibration towards higher Δ_{47} values for temperatures below 15 °C. At the same time, the variability of the benthic Δ_{47} data at the cold end of the calibration is relatively large. This can be explained by individual data points that contain less replicate measurements due to sample limitations.

The planktonic foraminiferal Δ_{47} -T data from Breitenbach et al. (2018) are characterized by a larger scatter. While all four datasets presented in Fig. 8 overlap for the warm end of the Δ_{47} -T calibration, Δ_{47} values at the cold end (<13 °C) tend to be lower by ~ 0.02 – 0.03 ‰ in the Breitenbach dataset. Breitenbach et al. (2018) acknowledge the small number of samples and replicates as well as the relatively large scatter of the dataset, which was generated with the primary purpose of comparing Δ_{47} and Mg/Ca.

The data from Peral et al. (2018) show excellent agreement with our measurements, with confidence intervals overlapping for the whole temperature range. This is particularly noteworthy as the two datasets were derived with completely different analytical setups: In this study, samples were digested at 70 °C in a Kiel IV carbonate preparation device with a short Porapak column and subsequently measured on a Thermo Fisher Scientific MAT 253 Plus in microvolume mode with the LIDI approach. In contrast, Peral et al. (2018) used a common acid bath operated at 90 °C, a GC column for contaminant removal, and carried out the isotope measurements on a VG Isoprime mass spectrometer under constant gas pressure. The good agreement of the data provides further evidence that different measurement techniques provide comparable Δ_{47} data as long as they are corrected using the same carbonate standards (in this case ETH 1-4; Bernasconi et al. 2018) and the “Brand parameters” for the ^{17}O abundance correction (Daëron et al., 2016; Schauer et al., 2016).

Based on these considerations, the various recent datasets containing foraminiferal Δ_{47} data with comparable data treatment were combined to enhance the accuracy of an overarching Δ_{47} -T calibration valid for all foraminiferal species. We excluded the Δ_{47} data of Breitenbach et al. (2018) due to the small number of replicate measurements (although we report a version of a combined foraminiferal-based calibration including this dataset in Table 4). The resulting Δ_{47} -T calibration encompassing the data of Peral et al. (2018), Piasecki et al. (2019) and this study (Eq. (2), Fig. 8) falls within the error of the regression exclusively derived from our data (which is characterized by a slightly flatter slope) and emphasizes the conformity and compatibility of the three Δ_{47} datasets:

$$\Delta_{47} = (0.0431 \pm 0.0016) * 10^6/T^2 + (0.1876 \pm 0.0189) (T \text{ in K}) \quad (2)$$

The recalculated version of the Kele et al. (2015) calibration (see Bernasconi et al., 2018) lies within the confidence interval of the combined foraminiferal Δ_{47} -T calibration presented here. For the calibrated temperature range our combined calibration yields temperature estimates within 1 °C of the Kele et al. (2015) calibration with the largest difference at the cold end of the calibrated temperature range. Given the fact that the Kele et al. (2015) calibration used the same carbonate standards for the corrections, this

agreement suggests that foraminifers follow the same Δ_{47} -T relationship as the travertines. We note that this agreement between our combined foraminifer-based calibration and the Kele travertine calibration does not exclude the possibility that all of these carbonates are influenced by some degree of disequilibrium fractionation (Watkins and Hunt, 2015; Daeron et al., 2019).

For future studies using foraminifer samples we recommend applying our combined foraminifer-based calibration (Eq. (2)) rather than the recalculated travertine calibration of Kele et al. (2015). Although the Kele et al. (2015) calibration has the advantage of covering a much wider temperature range our combined calibration is based on a large number of foraminifer samples from different studies and laboratories. Hence it is characterized by a smaller uncertainty within the normal ocean temperature range compared to the Kele et al. (2015) calibration. However, the reconstructed temperatures applying either of the two calibrations fall within less than 1 °C of each other. Using the long-integration dual-inlet (LIDI) method a sample size of 2–5 mg of foraminifers is enough for 20 to 40 replicate measurements, which is the equivalent of a temperature uncertainty of 1.5 °C or less on the measurement.

4.5. Water column temperature gradients

A widely accepted approach to gain a deeper understanding on past oceanographic changes is to combine geochemical information (e.g. combined analyses of foraminiferal Mg/Ca and $\delta^{18}\text{O}$) from calcitic tests of shallow and deep-dwelling foraminifer species, allowing reconstruction of water column

stratification. Based on the notion that there are no discernible species effects on the Δ_{47} -T calibration presented above (Eq. (2)) and the close agreement with the travertine-based Kele calibration (Kele et al., 2015), we test how reliably vertical temperature gradients can be reconstructed from foraminiferal Δ_{47} data. We compare Δ_{47} -derived temperatures from various species from two Pacific and Indian Ocean sites to annual mean water temperatures and seasonal extremes at these locations (Locarnini et al., 2010) (Fig. 9). To avoid circular reasoning, the Δ_{47} -temperature estimates were derived from the Kele calibration and plotted at the respective assumed calcification depths of the species, based on the available ecological information (c.f. Table 3). This exercise should be seen as a feasibility study.

Within error, the Δ_{47} -temperature estimates from almost all foraminifer species compare to the annual mean temperature at the respective sample locations. The absolute temperature difference of ~ 15 °C between the two sites is well reflected in the Δ_{47} -temperature signal. On the vertical scale, shallow-dwelling species commonly show higher Δ_{47} -temperatures than deep-dwelling species, and the reconstructed temperature differences reflect the different gradients at the two sites very well. Only *G. menardii* and *G. ruber* from site WIND 33B in the Indian Ocean yield Δ_{47} -temperatures that appear too cold for their assumed calcification depths (by 5 and 6 °C, respectively, Fig. 9). The calcification temperature reconstructed for *G. menardii* suggests a habitat in the lower thermocline at this site, lower than commonly assumed, which is also seen in the deeper $\delta^{18}\text{O}$ -based apparent calcification depth (Table 3). The apparent cold bias of *G. ruber* is a recurrent feature

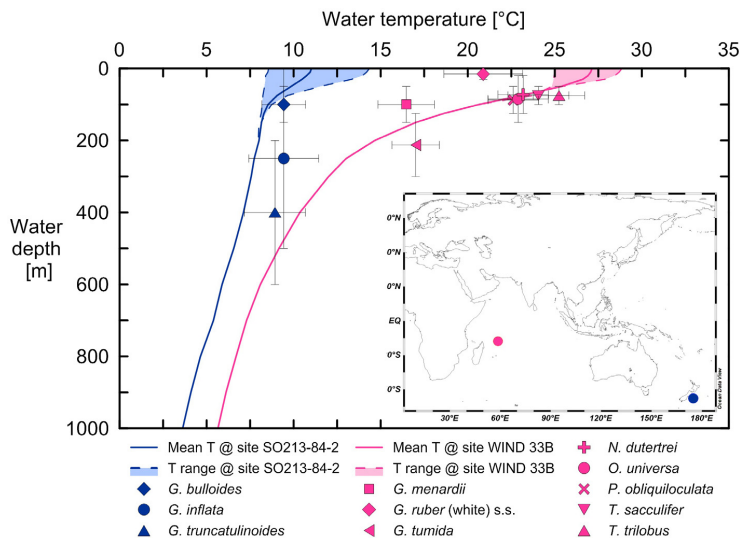


Fig. 9. Atlas-based mean annual water temperature (solid lines) and seasonal temperature range (dashed lines) (Locarnini et al., 2010) for sites SO213-84-2 (blue) and WIND 33-B (pink) and clumped isotope temperatures (using the calibration published by Kele et al., 2015, recalculated by Bernasconi et al. (2018)) plotted against water depth/assumed calcification depth (Table 3). Error bars in x-direction represent the temperature uncertainty due to the standard mean error of the measurement while the error bars in y-direction show the uncertainty of the calcification depth based on the available information presented in Table 3.

observed at various sites and ocean settings in this study as discussed above. Overall, this exercise demonstrates that Δ_{47} can be used to reconstruct vertical temperature gradients within the water column while avoiding the uncertainty introduced by the use of individual, species-specific calibrations for other foraminifer-based geochemical proxies.

5. CONCLUSION

By analyzing Δ_{47} in 14 species from 13 globally distributed core-top samples, this study confirms findings from previous studies (Tripati et al., 2010; Grauel et al., 2013; Peral et al., 2018) that found foraminifers to follow the same relationship between Δ_{47} and the carbonate formation temperature as inorganic calcite. The substantial number of different foraminifer species analysed here, as well as the large number of samples from different sites for some species greatly increases confidence in this finding. Although small species-specific effects within the analytical uncertainty cannot be completely ruled out, no significant systematic effect could be identified in this study. The only possible deviation from the Δ_{47} -T relationship that cannot be explained by the uncertainty associated with foraminiferal ecology is the mixed-layer species *G. ruber*, showing apparent cold biases in some samples. However, the results for this species remain inconclusive, warranting a more detailed study on the clumped isotope signal in *G. ruber*.

We demonstrate that results from different laboratories and various measurement setups are in good agreement when the Δ_{47} data are corrected using the same carbonate standards and the latest ^{17}O abundance correction parameters. The combination of natural variability, relatively large uncertainties of the estimated calcification temperatures and the comparatively small natural temperature range affect the precision of any Δ_{47} -T calibration based only on foraminifers. We minimize this problem by combining several available foraminifer-based calibrations and calculating a common Δ_{47} -T calibration. Within the error, this combined calibration is identical to the recalculated travertine calibration of Kele et al. (2015) (see Bernasconi et al., 2018). Temperatures reconstructed using either of the two calibrations fall within less than 1 °C of each other. Because of the smaller uncertainty within the ocean temperature range, we recommend using our combined calibration (Eq. (2)) for foraminifer samples. Finally, we show that the reconstruction of temperature profiles through the water column from clumped isotope measurements is feasible using micro-volume measurements on different species within the same sample.

Declaration of Competing Interest

The authors declare that they have no known competing financial interests or personal relationships that could have appeared to influence the work reported in this paper.

ACKNOWLEDGEMENTS

We thank Eystein Jansen at the University of Bergen and NORCE Norwegian Research Centre AS and Trond

Dokken and Bjørg Risebrobakken at NORCE for the provision of sample material. We would also like to thank Henrik Sadatzki at the University of Bergen for helping with the sample preparation. Radiocarbon dates for the GS15 samples were kindly provided by the ice2ice project funded by the European Research Council under European Community's Seventh Framework Programme (FP7/2007-2013) ERC grant agreement 610055. We thank Eivind W. N. Støren for access to the facilities of EARTHLAB and Enver Alagoz, Pål Tore Mørkved and the clumped isotope group at the University of Bergen for laboratory assistance and technical support during the analysis. We are grateful to Alison Piasecki for discussions and input. We also thank the reviewers for the constructive comments that helped to improve the manuscript. This work was funded by the Trond Mohn Foundation and the European Research Council (ERC) under the European Union's Horizon 2020 research and innovation programme (grant agreement No 638467). The UCLA contribution was supported by the Department of Energy through BES grant DE-FG02-13ER16402.

RESEARCH DATA

The raw replicate level data of this study are available at EarthChem (URL: <https://doi.org/doi:10.1594/IEDA/111435>).

APPENDIX A

See Figs. A1 and A2 and Table A1–A3.

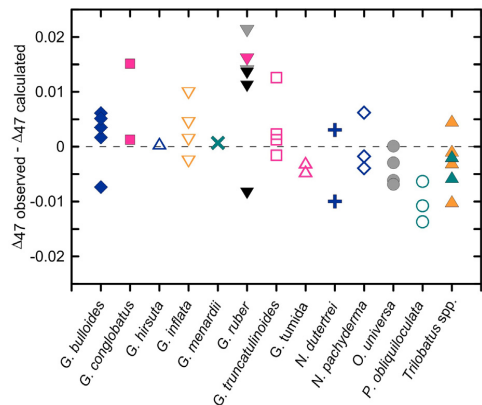


Fig. A1. Residual values for the resulting linear regression after species-specific disequilibrium correction factors (Appendix Table A2) were applied. The data are differentiated for each species (displayed by different symbols and colors as in Fig. 5B). Applying species-specific disequilibrium corrections to the $\delta^{18}\text{O}_{\text{calcite}}$ data prior to calculating the calcification temperature does not result in smaller residual values compared to Fig. 6A.

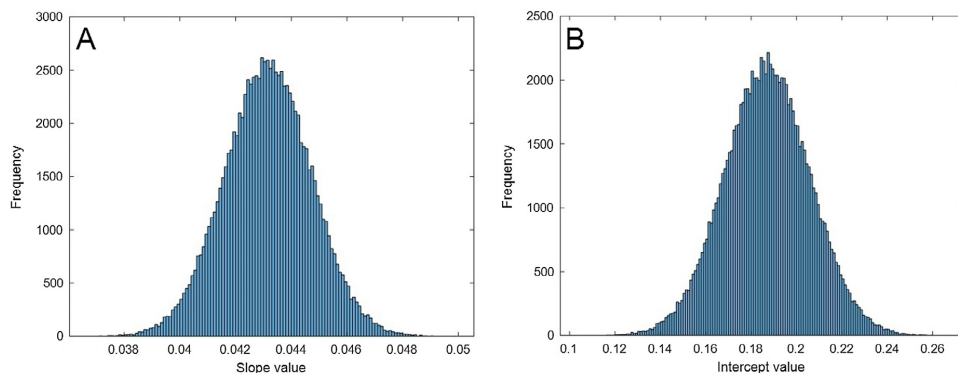


Fig. A2. Histograms showing the distribution of slopes (A) and intercepts (B) of the combined calibration across the 100,000 iterations calculated.

Table A1

External reproducibility of standard measurements. For the measuring interval from October 2016 to October 2017, the carbonate standards ETH 1, 3 and 4 were used for correction and the carbonate standard ETH 2 for monitoring. From November 2017 to March 2018, ETH 1, 2 and 3 were utilized for correction and ETH 4 for monitoring.

Standard	$\delta^{13}\text{C}$ VPDB SD external	$\delta^{18}\text{O}$ VPDB SD external	Δ_{47} CDES SD external
<i>Measurement interval from 2016/10/21 13:14 to 2017/10/14 17:06</i>			
ETH-1 (n = 957)	0.021	0.042	0.036
ETH-2 (n = 967), monitoring	0.022	0.045	0.035
ETH-3 (n = 982)	0.027	0.048	0.033
ETH-4 (n = 967)	0.020	0.042	0.031
<i>Measurement interval from 2017/11/30 16:17 to 2018/03/14 07:29</i>			
ETH-1 (n = 458)	0.045	0.087	0.037
ETH-2 (n = 402)	0.061	0.097	0.034
ETH-3 (n = 460)	0.063	0.106	0.036
ETH-4 (n = 456), monitoring	0.059	0.112	0.038

Table A2

Disequilibrium offset correction factors tested for the $\delta^{18}\text{O}_{\text{calcite}}$ measurements that were used to estimate calcification temperatures.

Species	Disequilibrium offset correction	Reference
<i>Globigerina bulloides</i>	0.25	Niebler et al. (1999)
<i>Globigerinoides conglobatus</i>	-0.2	Niebler et al. (1999)
<i>Globigerinoides ruber pink</i>	-0.4	Steph et al. (2009)
<i>Globigerinoides ruber white s.l.</i>	-0.4	Steph et al. (2009)
<i>Globigerinoides ruber white s.s.</i>	-0.4	Steph et al. (2009), Rippert et al. (2016)
<i>Globorotalia hirsuta</i>	-0.15	Niebler et al. (1999)
<i>Globorotalia inflata</i>	0	Niebler et al. (1999), Cl�eroux et al. (2013)
<i>Globorotalia menardii</i>	-0.2	Niebler et al. (1999), Steph et al. (2009)
<i>Globorotalia truncatulinoides</i>	-0.05	Niebler et al. (1999), Cl�eroux et al. (2013)
<i>Globorotalia tumida</i>	0	Niebler et al. (1999), Steph et al. (2009), Cl�eroux et al. (2013)
<i>Neogloboquadrina dutertrei</i>	-0.27	Niebler et al. (1999), Cl�eroux et al. (2013)
<i>Neogloboquadrina pachyderma</i>	-0.75	Niebler et al. (1999)
<i>Orbulina universa</i>	-0.3	Niebler et al. (1999)
<i>Pulleniatina obliquiloculata</i>	-0.3	Niebler et al. (1999)
<i>Trilobatus sacculifer</i>	-0.6	Steph et al. (2009), Rippert et al. (2016)
<i>Trilobatus trilobus</i>	-0.6	Steph et al. (2009), Rippert et al. (2016)

Table A3

Correlation coefficients (Pearson's product-moment correlation), slopes and intercepts calculated using various calcification temperatures for the following linear regression: $\Delta_{47} = (m \pm SE) * 10^6/T^2 + (b \pm SE) (T \text{ in K})$.

Method used to estimate calcification temperature	Correlation coefficient	Slope (m)	SE	Intercept (b)	SE
Method 1 – World Ocean Atlas 2009	−0.9120348	0.0375	0.0022	0.2543	0.0269
Method 2 – Kim and O'Neil, 1997	−0.9494287	0.0360	0.0018	0.2677	0.0219
Method 2 – Shackleton, 1974	−0.9493258	0.0415	0.0021	0.2054	0.0253
Method 3 – Shackleton, 1974	−0.947849	0.0397	0.0021	0.2259	0.0255
Method 3 – Shackleton, 1974 – disequilibrium-corrected	−0.9487466	0.0411	0.0021	0.2056	0.0263

REFERENCES

- Bajnai D., Fiebig J., Tomasovych A., Milner Garcia S., Rollion-Bard C., Raddatz J., Löffler N., Primo-Ramos C. and Brand U. (2018) Assessing kinetic fractionation in brachiopod calcite using clumped isotopes. *Sci. Rep.* **8**, 533.
- Barker S., Greaves M. and Elderfield H. (2003) A study of cleaning procedures used for foraminiferal Mg/Ca paleothermometry. *Geochem. Geophys. Geosyst.* **4**, n/a-n/a.
- Bemis B. E., Spero H. J., Bijma J. and Lea D. W. (1998) Reevaluation of the oxygen isotopic composition of planktonic foraminifera: experimental results and revised paleotemperature equations. *Paleoceanography* **13**, 150–160.
- Bernasconi S. M., Hu B., Wacker U., Fiebig J., Breitenbach S. F. and Rutz T. (2013) Background effects on Faraday collectors in gas-source mass spectrometry and implications for clumped isotope measurements. *Rapid Commun. Mass Spectrom.* **27**, 603–612.
- Bernasconi S. M., Müller I. A., Bergmann K. D., Breitenbach S. F. M., Fernandez A., Hodell D. A., Jaggi M., Meckler A. N., Millan I. and Ziegler M. (2018) Reducing uncertainties in carbonate clumped isotope analysis through consistent carbonate-based standardization. *Geochem. Geophys. Geosyst.*
- Bigeleisen J. and Mayer M. G. (1947) Calculation of equilibrium constants for isotopic exchange reactions. *J. Chem. Phys.* **15**, 261.
- Bonifacie M., Calmels D., Eiler J. M., Horita J., Chaduteau C., Vasconcelos C., Agrinier P., Katz A., Passey B. H., Ferry J. M. and Bourrand J.-J. (2017) Calibration of the dolomite clumped isotope thermometer from 25 to 350°C, and implications for a universal calibration for all (Ca, Mg, Fe)CO₃ carbonates. *Geochim. Cosmochim. Acta* **200**, 255–279.
- Brand W. A., Assonov S. S. and Coplen T. B. (2010) Correction for the 17O interference in δ (13C) measurements when analyzing CO₂ with stable isotope mass spectrometry (IUPAC Technical Report). *Pure Appl. Chem.* **82**, 1719–1733.
- Brassell S., Eglinton G., Marlowe I., Pflaumann U. and Sarnthein M. (1986) Molecular stratigraphy: a new tool for climatic assessment. *Nature* **320**, 129–133.
- Breitenbach S. F. M., Mleneck-Vautraviers M. J., Grauel A.-L., Lo L., Bernasconi S. M., Müller I. A., Rolfe J., Gázquez F., Greaves M. and Hodell D. A. (2018) Coupled Mg/Ca and clumped isotope analyses of foraminifera provide consistent water temperatures. *Geochim. Cosmochim. Acta* **236**, 283–296.
- Cléroux C., deMenocal P., Arbuszewski J. and Linsley B. (2013) Reconstructing the upper water column thermal structure in the Atlantic Ocean. *Paleoceanography* **28**, 503–516.
- Curry W. B., Thunell R. C. and Honjo S. (1983) Seasonal changes in the isotopic composition of planktonic foraminifera collected in Panama Basin sediment traps. *Earth Planet. Sci. Lett.* **64**, 33–43.
- Daëron M., Blamart D., Peral M. and Affek H. (2016) Absolute isotopic abundance ratios and the accuracy of Δ_{47} measurements. *Chem. Geol.* **442**, 83–96.
- Daëron M., Drysdale R. N., Peral M., Huyghe D., Blamart D., Coplen T. B., Lartaud F. and Zanchetta G. (2019) Most Earth-surface calcites precipitate out of isotopic equilibrium. *Nat. Commun.* **10**, 429.
- Davies A. J. and John C. M. (2019) The clumped (13C18O) isotope composition of echinoid calcite: further evidence for “vital effects” in the clumped isotope proxy. *Geochim. Cosmochim. Acta* **245**, 172–189.
- de Nooijer L. J., Spero H. J., Erez J., Bijma J. and Reichart G. J. (2014) Biomineralization in perforate foraminifera. *Earth Sci. Rev.* **135**, 48–58.
- Defliese W. F., Hren M. T. and Lohmann K. C. (2015) Compositional and temperature effects of phosphoric acid fractionation on Δ_{47} analysis and implications for discrepant calibrations. *Chem. Geol.* **396**, 51–60.
- Dennis K. J., Affek H. P., Passey B. H., Schrag D. P. and Eiler J. M. (2011) Defining an absolute reference frame for ‘clumped’ isotope studies of CO₂. *Geochim. Cosmochim. Acta* **75**, 7117–7131.
- Deuser W. and Ross E. (1989) Seasonally abundant planktonic foraminifera of the Sargasso Sea; succession, deep-water fluxes, isotopic compositions, and paleoceanographic implications. *J. Foraminiferal Res.* **19**, 268–293.
- Eiler J. M. (2007) “Clumped-isotope” geochemistry—the study of naturally-occurring, multiply-substituted isotopologues. *Earth Planet. Sci. Lett.* **262**, 309–327.
- Eiler J. M. and Schauble E. (2004) 18O13C16O in Earth's atmosphere. *Geochim. Cosmochim. Acta* **68**, 4767–4777.
- Emiliani C. (1966) Isotopic paleotemperatures. *Science* **154**, 851–857.
- Epstein S., Buchsbaum R., Lowenstam H. and Urey H. C. (1951) Carbonate-water isotopic temperature scale. *GSA Bull.* **62**, 417–426.
- Epstein S., Buchsbaum R., Lowenstam H. A. and Urey H. C. (1953) Revised carbonate-water isotopic temperature scale. *Geol. Soc. Am. Bull.* **64**, 1315–1326.
- Evans D., Sagoo N., Renema W., Cotton L. J., Müller W., Todd J. A., Saraswati P. K., Stassen P., Ziegler M., Pearson P. N., Valdes P. J. and Affek H. P. (2018) Eocene greenhouse climate revealed by coupled clumped isotope-Mg/Ca thermometry. *Proceedings of the National Academy of Sciences.*
- Ezard T. H. G., Edgar K. M. and Hull P. M. (2015) Environmental and biological controls on size-specific $\delta^{13}\text{C}$ and $\delta^{18}\text{O}$ in recent planktonic foraminifera. *Paleoceanography* **30**, 151–173.
- Fernandez A., Müller I. A., Rodríguez-Sanz L., van Dijk J., Looser N. and Bernasconi S. M. (2017) A reassessment of the precision of carbonate clumped isotope measurements: implications for calibrations and paleoclimate reconstructions. *Geochem. Geophys. Geosyst.* **18**, 4375–4386.
- Fujiki T., Takagi H., Kimoto K., Kurasawa A., Yuasa T. and Mino Y. (2014) Assessment of algal photosynthesis in planktic foraminifera by fast repetition rate fluorometry. *J. Plankton Res.* **36**, 1403–1407.
- Ghosh P., Adkins J., Affek H., Balta B., Guo W., Schauble E. A., Schrag D. and Eiler J. M. (2006) 13C–18O bonds in carbonate minerals: a new kind of paleothermometer. *Geochim. Cosmochim. Acta* **70**, 1439–1456.

- Ghosh P., Eiler J., Campana S. E. and Feeney R. F. (2007) Calibration of the carbonate 'clumped isotope' paleothermometer for otoliths. *Geochim. Cosmochim. Acta* **71**, 2736–2744.
- Gonfiantini R., Stichler W. and Rozanski K. (1995) Reference and intercomparison materials for stable isotopes of light elements. *IAEA TECDOC* **825**, 67–74.
- Grauel A.-L., Schmid T. W., Hu B., Bergami C., Capotondi L., Zhou L. and Bernasconi S. M. (2013) Calibration and application of the 'clumped isotope' thermometer to foraminifera for high-resolution climate reconstructions. *Geochim. Cosmochim. Acta* **108**, 125–140.
- Groeneveld J. and Chiessi C. M. (2011) Mg/Ca of Globorotalia inflata as a recorder of permanent thermocline temperatures in the South Atlantic. *Paleoceanography* **26**, n/a-n/a.
- Henkes G. A., Passey B. H., Wanamaker A. D., Grossman E. L., Ambrose W. G. and Carroll M. L. (2013) Carbonate clumped isotope compositions of modern marine mollusk and brachiopod shells. *Geochim. Cosmochim. Acta* **106**, 307–325.
- Ho S. L., Mollenhauer G., Fietz S., Martínez-García A., Lamy F., Rueda G., Schipper K., Méheust M., Rosell-Melé A., Stein R. and Tiedemann R. (2014) Appraisal of TEX86 and TEX86L thermometries in subpolar and polar regions. *Geochim. Cosmochim. Acta* **131**, 213–226.
- Hu B., Radke J., Schluter H. J., Heine F. T., Zhou L. and Bernasconi S. M. (2014) A modified procedure for gas-source isotope ratio mass spectrometry: the long-integration dual-inlet (LIDI) methodology and implications for clumped isotope measurements. *Rapid Commun. Mass Spectrom.* **28**, 1413–1425.
- Huntington K. W., Eiler J. M., Afek H. P., Guo W., Bonifacie M., Yeung L. Y., Thiagarajan N., Passey B., Tripathi A., Daeron M. and Came R. (2009) Methods and limitations of 'clumped' CO₂ isotope (Delta47) analysis by gas-source isotope ratio mass spectrometry. *J. Mass Spectrom.* **44**, 1318–1329.
- Hut, G. (1987) Consultants' group meeting on stable isotope reference samples for geochemical and hydrological investigations.
- Hönisch B. and Hemming N. G. (2004) Ground-truthing the boron isotope-paleo-pH proxy in planktonic foraminifera shells: partial dissolution and shell size effects. *Paleoceanography* **19**.
- Jentzen A., Nürnberg D., Hathorne E. C. and Schönfeld J. (2018) Mg/Ca and $\delta^{18}\text{O}$ in living planktic foraminifers from the Caribbean, Gulf of Mexico and Florida Straits. *Biogeosciences* **15**, 7077–7095.
- John C. M. and Bowen D. (2016) Community software for challenging isotope analysis: first applications of 'Easotope' to clumped isotopes. *Rapid Commun. Mass Spectrom.* **30**, 2285–2300.
- Kele S., Breitenbach S. F. M., Capezzuoli E., Meckler A. N., Ziegler M., Millan I. M., Kluge T., Deák J., Hanselmann K., John C. M., Yan H., Liu Z. and Bernasconi S. M. (2015) Temperature dependence of oxygen- and clumped isotope fractionation in carbonates: a study of travertines and tufas in the 6–95°C temperature range. *Geochim. Cosmochim. Acta* **168**, 172–192.
- Kelson J. R., Huntington K. W., Schauer A. J., Saenger C. and Lechler A. R. (2017) Toward a universal carbonate clumped isotope calibration: diverse synthesis and preparatory methods suggest a single temperature relationship. *Geochim. Cosmochim. Acta* **197**, 104–131.
- Kim S.-T. and O'Neil J. R. (1997) Equilibrium and nonequilibrium oxygen isotope effects in synthetic carbonates. *Geochim. Cosmochim. Acta* **61**, 3461–3475.
- Laskar A. H. and Liang M.-C. (2016) Clumped isotopes in near-surface atmospheric CO₂ over land, coast and ocean in Taiwan and its vicinity. *Biogeosciences* **13**, 5297–5314.
- Lea D. W., Mashiotta T. A. and Spero H. J. (1999) Controls on magnesium and strontium uptake in planktonic foraminifera determined by live culturing. *Geochim. Cosmochim. Acta* **63**, 2369–2379.
- LeGrande A. N. and Schmidt G. A. (2006) Global gridded data set of the oxygen isotopic composition in seawater. *Geophys. Res. Lett.* **33**.
- Leutert T. J., Sexton P. F., Tripathi A., Piasecki A., Ho S. L. and Meckler A. N. (2019) Sensitivity of clumped isotope temperatures in fossil benthic and planktic foraminifera to diagenetic alteration. *Geochim. Cosmochim. Acta* **257**, 354–372.
- Locarnini R., Mishonov A., Antonov J., Boyer T., Garcia H., Baranova O., Zweng M. and Johnson D. (2010) *World Ocean Atlas 2009, Volume 1: Temperature*. S. Levitus, Ed. NOAA Atlas NESDIS 68. US Government Printing Office, Washington, DC, p. 184.
- Marchitto T. M., Curry W. B., Lynch-Stieglitz J., Bryan S. P., Cobb K. M. and Lund D. C. (2014) Improved oxygen isotope temperature calibrations for cosmopolitan benthic foraminifera. *Geochim. Cosmochim. Acta* **130**, 1–11.
- Meckler A. N., Ziegler M., Millan M. I., Breitenbach S. F. and Bernasconi S. M. (2014) Long-term performance of the Kiel carbonate device with a new correction scheme for clumped isotope measurements. *Rapid Commun. Mass Spectrom.* **28**, 1705–1715.
- Molina-Kescher M., Frank M. and Hathorne E. C. (2014) Nd and Sr isotope compositions of different phases of surface sediments in the South Pacific: Extraction of seawater signatures, boundary exchange, and detrital/dust provenance. *Geochem. Geophys.* **15**, 3502–3520.
- Mulitza S., Dürkoop A., Hale W., Wefer G. and Stefan Niebler H. (1997) Planktonic foraminifera as recorders of past surface-water stratification. *Geology* **25**, 335.
- Niebler H.-S., Hubberten H.-W. and Gersonde R. (1999) Oxygen isotope values of planktic foraminifera: a tool for the reconstruction of surface water stratification. In *Use of Proxies in Paleoceanography*. Springer, pp. 165–189.
- Nürnberg D., Bijma J. and Hemleben C. (1996) Assessing the reliability of magnesium in foraminiferal calcite as a proxy for water mass temperatures. *Geochim. Cosmochim. Acta* **60**, 803–814.
- O'Neil J. R., Clayton R. N. and Mayeda T. K. (1969) Oxygen isotope fractionation in divalent metal carbonates. *J. Chem. Phys.* **51**, 5547–5558.
- Pearson P. N. (2012) Oxygen isotopes in foraminifera: overview and historical review. *Paleontol. Soc. Pap.* **18**, 1–38.
- Peral M., Daëron M., Blamart D., Bassinot F., Dewilde F., Smialkowski N., Isguder G., Bonnin J., Jorissen F., Kissel C., Michel E., Vázquez Riveiros N. and Waelbroeck C. (2018) Updated calibration of the clumped isotope thermometer in planktonic and benthic foraminifera. *Geochim. Cosmochim. Acta* **239**, 1–16.
- Petersen S. V., Deffense W. F., Saenger C., Daëron M., Huntington K. W., John C. M., Kelson J. R., Bernasconi S. M., Coleman A. S., Kluge T., Olack G. A., Schauer A. J., Bajnai D., Bonifacie M., Breitenbach S. F. M., Fiebig J., Fernandez A. B., Henkes G. A., Hodell D., Katz A., Kele S., Lohmann K. C., Passey B. H., Peral M. Y., Petrizzo D. A., Rosenheim B. E., Tripathi A., Venturelli R., Young E. D. and Winkelstern I. Z. (2019) Effects of improved 17O correction on inter-laboratory agreement in clumped isotope calibrations, estimates of mineral-specific offsets, and temperature dependence of acid digestion fractionation. *Geochem. Geophys. Geosyst.*
- Piasecki A., Bernasconi S. M., Grauel A.-L., Hannisdal B., Ho S. L., Leutert T. J., Marchitto T. M., Meinicke N., Tisserand A. and Meckler N. (2019) Application of clumped isotope thermometry to benthic foraminifera. *Geochem. Geophys. Geosyst.*
- Polik C. A., Elling F. J. and Pearson A. (2018) Impacts of paleoecology on the TEX86 sea surface temperature proxy in

- the pliocene-pleistocene mediterranean sea. *Paleoceanogr. Paleoceanol.* **33**, 1472–1489.
- Prahl F. G., Muehlhausen L. A. and Zahnle D. L. (1988) Further evaluation of long-chain alkenones as indicators of paleoceanographic conditions. *Geochim. Cosmochim. Acta* **52**, 2303–2310.
- Raddatz J., Nürnberg D., Tiedemann R. and Rippert N. (2017) Southeastern marginal West Pacific Warm Pool sea-surface and thermocline dynamics during the Pleistocene (2.5–0.5 Ma). *Palaeogeogr. Palaeoclimatol. Palaeoecol.* **471**, 144–156.
- Regenberg M., Nürnberg D., Steph S., Groeneveld J., Garbeschönberg D., Tiedemann R. and Dullo W.-C. (2006) Assessing the effect of dissolution on planktonic foraminiferal Mg/Ca ratios: Evidence from Caribbean core tops. *Geochim. Geophys. Geosyst.* **7**.
- Regenberg M., Steph S., Nürnberg D., Tiedemann R. and Garbeschönberg D. (2009) Calibrating Mg/Ca ratios of multiple planktonic foraminiferal species with $\delta^{18}\text{O}$ -calcification temperatures: paleothermometry for the upper water column. *Earth Planet. Sci. Lett.* **278**, 324–336.
- Rink S., Kühl M., Bijma J. and Spero H. (1998) Microsensor studies of photosynthesis and respiration in the symbiotic foraminifer *Orbulina universa*. *Mar. Biol.* **131**, 583–595.
- Rippert N., Nürnberg D., Raddatz J., Maier E., Hathorne E., Bijma J. and Tiedemann R. (2016) Constraining foraminiferal calcification depths in the western Pacific warm pool. *Mar. Micropaleontol.* **128**, 14–27.
- Saenger C., Affek H. P., Felis T., Thiagarajan N., Lough J. M. and Holcomb M. (2012) Carbonate clumped isotope variability in shallow water corals: temperature dependence and growth-related vital effects. *Geochim. Cosmochim. Acta* **99**, 224–242.
- Schauble E. A., Ghosh P. and Eiler J. M. (2006) Preferential formation of ^{13}C – ^{18}O bonds in carbonate minerals, estimated using first-principles lattice dynamics. *Geochim. Cosmochim. Acta* **70**, 2510–2529.
- Schauer A. J., Kelson J., Saenger C. and Huntington K. W. (2016) Choice of (17) O correction affects clumped isotope (Δ_{47}) values of CO_2 measured with mass spectrometry. *Rapid Commun. Mass Spectrom.* **30**, 2607–2616.
- Schiebel R. and Hemleben C. (2017) *Planktic Foraminifers in the Modern Ocean*. Springer.
- Schlitzer, R. (2018) Ocean data view. <http://odv.awi.de>.
- Schmid T. W. and Bernasconi S. M. (2010) An automated method for 'clumped-isotope' measurements on small carbonate samples. *Rapid Commun. Mass Spectrom.* **24**, 1955–1963.
- Schmuker B. and Schiebel R. (2002) Planktic foraminifers and hydrography of the eastern and northern Caribbean Sea. *Mar. Micropaleontol.* **46**, 387–403.
- Schouten S., Hopmans E. C., Schefuß E. and Sinninghe Damsté J. S. (2002) Distributional variations in marine crenarchaeotal membrane lipids: a new tool for reconstructing ancient sea water temperatures? *Earth Planet. Sci. Lett.* **204**, 265–274.
- Shackleton, N. (1974) Attainment of isotopic equilibrium between ocean water and the benthonic foraminifera genus *Uvigerina*: isotopic changes in the ocean during the last glacial.
- Shackleton N. J., Wiseman J. D. H. and Buckley H. A. (1973) Non-equilibrium isotopic fractionation between seawater and planktonic foraminiferal tests. *Nature* **242**, 177.
- Spencer C. and Kim S.-T. (2015) Carbonate clumped isotope paleothermometry: a review of recent advances in CO_2 gas evolution, purification, measurement and standardization techniques. *Geosci. J.* **19**, 357–374.
- Spero H. J., Bijma J., Lea D. W. and Bemis B. E. (1997) Effect of seawater carbonate concentration on foraminiferal carbon and oxygen isotopes. *Nature* **390**, 497.
- Steph S., Regenberg M., Tiedemann R., Mulitza S. and Nürnberg D. (2009) Stable isotopes of planktonic foraminifera from tropical Atlantic/Caribbean core-tops: Implications for reconstructing upper ocean stratification. *Mar. Micropaleontol.* **71**, 1–19.
- Takagi H., Kimoto K., Fujiki T., Saito H., Schmidt C., Kucera M. and Moriya K. (2019) Characterizing photosymbiosis in modern planktonic foraminifera. *Biogeosciences* **16**, 3377–3396.
- Tang J., Dietzel M., Fernandez A., Tripati A. K. and Rosenheim B. E. (2014) Evaluation of kinetic effects on clumped isotope fractionation (Δ_{47}) during inorganic calcite precipitation. *Geochim. Cosmochim. Acta* **134**, 120–136.
- Tripati A. K., Eagle R. A., Thiagarajan N., Gagnon A. C., Bauch H., Halloran P. R. and Eiler J. M. (2010) ^{13}C – ^{18}O isotope signatures and 'clumped isotope' thermometry in foraminifera and coccoliths. *Geochim. Cosmochim. Acta* **74**, 5697–5717.
- Tripati A. K., Hill P. S., Eagle R. A., Mosenfelder J. L., Tang J., Schauble E. A., Eiler J. M., Zeebe R. E., Uchikawa J., Coplen T. B., Ries J. B. and Henry D. (2015) Beyond temperature: clumped isotope signatures in dissolved inorganic carbon species and the influence of solution chemistry on carbonate mineral composition. *Geochim. Cosmochim. Acta* **166**, 344–371.
- Tripati A. K., Sahany S., Pittman D., Eagle R. A., Neelin J. D., Mitchell J. L. and Beaufort L. (2014) Modern and glacial tropical snowlines controlled by sea surface temperature and atmospheric mixing. *Nat. Geosci.* **7**, 205.
- Turich C., Freeman K. H., Bruns M. A., Conte M., Jones A. D. and Wakeham S. G. (2007) Lipids of marine archaea: patterns and provenance in the water-column and sediments. *Geochim. Cosmochim. Acta* **71**, 3272–3291.
- Urey H. C. (1947) The thermodynamic properties of isotopic substances. *J. Chem. Soc. (Resumed)*, 562–581.
- Wacker U., Fiebig J., Tödter J., Schöne B. R., Bahr A., Friedrich O., Tütken T., Gischler E. and Joachimski M. M. (2014) Empirical calibration of the clumped isotope paleothermometer using calcites of various origins. *Geochim. Cosmochim. Acta* **141**, 127–144.
- Wang L. (2000) Isotopic signals in two morphotypes of *Globigerinoides ruber* (white) from the South China Sea: implications for monsoon climate change during the last glacial cycle. *Palaeogeogr. Palaeoclimatol. Palaeoecol.* **161**, 381–394.
- Wang Z., Schauble E. A. and Eiler J. M. (2004) Equilibrium thermodynamics of multiply substituted isotopologues of molecular gases. *Geochim. Cosmochim. Acta* **68**, 4779–4797.
- Watkins J. M. and Hunt J. D. (2015) A process-based model for non-equilibrium clumped isotope effects in carbonates. *Earth Planet. Sci. Lett.* **432**, 152–165.
- York D., Evensen N. M., Martinez M. L. and De Basabe Delgado J. (2004) Unified equations for the slope, intercept, and standard errors of the best straight line. *Am. J. Phys.* **72**, 367–375.
- Yu J., Thornalley D. J., Rae J. W. and McCave N. I. (2013) Calibration and application of B/Ca, Cd/Ca, and $\delta^{11}\text{B}$ in *Neogloboquadrina pachyderma* (sinistral) to constrain CO_2 uptake in the subpolar North Atlantic during the last deglaciation. *Paleoceanography* **28**, 237–252.
- Zaarur S., Affek H. P. and Brandon M. T. (2013) A revised calibration of the clumped isotope thermometer. *Earth Planet. Sci. Lett.* **382**, 47–57.
- Zachos J., Pagani M., Sloan L., Thomas E. and Billups K. (2001) Trends, rhythms, and aberrations in global climate 65 Ma to present. *Science* **292**, 686–693.
- Zeebe R. E. (1999) An explanation of the effect of seawater carbonate concentration on foraminiferal oxygen isotopes. *Geochim. Cosmochim. Acta* **63**, 2001–2007.

**Errata for
Clumped isotope thermometry in foraminifera - From
calibration to Plio-Pleistocene temperature
reconstructions in the Indo-Pacific Warm Pool**

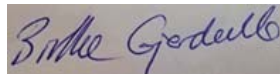
Niklas Meinicke



Thesis for the degree philosophiae doctor (PhD)
at the University of Bergen

09.06.2020 

(date and sign. of candidate)



(date and sign. of faculty)

Errata

Pages 1-30, 79-110 and 132-155 Order of literature references changed from alphabetical to chronological

Page 91 Incorrect unit for Mg/Ca ratios: “‰” – corrected to “mmol/mol”

Page 92 Incorrect unit for Mg/Ca ratios in Figure 2: “‰” – corrected to “mmol/mol”

Page 98 Incorrect figure caption for Figure 4: “Error bars for the Δ_{47} values represent 95% confidence intervals.” – corrected to “Error bars for the Δ_{47} values represent two standard errors of the mean.”

Page 99 Incorrect figure caption for Figure 5: “Error bars for the Δ_{47} values represent 95% confidence intervals.” – corrected to “Error bars for the Δ_{47} values represent two standard errors of the mean.”

Page 169 Missing units in table header: “Mg/Ca”, “Mn/Ca” and “Sr/Ca” – corrected to “Mg/Ca (mmol/mol)”, “Mn/Ca (mmol/mol)” and “Sr/Ca (mmol/mol)”



Graphic design: Communication Division, UIB / Print: Skjipes Kommunikasjon AS



uib.no

ISBN: 9788230854204 (print)
9788230855201 (PDF)